UCLouvain

epl

École polytechnique de Louvain

Towards paper-based biosensors:

Design considerations for lateral flow assay strips using magnetic iron oxide nanoparticles

Author: **Alexandre LOFFET**
Supervisor: **Jean-Pierre RASKIN**
Readers: **Annika GILLIS, Margo HAUWERT, Grégoire LEBRUN**
Academic year 2022–2023
Master [120] in Biomedical Engineering

Acknowledgements

I would like to thank several people that were of great help in the achievement of this master thesis.

First, I warmly thank Prof. Jean-Pierre Raskin for supervising this work and for his support to the project. Thank you to Prof. Annika Gillis for agreeing to be in my jury and for her nice welcome in her laboratory.

A special thank to Margo Hauwaert for her interesting remarks during the conception of this report and especially for her precious guidance and follow up during the year. Thank you also for the croissants and your patience during the long hours we spend with the scanning electron microscope looking at grey clouds to finally see the appearance of nanoparticles. I wish you the best for the end of your PhD thesis.

I have a special thought for Grégoire Le Brun whose training on manufacturing lateral flow assay was really valuable. As he initiated this thrilling project on lateral flow assay biosensor I hope he appreciates the progress of the project and new equipment in the lab as much as I did (The guillotine is amazing) and I wish him success for his PhD defense and his future projects.

Speaking of the training, I would like to thank Richard Ekoue Kouvahey for our mutual support, his good mood and his heady songs that he songs especially when tired. Good luck with finishing your master thesis.

I thank Sarah Vellemans who nicely took time to answer my questions on toxicity and for summarizing the part of the course she gives on environmental risk assessment.

Similarly, I am grateful to Montserrat Rivas Ardisana for taking time to answer some of my questions on lateral flow assay and for letting me benefit from her expertise/knowledge in the field of lateral flow assay.

Again I would like to thank Prof. Charles-André Fustin and Fabio Lucaccioni for their help and explanations related to the use and understanding the dynamic light scattering.

Lastly, as this master thesis is the conclusion of my studies I would like to thank my parents for their unconditional love and support during all those years. Without forgetting obviously my extraordinary sister, Hélène, without whom the exam sessions would have been very different.

Contents

Acronyms

AuNP Gold nanoparticle. 27, 28, 31, 38–40, 53–56, 58, 69–72, 75, 76

DLS Dynamic light scatering. 49, 50, 60, 62, 66, 67, 71, 73

IONP Iron oxide nanoparticle. 80–82, 85, 89–91

LFA Lateral Flow Assay. 1–3, 8–11, 20, 21, 23, 24, 27–36, 38, 39, 41, 45–47, 51–53, 56, 58, 65, 69, 71, 75–79, 82, 85, 86, 89–91

LOD limit of detection. 2, 36, 46, 78

MNP Magnetic nanoparticles. 2, 29–32, 38, 70

MNP@biotin Biotin coated magnetic nanoparticle. 42, 45, 46, 48, 53, 56, 65–67, 70, 71, 73–76, 78, 88, 90, 91, 93, 94

MNP@Neutravidine Neutravidin coated magnetic nanoparticle. 42, 45–48, 50, 53, 56–67, 70–76, 78, 85–88, 90, 91, 93–95

NP nanoparticles. 31, 32, 38, 57

PoC point-of-care. 1, 2, 9, 28, 90

QMRA Quantitative Microbial Risk Assessment. 3

SEM Scanning Electron Microscopy. 44, 48, 56, 61, 62

WHO World Health Organization. 2, 3, 79

Chapter 1

Introduction

Access to safe and clean drinking water is recognised by the UN as an human right. However, according to the World Health Organisation over 2 billion people live in water-stressed countries. Beside the lack of water, the difficulty to reach water sources and the eventual chemical contamination lies a microbiological hazard. Globally at least 2 billion people use a drinking water source potentially contaminated with faeces. Among these, over 368 million people are taking water from unprotected wells and springs and 122 million people collecting untreated surface water from lakes, ponds, rivers and streams. Microbial contamination of drinking-water as a result of contamination with faeces poses the greatest risk to drinking-water safety [1]. Microbiologically contaminated drinking water can transmit diseases such as diarrhoea, cholera, dysentery, typhoid and polio and is estimated to cause 485 000 diarrhoeal deaths each year. In the same way, pathogen contaminated water can also be harmful if it is used for cooking, growing food or for recreational purposes [1] [2] [3].

Being able to detect the contaminants in water is therefore crucial to prevent the propagation of water-based diseases. Traditional methods such as Most Probable Number (MPN), Enzyme-Linked Immunosorbent Assay (ELISA), Polymerase Chain Reaction (PCR), and their variations are able to reveal the presence or even to quantify the amount of pathogens but it comes with a cost. Indeed, those methods generally require an accessible laboratory containing specific material and the presence of skilled personal. As a result, those processes are time consuming and costly (e.g. up to 6 hours and more than 10$ per polymerase chain reaction test (PCR) [4]). Those factors can impede the monitoring of water, especially in crisis situations (earthquakes, floodings, war, etc.), in remote areas or in low and middle-income countries where there are few or no specific infrastructures and resources allocated to water monitoring [5].

Aside from the laboratory-based methods, biosensor technology has emerged as a promising solution to provide reliable, rapid, low-cost, end-user friendly and on site detection mean. Among the biosensors, defined as chemically sensing device that incorporates any biological or biologically derived material along with a physicochemical detector or a transducer [6], the lateral flow assay Lateral Flow Assay (LFA) stands out. LFA is an mature technology since it has been used for about 40 years for quick pregnancy tests and gained public appreciation more recently during the Covid-19 pandemia. This point-of-care (PoC) device, device that can provide rapid and on-site information [7], relies on a microfluidic stick where the sample is poured. The sample flows thanks

to capillarity and labels pre-disposed on the stick will attach the target analytes leading to a signal that can be assessed optically or with the use of a reader device. Lateral flow assay was the first PoC device to meet the World Health Organisation World Health Organization (WHO) ASSURED criteria (Affordable, Sensitive, Specific, User-friendly, Rapid and robust, Equipment-free (or simple), and Deliverable to end-users))[8] [9]. LFA are indeed relatively low-cost (less than 10 US$ per test), able to detect specific analytes in solution (such that it is used for HIV, COVID-19, pregnancy detection), rapid (less than 30 min for diagnosis), user friendly (no specific formation required), and usable on site [10]. However these PoC devices are not yet able to detect analytes in solution with the same limit of detection (LOD) and with an equal quantitative manner as their laboratory-based counterparts.

This is why the group working on LFA is heading towards a LFA that would not use gold nanoparticles traditionally employed to deliver an optical signal but iron oxide NP's instead as signal transducer. The goal is to take advantage of the iron oxide nanoparticles magnetic properties in order to use it as transducer for a portable magnetic device. This way, we would be able to quantify the amount of Magnetic nanoparticles (MNP) lying on the LFA stick and consequently to quantity of bacteria or other possible analytes linked to it. This could also improve the LOD in part because all the nanoparticles on the stick would contribute to the signal and not only the ones at the surface as it is the case with an optical detection. To carry out this project we need to develop and optimize several central components in different domains such as the LFA strip, the magnetic sensor and the bioreceptor responsible for the binding with the analyte in solution, the nanoparticles and the substrate.

To this journey towards a rapid, affordable and quantitative water quality monitoring device, I bring my contribution with this report. The purpose of this work is to design a prototype of magnetic nanoparticles based lateral flow assay which could be used as a first substrate to test the magnetic reader which is currently being designed. The structure of this work is strongly based on previous master thesis: "*Nanoparticles for paper-based biosensors and environmental impact assessment*" done by J. Vandeputte [11]. We will begin by explaining more in depth the issue linked to pathogens, exploring other biodetection means and explaining important theoretical background of the LFA in "State of the art" chapter, then the material and methods used in this work will be presented, the results will be exposed and then discussed. The concern posed by the possible toxicity of iron oxide nanoparticles will be investigated in the penultimate chapter and then you will find the conclusion of this work.

Chapter 2

State of the art

In this chapter we will firstly discover the sanitary problem caused by microorganisms and some current method of biodetection and their limitations. In a second part we will focus on the lateral flow assays, their advantage, working principle and components. Finally the use of magnetic nanoparticles in lateral flow assay is highlighted and as some means to improve the sensitivity of LFA are exposed.

2.1 Detection methods of microorganisms

Microbiological detection is tremendously important in food and water safety. Indeed, some microorganisms are pathogenic and can cause illness which can have dire consequences (485 000 diarrhoeal deaths each year [1]). According to the WHO, microbial contamination of drinking-water as a result of contamination with faeces poses the greatest risk to drinking-water safety [2]. In order to protect people, legal limits based on the dose-response of the pathogens have been put in place (e.g. for E.coli 0 Colony Forming Unit (CFU)/100mL in drinking water [12] and max. 2000 CFU/100mL in bathing water [13]). To monitor the risks Quantitative Microbial Risk Assessment (QMRA) systems combine information on the exposure, the potential number of people threatened and dose–response models to produce estimates of the probability of infection associated with exposure to pathogens in drinking-water. We can see in figure 2.1 a risk classification in function of the sanitary inspection as proposed by the WHO [14]. The use of biodetection methods indeed is only a part of the strategy. The organ in charge need to inform the public and provide viable alternative or promote suitable water treatment (other water source, boiling of the water, chlorine disinfection,...). The use of E. coli (or coliform bacteria present in animal gastrointestinal track) as an indicator of the fecal contamination is a well-established practice in the assessment of drinking-water quality. Even though in certain occasions it may not be sufficient (especially for waterborne outbreak due to enteric viruses or protozoa), in the majority of cases, monitoring for E. coli or thermotolerant coliforms (i.e. bacteria that can develop in human or animal intestinal track) provides a high degree of assurance because of their large numbers in polluted waters [2] [13] [14]. Of course, this is only an indicator of microbial contamination, other sources of pollution (chemicals, radiological) could make water unsafe.

E. coli count	Sanitary inspection risk score			
	0–2	3–5	6–8	9–10
>100	17	57	31	4
11–100	45	122	55	5
1–10	26	58	22	3
0	426	609	114	3

Low risk: no action required	Intermediate risk: low action priority	High risk: higher action priority	Very high risk: urgent action required

Figure 2.1: Assessment of priority remedial action for drinkable water sources in the framework of quantitative microbial risk assessment strategy [2]

The ability to detect the presence of microorganism or to quantify their concentration is therefore crucial to assess the risks and consequently to avoid waterborne outbreak [2]. A good biodetection method thus needs to be able to detect the presence of microorganisms with high accuracy and repeatability [15]. As we will see the methods depicted here after are able to assess the presence of microorganisms but each of them comes with drawbacks.

2.1.1 Culture based methods

The oldest methods of microbiological detection are based on microbiological culture. The principle is, at first sight, pretty straightforward. Collect a sample, give it the right conditions of pH, temperature, nutrients, incubation time, oxygen availability, etc. for bacteria to proliferate and then evaluate the amount of bacteria [6]. The amount of bacteria found is often reported in CFU, colony forming unit. The single colony consists of many bacterial cells which may have started from one cell or a group of cells [6]. We can see on the figure 2.2 the outcome of a bacterial culture in a Petri dish, the CFU are clearly visible. Several technique to count the bacteria or to evaluate the bacteria metabolic activities are possible some examples are presented here under.

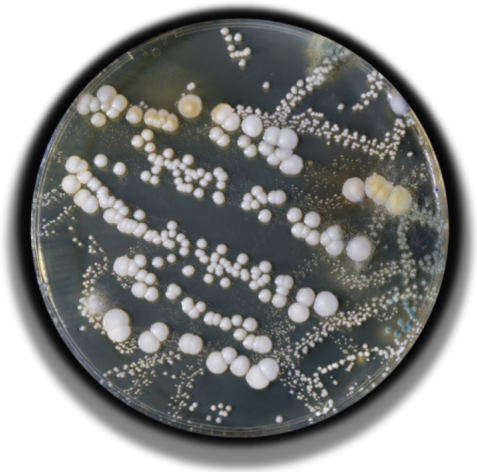

Figure 2.2: Bacterial culture in a Petri dish. The colony forming units resulting from exponential growth of single bacteria are clearly visible, image from [16]

Direct microscopy count The sample is observed with the a microscope in grided cover slip. The micro organisms can be distinguished by their morphologies as observed under a light, or fluorescence microscope after staining the cells. The number of bacteria on the grid is computed and reported in number of cells per milliliter [15].

Standard plate count Plate counts exploit the fact that individual microscopic cells quickly grow into a colony visible to the unaided eye if provided with suitable growth conditions [17]. It is then possible to count the colony forming unit (CFU) and estimate their total number (per ml or per g) by multiplying with the dilution factor of the initial solution spread onto the plate [15].

Most probable number Statistical method used to estimate the viable numbers of bacteria in a sample by inoculating broth in 10-fold dilutions and is based on the principle of extinction dilution. In clear, serial dilutions of the sample (10, 100, 1000, 10 000,...) in several exemplary (typically 3 or 5) are made. Then the diluted sample are incubated for a certain period of time (24 hours). After this incubation the presence of CFU in the sample is assessed and depending on the number of positive sample a statistical estimate of the MPN of bacteria can be made. The dilution at which no CFU is observed is also taken into account in the multiplying factor as we can see on the figure 2.3. This way a relatively good approximation of the number of CFU per mL in the original solution can be obtained [15] [17] [18].

Table A5.4 Example of multiplying factors for determination of the MPN for different dilutions of sample

	No. of tubes giving a positive reaction					Coded result chosen	Multiplying factor for MPN
Example	5 of 1 ml	5 of 0.1 ml	5 of 0.01 ml	5 of 0.001 ml	5 of 0.0001 ml		
1	5	5	2	0	0	5–2–0	100
2	5	5	4	1	0	5–4–1	100
3	5	3	0	0	0	5–3–0	10
4	5	5	5	3	1	5–3–1	1000
5	0	1	0	0	0	0–1–0	10

Figure 2.3: Most probable number (MPN) assessment, image from [19]

Those culture based techniques can also be coupled with biochemical identification (like API galleries), to identify precisely the type of bacteria. They are able to assess the presence of specific living cells and to approximate the concentration in the sample (MPN or direct microscopic count if no culture prior). Nevertheless these traditional techniques have some limitations. First, it does not allow to detect non culturable microorganisms like protozoa, viruses or bacteria in a Viable But Not Culturable state (VBNC). Culture-dependent methods only allow to detect organisms able to grow and compete under laboratory condition [5] [17]. Besides there are a lot of different culture media and the choice of the media is very important as it will favor the growth of some types of bacteria. [15]. There is indeed competition between the different microorganisms (that may not be all pathogens) if they were present in the sample [15]. Then, microbiological culture requires laborious work process of sample collection, serial dilution, plating on selective and suitable media and waiting for appropriate incubation time as well as all the apparatus needed for those operations. It must therefore be done in a laboratory by skilled personal and can take from

18 to 72 hours to grow the pathogens [6] which does not take into account the time required to bring the sample to the laboratory. Those methods are thus not appropriate to monitor water quality especially in low development countries.

2.1.2 Non culture based methods

In order to address the issues linked to the microbiological culture, other techniques using nucleic-acid sequence or immunology have been developed. Those indeed allow to detect not culturable microorganisms in a shorter period of time as we can see on the table 2.1 which summarizes their characteristics.

	Time to run the test	Limit of detection	Detection of bacteria	Quantification
Plate counting	24-72 hours	10^2 bacteria	Viable cells only	No
Most probable number	6-18 hours	2-300 bacteria	Viable cells only	Approximation possible
ELISA	2 to 4 hours	1 x 10^3 CFU/mL	Viable cells and VBNC	Possible if no enrichment
PCR	1 to 6 hours	3.5×10^3 CFU/mL	Viable cells and VBNC	Possible for qPCR

Table 2.1: Sum up of characteristics for some biodetection techniques [13] [5]

Enzyme-linked immunosorbent assay (ELISA)

The ELISA, acronym for Enzyme-Linked ImmunoSorbent Assay, is a widely used immunological approach in food investigation designed in the early 1970s. As we can see on figure 2.4 (in the case of a sandwich LFA), the base principle is to use antibodies to attach the analytes in the sample then to bind another antibody labelled with an enzyme (different variants exist with coloured or fluorescent labels). When washed to remove non bound antibodies and enzymes, a substrate is added to the well. The enzyme, that stayed in the well because of its attach to the analyte, will induce coloration of the well. Finally the intensity of this coloration can be quantified with absorbance measurements [6].

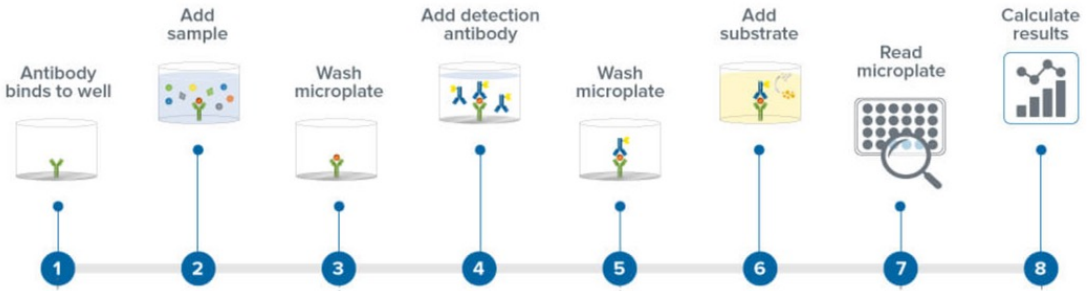

Figure 2.4: View of a sandwich ELISA process, image from [20]

The major advantages of ELISA over other approaches, are its high level of specificity, sensitivity, reproducibility, and simplicity [6]. ELISA is also quite cost effective but it still requires specific equipment and some time, about 2 to 4 hours to go through the process. A lot of variants were designed along the years, some use cultural enrichment to improve the limit of detection but it increase the duration of the assay. To diminish the process duration, a way is the automation which can be beneficial for time, efficiency yield, and reproducibility [20].

Polymerase chain reaction (PCR)

The late 1990s was the beginning of the molecular oriented identification with the development of PCR based reactions and first generation sequencing [6]. The polymerase chain reaction is nucleic-acid sequence based approaches that can detect microbial cells and their toxins, whereas immunological approach is not so specific for the detection of microorganisms and dependent on harboring proteins [6]. In short, the PCR makes multiple copies of a specific fragment of DNA (or RNA for RT-PCR) from a mixed pool of nucleic acid fragments and permits detection of sequences originally present at very low densities. As we can see on the figure 2.5 (left), the process include 3 steps:

1. Double-stranded DNA (dsDNA) is heat denatured
2. Primers align to the single DNA strands
3. The primers are extended by DNA polymerase

Hence is obtained two copies of the original DNA strand. This 3-steps cycle of denaturation, annealing, and elongation is repeated approximately 20-40 times and the amplified product can then be analyzed [21]. After PCR amplification, fragments are separated by electrophoresis in a polymer gel on the basis of their length or nucleotide composition. Depending on the length and thus on molecular mass of the fragments they will progress to a certain extend. The result, as we can see on figure 2.5 (right), is a collection of bands corresponding to the molecular mass that constitute a fingerprint of the DNA/RNA present in the sample. This way PCR is able to detect specific strains, species, or phylogenetic groups in environmental samples. Two important considerations however are that amplification efficiency varies among DNA sequences. Therefore 'simple' PCR results are rarely considered to be quantitative,and DNA sequence with low amplification efficiency could conceivably be prominent in the environment but not appear in PCR-based diversity measurement [17]. Variants of PCR were established notably the Reverse Transcriptase PCR (RT-PCR) which allows to amplify RNA or the quantitative PCR (qPCR sometimes called real time PCR). For quantitative PCR the principle is to use dyes that become fluorescent when incorporated to the replicated DNA (Taq-Man or SYBR green procedures). In this way, the fluorescence is indicative of the amount of DNA copies that are made and it becomes possible to determine with more certainty the number of genomes per volume of water for a specific bacterial species [13].

In this way, the fluorescence is indicative of the amount of DNA copies that are made and it becomes possible to determine with more certainty the number of genomes per volume of water for a specific bacterial species.

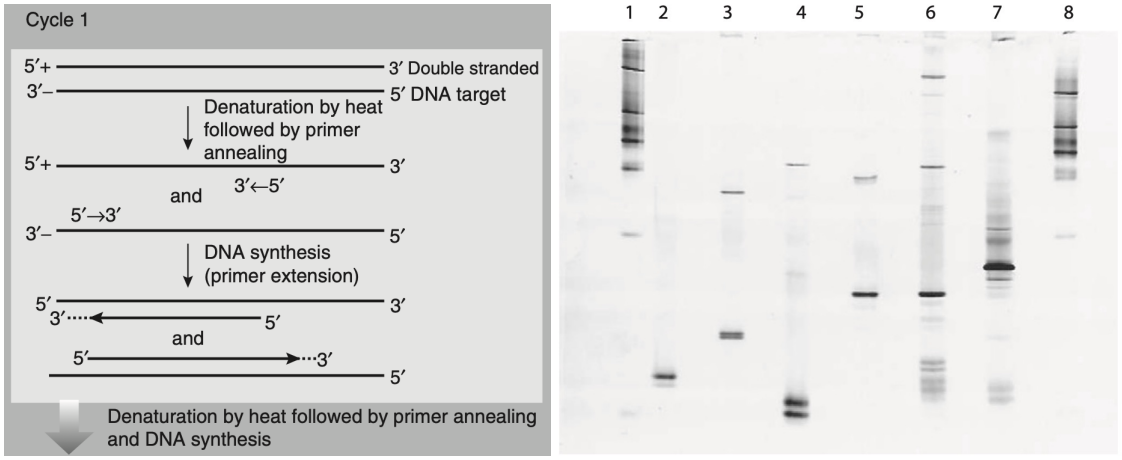

Figure 2.5: *Left*: Scheme of a cycle in polymerase chain reaction. *Right*: Inverted image of fluorescently stained polyacrylamide gel showing DNA bands in electrophoresis, images from [17]

We can see on the figure 2.6 a comparison in term of diagnostic speed and analytical sensitivity between ELISA, PCR and lateral flow assay (LFA) , point-of-care device that will be explained in depth in the next section. The advantage of LFA appears quite clearly in terms of time detection and this does not take into account the time needed to bring the sample from the tested site to the laboratory. Indeed a laboratory is required to perform PCR and ELISA tests but not for the LFA which , as point-of-care device, can be run on-site. The lateral flow assay is also way less expensive than the other techniques indeed the test takes less than 1$ USD [22] whereas PCR is estimated to cost around 10$ USD per test [4]. We can however notice that the limit of detection is several order of magnitudes higher for the existing commercial LFA than for the other techniques. This gap can yet be reduced with so-called signal-amplified LFAs, in fact lateral flow assay using other types of labels (such as magnetic ones) as we will see on the following section.

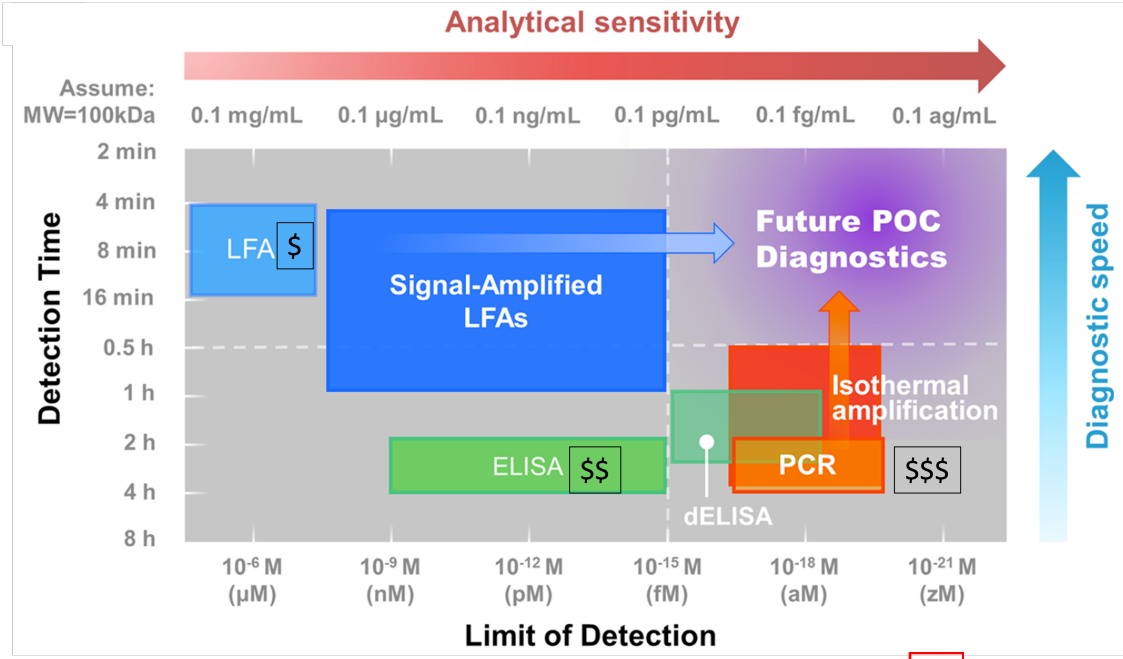

Figure 2.6: Comparison between the analytical sensitivity and diagnostic speed of LFA for an analyte having a molecular weight of 100kDa, image from [23]

2.2 Lateral flow assay

In order to overcome the limitations a of conventional biodetection methods, point of care PoC devices were developed. Among which biosensors such as lateral flow assays LFAs that were the firsts to meet the ASSURED requirement (Affordable, Sensitive, Specific, User-friendly, Rapid and robust, Equipment-free (or simple), and Deliverable to end-users) [8]. Indeed, LFA is a mature technology. LFA were firstly introduced for pregnancy auto-tests in the 1980's and are now widely used as 3 millions tests are sold each year in France [24]. More recently, LFA gained public recognition due to the COVID-19 pandemia. During the crisis, LFA were used for the first time as part of a large-scale testing strategy. By the end of May 2021 691 million LFA were distributed in the UK, outpacing RT-PCR (Reverse-transcriptase PCR) testing [25]. This intensive use of LFA gives a valuable feedback on the implementation of a monitoring system based on LFA [26]. Nevertheless, the LFAs used were not flawless. We can highlight their sensitivity ranging from 34.1% and 88.1% compared to a RT-PCR or the difficulty for the authorities to have a global view of the situation as only about 14% of the results were reported [27]. The next generation of LFA should address those issues, but before going into such considerations we will explore the operating principle of the LFA.

Figure 2.7: Commercial lateral flow assay for COVID-19 detection (*left*) or pregnancy test (*right*) [28]

2.2.1 Lateral Flow Assay: Working principle

Lateral flow assay sometimes also called, lateral flow test, lateral flow device or lateral flow immunoassay relies on a simple principle. A aqueous sample containing the analyte of interest is poured on the extremity of the stick and flows thanks to capillarity to the other end. During the process, functionalised nanoparticles pre-positioned on the stick will resolubilize, bind to the analyte of interest, continue to flow and bind on control or test line consisting of bioreceptors, molecules stuck to the membrane that will bind specifically the analyte or the nanoparticles. This will cause the nanoparticles to accumulate on one or both lines depending on the positive or negative test result and the format of the test (as we can see on figure 2.9). The flow test generally takes from 10 to 30 minutes to be completed depending on the type of analyte, the mean of detection or the kind of stick used. It is a big advantage over other biodetection methods. For the sake of clarity in this work, as in Parolo and al. "Tutorial: design and fabrication of nanoparticle- based lateral-flow immunoassays" [29], the name detection bioreceptor is used for bioreceptors attached

to the nanoparticles and the name capture bioreceptor is used for bioreceptors immobilized on the stick.

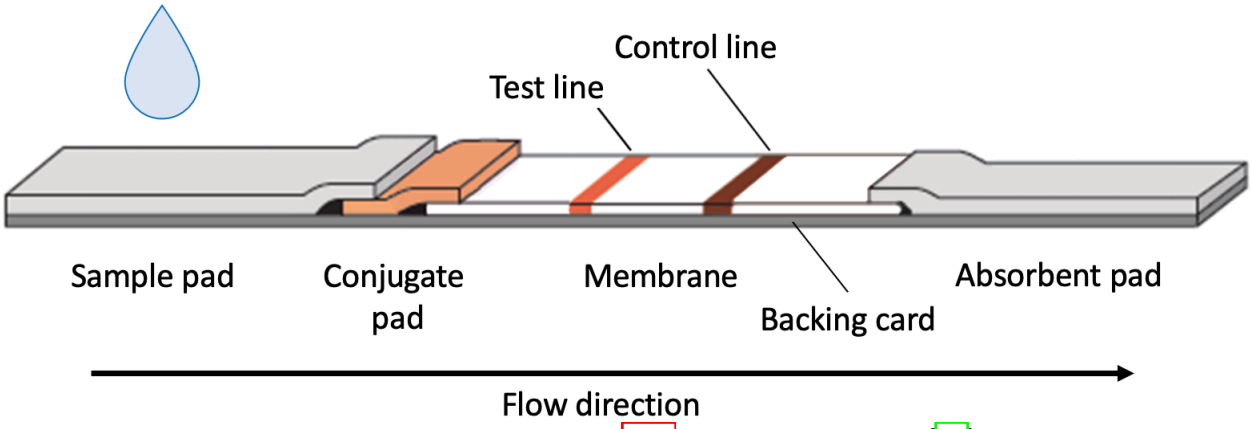

Figure 2.8: Composition of a LFA stick, adapted from [30]

We can see on the figure 2.8 here above the main parts of a lateral flow assay stick. It is generally composed of 4 important parts: the sample pad, the conjugate pad, the membrane and the absorbent pad. The sample pad which can modulate the sample and promote a good flow for the next pad, the conjugate pad where the previously functionalized nanoparticles are placed waiting for resolubilisation. Then comes the membrane or analytical pad where the control and test lines are predisposed and finally the wicking or absorbent pad which ensures the continuation of the flow after the water front has reached the end of the membrane so that a maximum of the analytes and the nanoparticles passes through the test and control lines. We can also mention the backing card which does not get involved in the flow but provide a support to glue the different pads and ensures the cohesion of the whole. The role, specificity and materials used for each pad are explained more in details within the next sections but first we will explore more in depth the 2 main formats of the lateral flow. We can see on the figure 2.9, those 2 sensing strategies: the sandwich LFA and the competitive LFA.

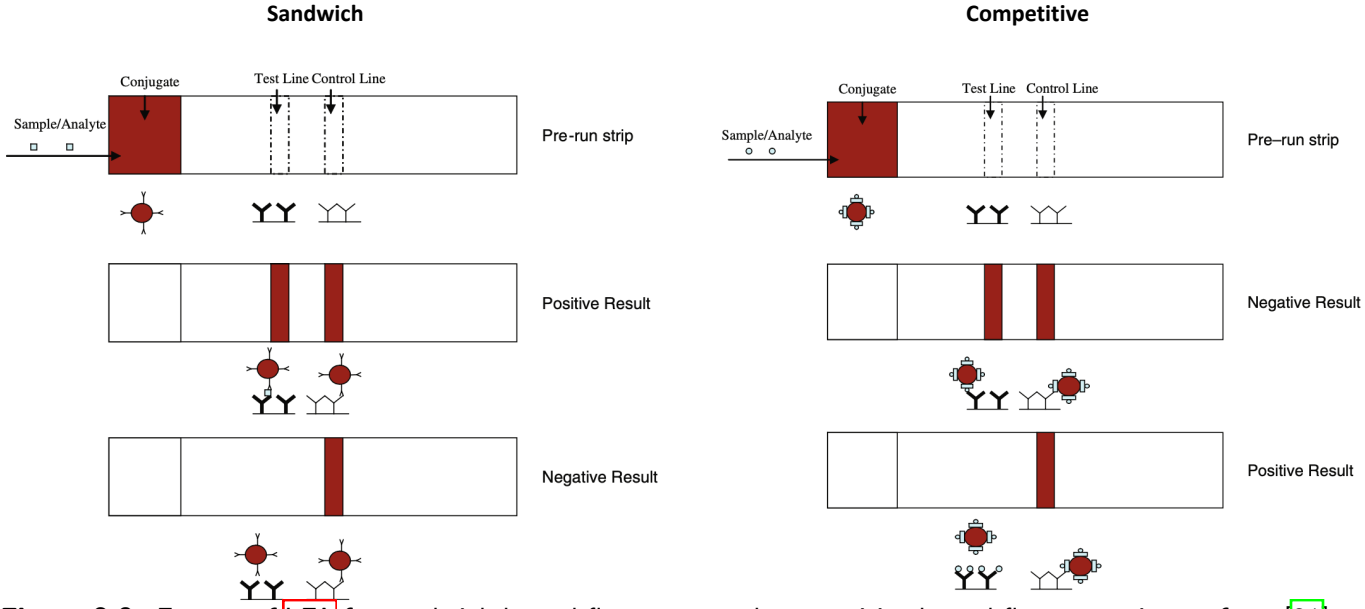

Figure 2.9: Format of LFA for sandwich lateral flow assay and competitive lateral flow assay, image from [31]

Sandwich LFA Probably the most common strategy, this format is suited for big or mid-size analytes (>1kDa) which have multiple antigenic or binding sites. Indeed as its name suggests, at the end of the test, the target analyte must be taken in a "sandwich", i.e. be linked to the detection bioreceptor which is attached to the nanoparticles and to the capture bioreceptor which is anchored to the membrane hence revealing the test line. The control line, always placed after the test line following the flow direction, is formed by capture bioreceptors binding specifically the detection bioreceptors fixed on the nanoparticles. In this way, a control line appears ensuring the proper operation of the device. Therefore when there is no target analyte in the solution, the complex detection bioreceptors-analyte-capture bioreceptors cannot form, there is no binding on the test line and all the nanoparticles bind to the control line as we can see on figure 2.9. When on the contrary, there are analytes in solution, the complex is formed and 2 lines appear. Sandwich LFA however present a notable downside, they are more prone to false-positive results than competitive assays [32] [29].

Competitive LFA In competitive lateral flow assay the analyte enters in competition with a bioreceptor to bind a second bioreceptor. There are two types of competitive lateral flow assay: when the target analyte and the detection bioreceptor on the functionalized nanoparticle compete to bind at the test line (as we can see on figure 2.9) and when the target analyte and the capture bioreceptor at the control line compete to bind the capture bioreceptor on the nanoparticle. The competitive LFA is suitable for detecting small analytes (< 1kDa) [32] [29].

As we began to find out, lateral flow assay is more complex than it may seem at first glance. Indeed it combines several components which have their requirements, are interdependent and act on different time and length scales. The figure 2.10 illustrates this quite well. It also mentions some parameters that can be modified to improve the performance and that will impact components on different scales. In the following sections are explained more in details all those components and how they can affect the performances of LFA.

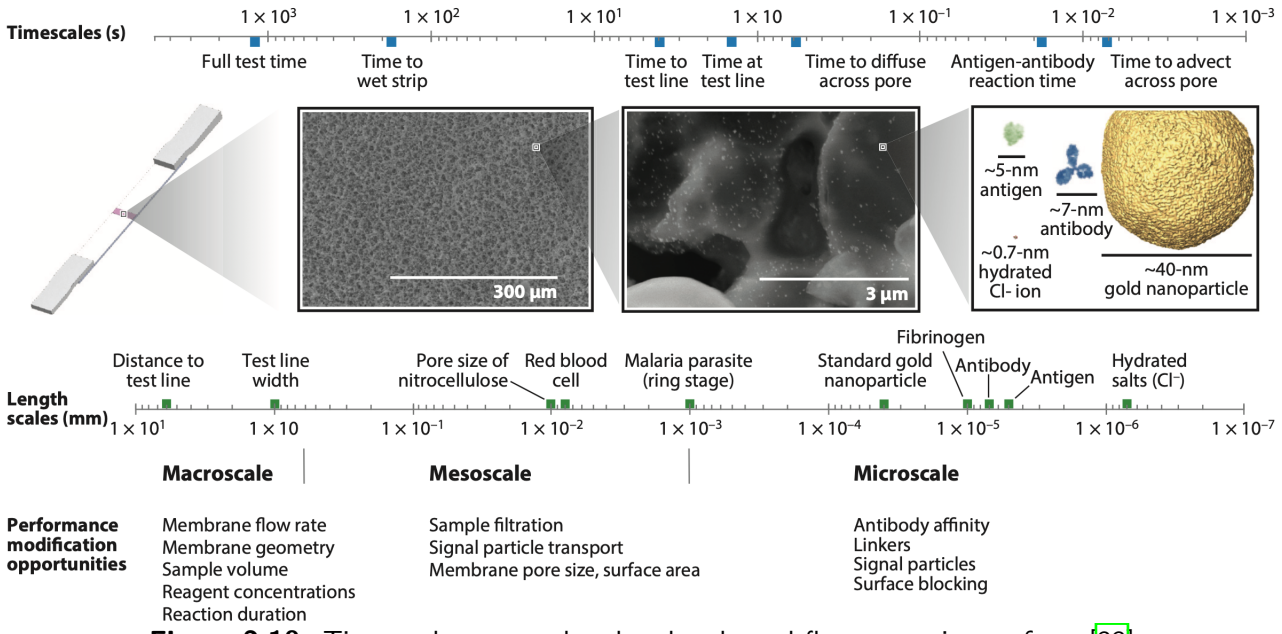

Figure 2.10: Time and space scale related to lateral flow assay, image from [33]

Sample pad

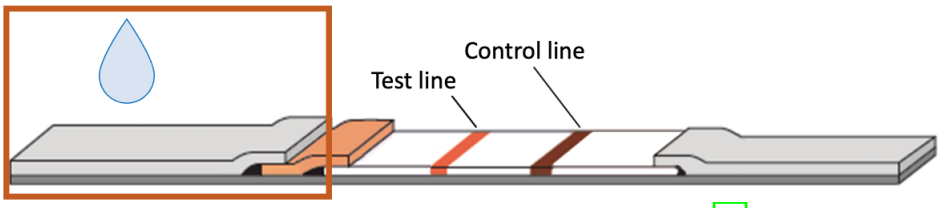

Figure 2.11: Sample pad, adapted from [30]

The sample pad is the portion where the aqueous sample is poured. It is important because it is the first contact between the sample and the stick as we can see in figure 2.11. The sample pad ensure therefore 2 main functions [29]:

- Provide an even flow for the next pad
- Standardize the buffer conditions of the sample

Lateral flow tests can be used in various domains: from clinical applications (e.g. blood, serum, plasma, saliva, nasal swabs samples) to environmental applications with water and soil samples, or else food and beverage industry applications with milk or liquid food samples. The sample pad therefore needs to be adapted to provide the good conditions of pH, ionic strength, viscosity and blocking capabilities for the test. To this end, the sample pad can be pretreated typically via immersion and drying [31]. Depending on requirements, these pretreatment solutions may contain buffering agents, detergents, blocking agents and preservatives. We can see in table 2.2 the parameters controlled by the pretreatment and some commonly used reagents that are used to fulfill 4 main tasks. Buffering agents aim to control pH and ionic strength, two parameters that can alter the sensitivity, reproducibility and specificity of the assay by impacting the interactions between receptors and analytes. The presence of detergents and surfactants (such as SDS or Tween 20 at a very low concentration) may promote resolubilization of the conjugate, reduce nonspecific binding of the conjugate, and possibly minimize adsorption of the analyte to the membrane. Finally aside from preservative that should not impact the flow, the blocking agent to diminish the nonspecific bindings and avoid to have to block/passivate the membrane [34] [29] as we will see later on.

Pretreatment solution	Goal	Commonly used reagents
Buffering agent	Control pH and ionic strength	Phosphate, Tris, HEPES or Borate
Detergent	Minimize nonspecific binding and facilitate the flow of the detection labels	SDS , Tween 20 or Triton
Blocking agent	Minimize nonspecific binding	BSA, milk or Casein
Preservative	Avoid microbial contamination on the LFA strip	Sodium azide

Table 2.2: Reagents used for sample pad, based on [29]

Aside from regulating the composition of the sample, sample pad can also be used to physically control the rate at which liquid enters the next pad (conjugate pad) or to filter the sample. Depending on the size of the pores, it is able to retain the biggest components of the sample solution that otherwise could be blocked further in the detection region diminishing the sensitivity of the test [34].

Materials The materials used for the sample pad depend on the requirements of the application but the most common are cellulose and woven meshes like glass fiber [31]. The sample pad needs to be able to accept all the sample volume which makes the bed volume (also known as void volume or volume of air) an important parameter to consider. It also should be strong enough to be handled during the fabrication process.
Cellulose fiber is cheaper, has typically bigger bed volumes (more than 25 μL/cm^2, although it obviously depends on the thickness) and has good tolerance toward the chemicals present in the sample pad buffer. Nonetheless, it is weaker for handling especially when wet which makes the manufacturing process more delicate particularly if a sample buffer is applied [29].
Glass fiber may be costlier but it has good tensile strength and handle well, even when wet. Meshes have very low bed volumes (1 -2 μL/cm^2), meaning that it retains very little sample volume but also that it cannot accept a lot of sample volume at once otherwise the stick will be flooded. Another big drawback is that it is impractical to treat them with enough sample pad buffer solutes to modify the protein content, pH, ionic strength or viscosity of the test sample [34].

Conjugate pad

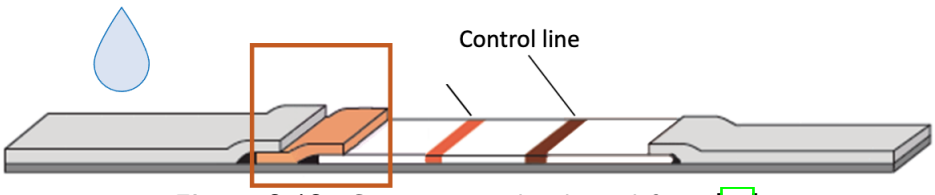

Figure 2.12: Conjugate pad, adapted from [30]

Once the sample loaded on the sample pad, it will flow thanks to capillarity through the conjugate pad. The conjugate pad is the part of the stick that contains the functionalized, or conjugated, nanoparticles. It has 3 main functions [29]:

- Fix and preserve the nanoparticles previously labelled with bioreceptors
- Release efficiently and in a reproducible manner the nanoparticles upon wetting
- Provide the first interaction between the targeted analytes and the bioreceptors

The conjugate pad has therefore a central role in the lateral flow test, poor conjugate pad designing or manufacturing could drastically hinder the release of nanoparticles diminishing the assay's sensitivity. A good conjugate pad should ensure low non-specific binding (to avoid the retention of the nanoparticles or the target on the conjugate pad), consistent flow and bed volume (achieving a homogeneous and reproducible flow along the width of the membrane is essential to obtain reproducible results) and enough mechanical strength for the manufacturing process [29]. In order

to achieve its role, the choice of the material, the treatments applied on the pad and the loading of the bioreceptor-nanoparticle conjugate are determining. We can see on the table 2.3 some reagents used. The stabilizing reagents typically protect the bioreceptor's properties because the hydroxyl groups of sugar molecules replace the water around the protein upon drying, ensuring they keep the same conformation. Those reagents then promote rapid resolubilization because they are solved easily when aqueous sample enters the conjugate pad [29] [32].

Conjugate pad buffer components	Goal	Commonly used reagents
Buffering agent	Control pH and ionic strength	Phosphate and Borate buffer
Stabilizing and resolubilisation reagents	Preserve the native conformation of the proteins and promote quick resolubilisation upon rewetting	Sucrose or trehalose
Detergent/surfactant	Promote the flow, impede non-specific adsorption	Tween 20, SDS or Triton

Table 2.3: Reagents used for conjugate pad buffer, based on [29] and [34]

There are two main ways to load the conjugated nanoparticles on the conjugate pad. The first is to dip the conjugate pad into the conjugate pad buffer containing the functionalized nanoparticles. The second is to use an air jet dispenser. The second option has the advantage of providing a more uniform loading which diminishes stick to stick variability. Once the nanoparticles loaded, a crucial step remains: the drying of the conjugate pad. The drying process is crucial to maintain the stability of the dried bioreceptor-nanoparticle conjugate and determines the release efficiency from the membrane. Failing to completely dry the conjugate pad may generate a syrup-like solution unable to run through the membrane [29]. In mass production heat-induced drying is usually used due to its convenience, but when applicable, vacuum drying is preferred because it does not affect the stability of the molecules and promote a more uniform distribution of the nanoparticles [31].

Materials The most commonly used materials are glass fiber, polyesters and cellulose. Each of those materials have low non-specific bindings, consistent flow characteristics and low extractables, i.e. particles that can clog the membrane at the conjugate pad/membrane interface. They have flaws: glass fiber is more difficult to slit and cellulose is very weak when wet. Glass fiber is generally used because it has low hold-up volume, about 1 or 2 μL/cm^2 against 50 and 15 μL/cm^2 for cellulose and polyester respectively. Compared to polyester and especially cellulose, glass fiber should retain less solution allowing more nanoparticles to go into the membrane [34].

Membrane

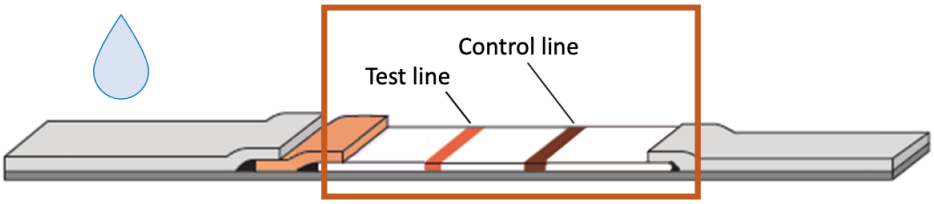

Figure 2.13: Membrane, adapted from [30]

The membrane sometimes called detection pad or the analytical region is the the part of the stick where the outcome appears thanks to the capture bioreceptors previously attached to the membrane forming the control and test lines as we can see on figure 2.13. It fulfils 3 main functions [29]:

- Promote an homogeneous flow
- Provide a good substrate for attaching the capture bioreceptors
- Minimize low non specific binding

The role of the membrane is thus central in the lateral flow test because it is where the outcome of the test is reported. A good flow of the analytes and the nanoparticles, with low non specific binding, and a good fixation of the capture bioreceptors on the membrane is crucial for achieving a good sensitivity and a high signal-to-noise ratio.

Materials The most commonly used material for the membrane is nitrocellulose. Several attempts have been made to introduce the use of other material types such as nylon and polyvinylidene fluorid. However, those attempts have had limited success, apparently due to factors including cost, limited utility, the need for education regarding new chemistry and processing requirements, and resistance to change due to the large bank of existing experience in the use of nitrocellulose [31]. We will therefore focus this section on the use of nitrocellulose as membrane.

Nitrocellulose has several advantages among which its low price, its strong binding to proteins (enabling the fixation of capture bioreceptors) and its tuneable capillary flow time and pore size [29]. Three manufacturing methods are shown with their specificity as we can see on the figure 2.14. The first technique, the phase inversion technique developed in early 1900, is appropriate to manufacture nitrocellulose for lateral flow assay [35]. On an industrial scale, a lacquer consisting in nitrocellulose polymer dissolved in a mixture of solvents, nonsolvents and wetting agent (to make the final nitrocellulose hydrophilic) is spread on a moving belt. The belt carries the lacquer into a series of chambers where air flow, temperature, and humidity are adjusted to control the evaporation rate of the solvents from the lacquer. As the solvents evaporate, the nitrocellulose strands migrate within the liquid phase, eventually reaching a concentration where they precipitate. The size of the pores within the structure is dictated by the evaporation rate, with more open structures achieved by reducing the evaporation rate. In this way is achieved nitrocellulose with pore sizes ranging from 3 to 20 μm. Below this range, the lateral flow rate is too slow to be

practical and above this range, it is complicated to obtain a nitrocellulose membrane with uniform properties with current technologies [36].

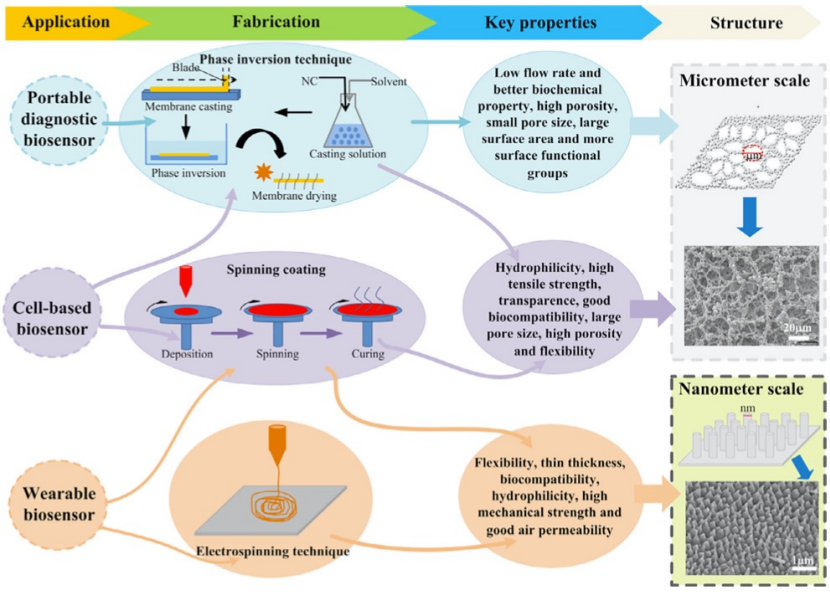

Figure 2.14: Fabrication techniques achieving nitrocellulose with different properties, image from [35]

Being able to tune the flow rate is important because it will impact the sensitivity and specificity of the test. We can observe on table 2.4 the capillary speed, pore size, sensitivity and specificity of 3 UniSart® nitrocellulose membranes produced by Satorius. Commercial membranes are generally defined by their capillary flow time, which is the time required for the sample front to cover a certain distance (generally expressed as seconds by 4 cm) [29]. It is an easier characteristic to identify than the pore size which is subjected to more variation depending on the technique used to take the measure [34]. As we can see on the table, the sensitivity diminishes with increasing capillary speed. It is because high flow rate will let less time for interaction between the targeted analytes and the bioreceptors leading to a decrease of the sensitivity if the time does not match the reaction constant. On the other hand, the more the flow is fast the less it will give time for non specific interactions leading to a better specificity.

Membrane name	Capillary speed down web, purified water [s/4cm]	Nominal pore size	Relative sensitivity	Relative specificity
CN 95	65-115 s	10 – 12μm	Low	High
CN140	90-150 s	about 8 μm	↓	↑
CN180	135-175 s	about 5 μm	High	Low

Table 2.4: Satorius's UniSart® nitrocellulose membrane characteristics based on [37]

Nonetheless nitrocellulose has also some downsides. It is an hydrophobic material and to ensure a good flow, the membrane needs to be hydrophilic. Luckily it is possible to make nitrocellulose hydrophilic by adding rewetting agents during the membrane production process as we saw earlier.

Besides, chemistries that make the membrane wettable with aqueous solution do not significantly diminish protein adsorption [36]. Another downside of nitrocellulose is that it is quite brittle but this can be partly overcome by casting the nitrocellulose on a backing (generally consisting of polyester). This polyester backing does not interfere with the function of the nitrocellulose while significantly improving its handling properties however the membrane is still to be handled carefully.

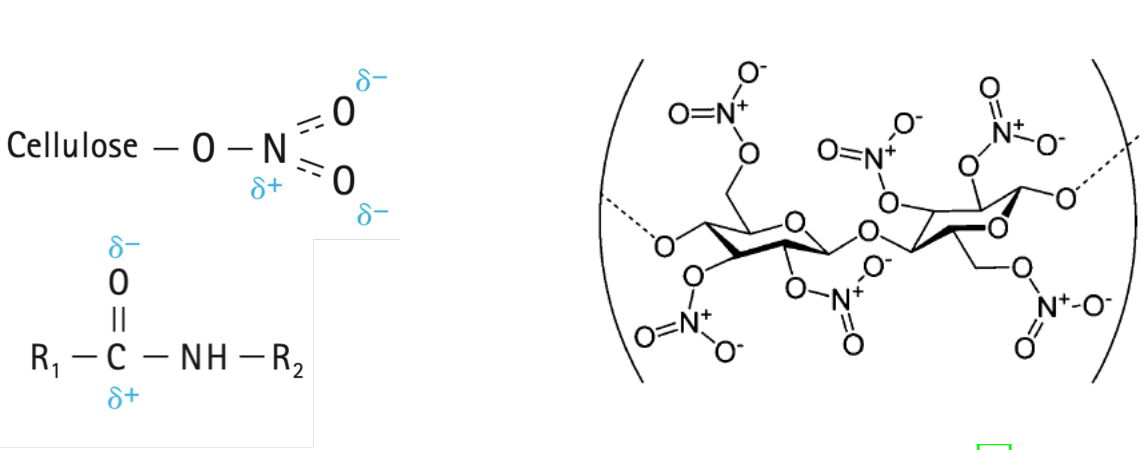

Figure 2.15: *Left:* Chemical structures of functional groups of nitrocellulose and proteins [34]
Right: Chemical structure of nitrocellulose [38]

A key ability of the nitrocellulose membrane is to be able to fix the capture bioreceptors in order to form the test and control lines. The commonly accepted model for binding of protein to nitrocellulose is that proteins are initially attracted to the membrane surface by electrostatic attraction. Indeed we can see on figure 2.15 the dipoles due to the nitrate ester of the nitrocellulose that will interact with the amino acids of the capture bioreceptors. When the membrane is dried, the fixation is then accomplished by a combination of hydrophobic and hydrogen bonds [31]. In order to promote the anchoring of the capture bioreceptors some reagents may be used in an immobilization buffer. In general, to maximise the adsorption, antibodies and other proteins should be applied to the membrane in buffers at a low concentration that are preferably free of salt, surfactants, and sugars to avoid interfering with the adsorption process [31]. We can see some examples of immobilization reagents sometimes used in the table 2.5. Buffer with high ionic strength are to be avoided because they could screen the membrane's electric charges. A pH within the unit of the capture bioreceptor isoelectric point is preferred to promote its binding to the membrane and its stability [29].

Immobilization buffer components	Goal	Commonly used reagents
Buffering agent	Maintain the stability of the capture bioreceptors	Ammonium acetate or phosphate buffers at low concentration (10mM)
Stabilizing reagents	Stabilize the capture bioreceptor once the membrane dried	Lactose (0.1% (wt/vol)) or trehalose (1% (wt/vol))
Alcohols	Reduce solution's surface tension, viscosity and static repulsion	Methanol, ethanol or isopropanol in concentrations ranging from 1 to 10 % (vol/vol)

Table 2.5: Reagents sometimes used for immobilizing the capture bioreceptors, based on [29]

In addition to immobilization buffers which are specially intended to promote the anchoring of the capture bioreceptors, it is also possible to treat the membrane in order to reduce non-specific interactions with the membrane. If the use of a blocking buffer is decided, it is imperative to do it after the total immobilization of the capture bioreceptors otherwise it could impede the adsorption of the bioreceptors. Some of the reagents used to this purpose are listed on table 2.6. The blocking process consist in at least three steps. First the blocking buffer is applied by dipping the membrane into the buffer, then the excess blocking agent are removed by dipping the membrane at least two times in the washing buffer[29]. It is important to wash the membrane immediately after the blocking step because molecules not adsorbed to the nitrocellulose can dry and form crystals in the pores, hindering or blocking sample flow [36].

Blocking the membrane	Goal	Commonly used reagents
Blocking buffer	Reduce non specific interaction of functionalised nanoparticles or target analyte with the membrane	BSA (66 kDa) 1–2% , IgG (150 kDa) 1–2% , gelatine (60 kDa) 0.1–0.5% , casein (25 kDa) 1–2% , polyvinylpyrrolidone (8–10 kDa) 0.5–1% and polyvinyl alcohol (PVA,8–10 kDa) 0.1–1%
Washing buffer	Remove the excess blocking agents	SDS 0.005–0.01% (wt/vol)

Table 2.6: Reagents used for blocking the membrane (percentage in weight per volume), based on [29]

As we can see on the table, the washing reagent is generally the SDS (Sodium dodecyl sulfate) a detergent (amphiphilic). The blocking reagents often used are of different type: bulking proteins like bovine serum albumin (BSA) or casein that compete for binding sites to prevent non-specific binding or else polymers like polyvinylpyrrolidone (PVP) that interfere with protein binding by a combination of bulking and interfering with hydrogen and hydrophobic bondings [31]. Anyhow, the blocking agent should be smaller than the capture bioreceptor, in order to avoid steric hindrance that may affect the binding between the bioreceptor and the analytes [29]. Some reports that the blocking (i.e. coating uniformly the membrane with a single chemical species) could also benefits the flow consistency through the membrane [31]. Membrane blocking is however a tedious process

that requires several steps of blocking, washing and a drying for long time. Other strategies to reduce the non-specific interactions can therefore be preferred like loading blocking agent in the sample pad or the conjugate pad although this is thought to be less efficient [34].

Absorbent pad

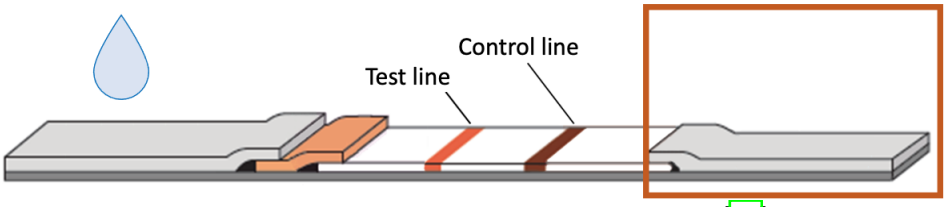

Figure 2.16: Absorbent pad, adapted from [30]

The absorbent pad, sometimes also called wicking pad, is at the same time the engine and the trash can of the strip. It is placed after the membrane to pull all the fluid so that a maximum of the labels will go through the test and control lines and ensure that the remaining labels that did not bind do not stay on the membrane which would make background noise [29]. The dimensions of the absorbent pad should be evaluated based on the volume of liquid that must pass through the membrane to ensure that a maximum of the potential analytes and nanoparticles flows through the test and control lines [31].

Materials The absorbent pad is, unless rare exceptions, not treated and the choice of material relies mainly on the cost and on the absorptive capacity. Cotton threads are attractive for LFA development because of their flexibility and wicking properties but cellulose is generally used because of its ubiquitous availability, absorptive capacity, biodegradability and patterning capabilities [31].

2.2.2 Assembly workflow of LFA

Now that we have seen the different parts of the lateral flow assay stick, we can visualize the manufacturing of the stick. As we can see on the figure 2.17, each pad is processed independently before being assembled. The conjugate pad and the sample pad are pre-treated then dried if necessary then the functionalized nanoparticles are placed on the conjugate pad and dried. For the membrane the first step is to fix the capture bioreceptors to form the test and control lines then to block the membrane if necessary. Once each pad fully dried, they are assembled on a backing card that will ensure the coherence of the whole. This assembly is sometimes called the lamination because each pad has to recover the neighboring pad (as it is shown on figure 2.16) to ensure a consistent flow. The backing card consist generally of polyvinyl chloride (PVC), polystyrene, or polyester with adhesive layer on one side. There are less requirement on the backing card because it is not involved directly in the flow, it has limited contacts with the sample. Nevertheless, the backing should be thick enough to support the different components of the stick but no too thick as it could create cutting problem, typical thickness vary from 0.2 to 0.5 mm [36]. Next, the assembled cards are cut into strips of typically 3 to 5 mm width and those strips are placed into a housing cassette. In the vast majority of the cases, the cassette is in plastic for ease and economical reason. The importance of the housing should not be under-estimated. Beside the marketing aspect, the

housing must be dimensioned to support the strip, to allow a proper fluid flow and to let apparent the control and test lines through a viewing window. Proper housing design should ensure that the overlapping between pads are pressed together to maintain contact between the different pads but not too tight as it could have deleterious effects on the sample flow [36]. Similarly a dimension problem that would let a gap between the sample pad and the housing could result in the sample running across and pool inside the housing. The depth of the well and the internal dimensions of the housing have to be determined to allow full contact without completely crushing the sample pad which could limit the rate of sample absorption [31] . Last but not least the housing should prevent any compression of the absorbent pad which could induce flowing in the wrong direction leading to a false positive outcome [36].

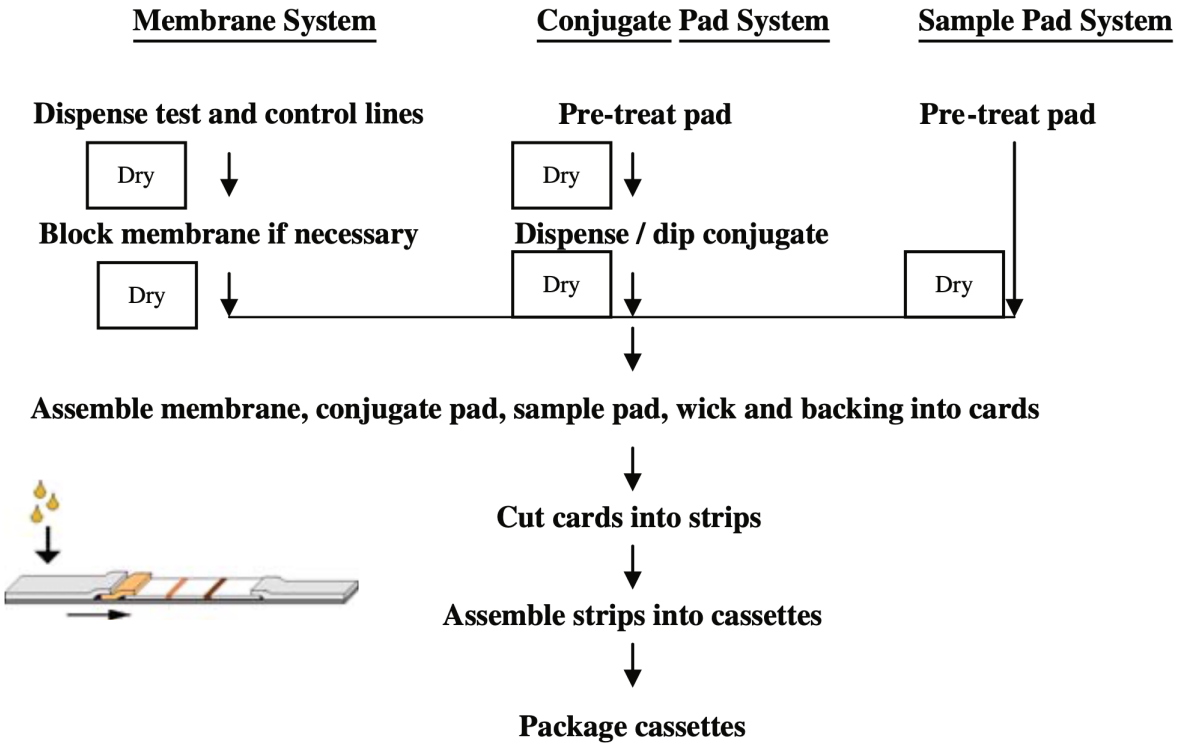

Figure 2.17: Manufacture workflow of lateral flow assay stick, image from[31]

Finally, the cassette is generally placed into a sealed bag, protected from light, with desiccant and sometimes other material required to run the test for the specific application of the LFA [31]. As the ambient conditions during the manufacturing process can impact the sensitivity of the test, attention should be given. Optimal conditions for the binding of bioreceptors to the nitrocellulose membrane are 25–50% relative humidity at room temperature and once bound, 20% relative humidity prior to packaging is preferred [22] .

2.2.3 Bioreceptors

The bioreceptors are at the very heart of the lateral flow assay, if the bioreceptors are not meticulously selected for the specific application, no amount of optimization will be able to overcome this inherent defect [31]. Good bioreceptors need [31] [29]:

- To be stable i.e. keep its structure and functionality in various environments (different temperatures, humidity percentages and pressures), and, above all, after drying
- To have fast association kinetics
- To have strong binding affinity for the target molecules
- To have low binding affinity for other molecule to avoid non specific binding
- To be able to be attached on the membrane or on the nanoparticles without loosing its binding affinity for target molecules

Moreover, concerns about the variability, the ease of production/supply and the cost may arise. The bioreceptors can indeed represent a big part of the total cost of the device [22]. For the conjugation with the nanoparticle, the chemistry process and the concentration needs to be adapted to the different kind of detection bioreceptors and nanoparticles. For the capture bioreceptor there are two main ways to display them into the membrane to form the control and test line: via contact or non contact. Non-contact method such as with air jet are preferred because there is no risk of damaging the membrane. [36] There are also different drying methods, forced air oven at elevated temperature, ambient drying conditions or drying under vacuum. Vacuum drying promotes a more uniform drying of the capture bioreceptors and is to be preferred if heating can impact the activity of the bioreceptor. Nonetheless it is difficult to upscale for industrial production [31]. Another parameter that can be optimized is the capture bioreceptor concentration at the test and control lines. Intuitively, the more concentrated the bioreceptors are, the more nanoparticles can bind achieving an higher signal. Excess amount of bioreceptors can however increase the steric hindrance effect which may decrease the binding efficacy [32] [29]. The concentration of bioreceptor can also be optimised for the functionalization, the conjugation to the nanoparticle as we will see after the presentation of three possible bioreceptors.

Antibodies

Antibodies, also known as an immunoglobulins, are large (about 150 kDa for IgG antibodies [39]) proteins produced by lymphocyte B cells from the immune system that aim at identifying and neutralizing foreign objects [40]. Antibodies possess detection regions (i.e. paratopes) that bind specifically to epitopes detecting antigens. LFA took advantage of this affinity and specificity in early development [36]. Indeed antibodies are commonly used and lateral flow assay using these are sometimes called lateral flow immunoassay.

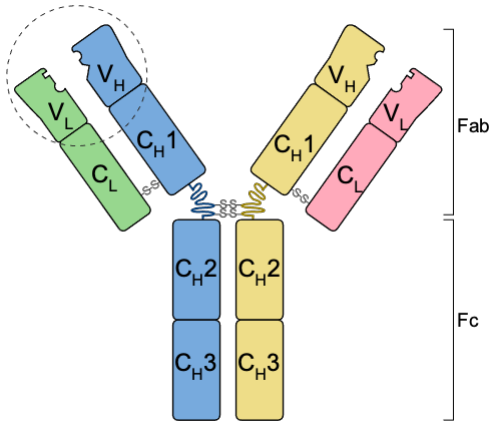

Figure 2.18: Scheme of a antibody structure, Fab: antigen-binding fragments ,Fc: crystallisable fragment, image from[40]

We can see on the figure 2.18 a scheme of antibody valid for IgG, IgD and IgE. It is composed by 2 heavy chains in blue and yellow and by 2 light chains in pink and green linked by a disulfide bridge. The dotted circle shows the paratope. Two way to obtain antibody are possible resulting in 2 types of antibodies: mono- and poly-clonal antibodies. Antigen-binding fragments of antibody can also be used because they show less non specific binding but the downside is that they are less stable [29].

Polyclonal antibodies Polyclonal antibodies are produced by initially injecting an animal with an antigen followed by a series of boosts, typically at 3–6 week intervals [31]. Its immune system will produce a range of different antibodies that bind to different epitopes of the antigen that are collected from the plasma [36]. It requires to dispose from the antigen but it is an easier process than to obtain monoclonal antibodies. In a typical polyclonal antibody preparation, only 0.2–2% of the total anti- body are directed against the antigen of interest. The rest are not specific for the target antigen and can compete with the specific antibodies during the conjugation or the attachment on the membrane. This is why a purification step is required [31]. Polyclonal antibodies are cheaper than monoclonal ones but also less specific and show bigger variation between different batches [29].

Monoclonal antibodies Monoclonal antibodies are produced by fusing a specific type of antibody-producing cell with a myeloma cell to create a hybridoma cell line that grow indefinitely in culture and produces identical antibodies that bind to a single specific epitope on an antigen [36]. This process is challenging so that it leads to higher cost (about 10 to 20 times) than polyclonal antibodies but monoclonal antibodies have higher specificity and are less prone to variation between different batches [29].

Aptamers

Aptamers are artificial, short, single stranded oligonucleotides (RNA or DNA) with molecular weight ranging 10 and 30 kDa that can adopt specific three-dimensional conformations to combine with target analyte [41]. The aptamers are sometimes called chemical antibodies because of the similarity reached in terms of sensitivity and specificity. Aptamers are produced with the SELEX (systematic evolution of ligands exponential enrichment) process described on figure 2.19.

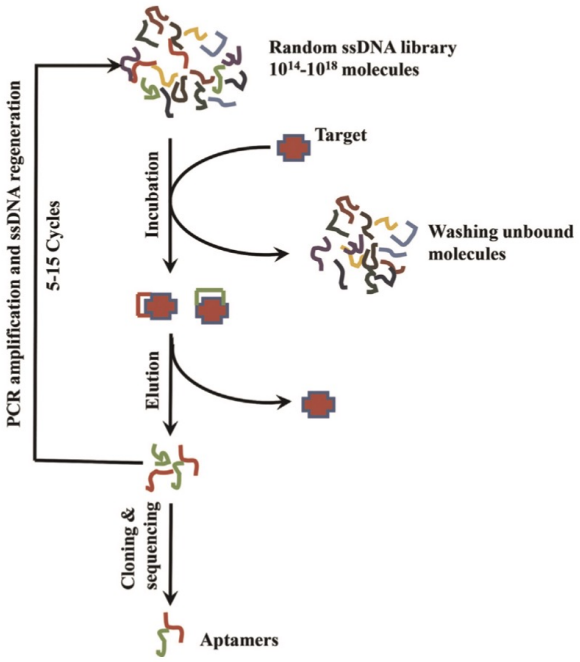

Figure 2.19: Scheme of the SELEX process, image from [42]

The SELEX process comprises 5 big steps [42]:

1. Incubation of the interest target with the random DNA library
2. Isolation of the DNA that binds to the target
3. DNA amplification by polymerase chain reaction (PCR)
4. Preparation of single-stranded DNAs for the next-round library (repeat those 4 steps for 5–15 cycles involving interval counter screening with non-target substances to remove nonspecific ssDNAs)
5. Finally cloning and sequencing of the enriched library

This artificial synthesis is not straightforward, indeed, many researchers found it inefficient to obtain a good aptamer with high specificity and sensitivity, especially for small-molecule targets that have few sites for aptamer binding or immobilization before SELEX [42]. Nevertheless, it allows to target specific molecule, even some that are to small to bind to antibodies or that do not trigger immune reaction. Compared to the conventional antibodies, aptamers possess several other advantages: they are generally cheaper, do not require animals exploitation, have higher stability (only in dehydrated form) and lower batch-to-batch variability [41] [42]. A big disadvantage comes however with the use of aptamers, their binding activity is highly dependent on the ionic strength of the buffer and the presence of interfering molecules in the buffer [29].

Phages proteins

Bacteriophages (or phages) are obligate intracellular viruses that infect bacteria and can have different life cycles. They major driver of horizontal gene exchange between bacteria [43]. There exists variation but we can see a representation of phage on the figure 2.20. It is composed of a capsid which contains the genome that will be injected into a bacteria. To inject the genome, bacteriophages are able to recognise and bind specifically to certain types of bacteria. Their endolysin, which mediates the disruption of host cells and the release of progeny bacteriophages, generally possesses a cellular wall-binding domain (CBD or CWBD) that attaches endolysin to the carbohydrate ligand on the surface of the cellular wall of the host bacteria [44] [45]. Those cell wall binding domain have strong affinity and high specificity toward target bacteria which makes it a promising bioreceptor for lateral flow assay. Besides, the production of bacteriophages seems to be low cost and easily transposable to mass production. On the other side, most natural bacteriophages show rather high bacteria strain specificity which can be a downside for LFA application, the bioreceptor being too specific [44].

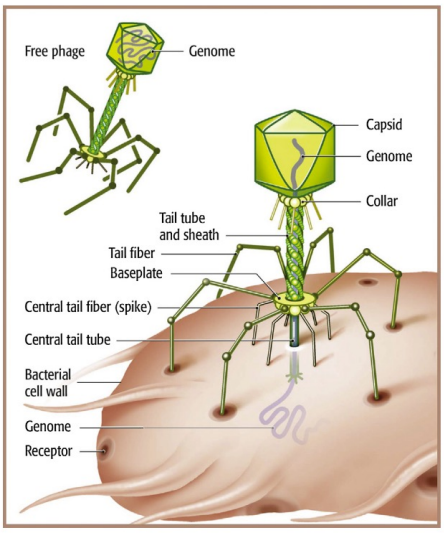

Figure 2.20: Scheme of bacteriophage, image from [43]

2.2.4 Functionalization

Functionalization is the final step in the design of nanoparticle for lateral flow assay. It will associate the detection bioreceptor to a nanoparticle and that way the nanoparticle will be able to generate a signal by binding specifically to the analyte or the capture bioreceptor at the control line. Besides the independent choice of nanoparticle and bioreceptor, the good conjugation of the 2 is crucial to achieve performing LFA and this should be taken into account in the choice of bioreceptor and nanoparticle as some conjugation are not possible with specific combination. The conjugation is generally classed into 2 kinds: Non-covalent and covalent conjugation. The non covalent conjugation relies on physical interaction such as electrostatic, hydrophilic-hydrophobic, and affinity interactions and is a spontaneous adsorption of the bioreceptor onto the nanoparticle. Non-covalent conjugation is generally simpler than covalent conjugation but has major weaknesses. It necessitates a high concentration of bioreceptor, the binding is impressed by changes in pH, the bioreceptors are randomly oriented (antibodie's paratope is not available for binding) and because the non-covalent bond is not strong as covalent, bioreceptors could be replaced by other molecules in biological samples [46] [47]. Another strategy can be to use mediator linker with high affinity such as biotin/avidin complex.

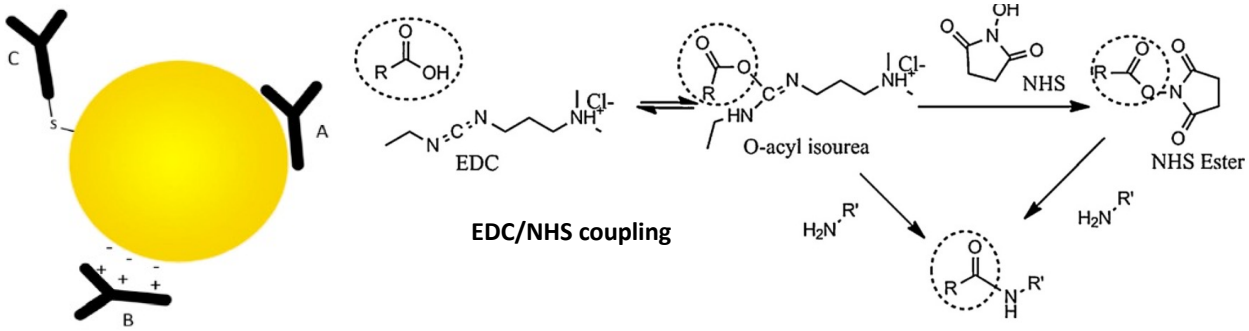

Figure 2.21: *Left:* Scheme of different interaction between antibodies and gold nanoparticle, A: hydrophobic interaction, B:ionic interaction and C covalent bond image from [46] *Right:* Scheme of carbodiimide coupling with EDC with and without NHS ester intermediate, image from [48].

The covalent binding is more complex to achieve but enables stronger attach to the nanoparticle. a lot of functional groups can be put into profit for different reactions such as carboxyl group for carbodiiminde coupling as presented on the right of the figure 2.21 but also amino, epoxide, thiol, aldehyde and alkyne/azide groups [47]. The principle of arbodiiminde coupling is, as we can see on the figure 2.21, EDC (N- ethyl N-[3-dimethylaminopropyl] carbodiimide) forms an intermediate compound with the carboxylic moiety. The activated group is reactive toward primary amines. In the case of primary amines present on the particle surface, active ester compounds (N-hydroxy-succinimide; NHS) can be used to equally form amide bonds. The covalent immobilization assembles a stronger bond and a more stable conjugate than physisorption but requires the right functional groups on the coating of the nanoparticle [46].

2.2.5 Nanoparticles in lateral flow assay

The last important component of lateral flow assay is the label that will reveal the presence of the analyte. The choice of the label is thus crucial because it will dictate the way of detection. We can see on the figure 2.22 the visual signal obtained with different types of nanoparticles. This gives a glimpse of what is possible but the optical detection is not the only one as we will see.

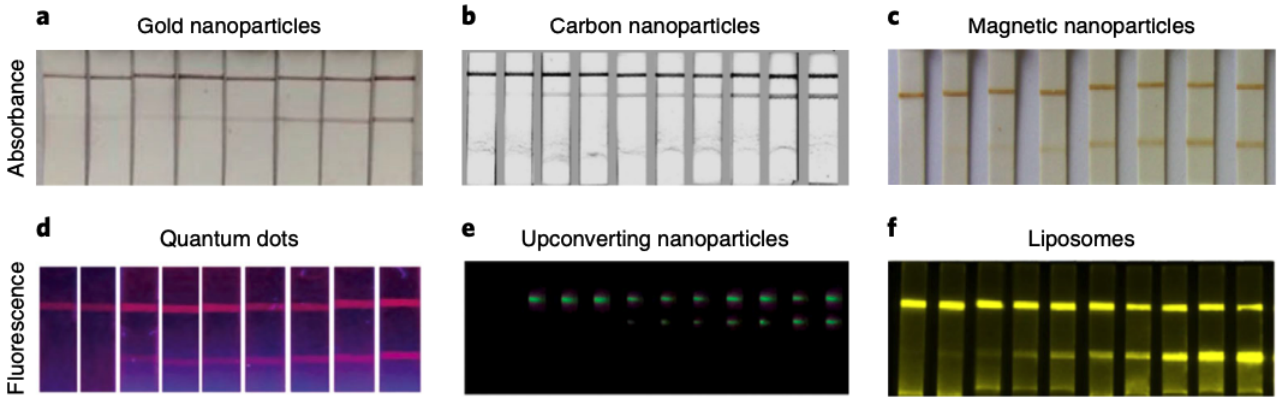

Figure 2.22: Signal produced by different types of labels. The images are taken from different articles that do not detect the same analyte with the same concentrations so this can not be used to comparate quantitatively the resulsts. Image from [29]

For decades, gold nanoparticles were used for optical detection but, as we will see, due to some limitations linked to gold nanoparticles other alternatives have emerged. For the choice of the label several parameters are to be taken into considerations among which [31]:

- What type of detection are we looking for (qualitative, semi-quantitative or quantitative) ?
- Will the label be stable at the environment under which the test is manufactured, performed, and stored?
- In which context the label will be used? What are the type of analyte or detection bioreceptors ? Which limit of detection is to be reached?
- Are there simple conjugation chemistries available to conjugate the detection bioreceptors without losing their affinity and specificity?

- Is the label easily producible in quantity with low variation and at low cost ?
- Does the label require specific equipment (reader) to transduce the signal?

Depending on the importance granted to those concerns some of the nanoparticles presented here under may be more suited than others. Of course this list is not exhaustive, other labels or combination of labels are possible. Emphasis is placed on gold nanoparticles and magnetic nanoparticles due to their use in this work. You can find on table 2.7 a sum up of the characteristics of the nanoparticles introduced here after.

Nanoparticles	Advantages	Disadvantages	Detection mean
Gold (AuNP)	**1)** Well known conjugation, **2)** Strong color	**1)** Quite expensive, **2)** Quantitative and thermal detection requires expensive extra hardware	Optical and/or thermal
Latex	**1)** Versatility **2)** Generally cheaper than AuNP **3)** Resistant to chemical and physical damage	**1)** Weaker signal than AuNP **2)** Less sensitive	Optical, fluorescent or magnetic depending on the load
Carbon	**1)** High signal-to-noise ratio **2)** Cheaper than AuNPs **3)** More stable	**1)** Unspecific adsorption **2)** Weaker signal	Optical
Liposomes	**1)** Loading of multiple labels **2)** Easy conjugation	**1)** Delicate to pH and ionic strength **2)**	Optical or fluorescent depending on the load
Quantum dots	**1)** Small-sized: fast assay **2)** Strong intensity	Difficult to synthetize and conjugate	Fluorescent
Up-converting nanoparticles	**1)** No UV source necessary **2)** Strong fluorescent signal	**1)** More expensive than QDs **2)** Requires extra hardware (NIR laser)	Fluorescent
Magnetic nanoparticles	**1)** Magnetic detection more precise and sensitive than the other [49] **2)** relatively inexpensive	Sensitivity related to the size of the particles: slow assays	Optical and magnetic

Table 2.7: Sum up of the the characteristics of the nanoparticles mentionned in this work, adapted from tables in [29] and [50]

Gold nanoparticles

Gold nanoparticle (AuNP) is to date the most widely used label in commercial lateral flow assay because of its interesting properties. Colloidal gold is fairly easy and inexpensive to produce with scaleable size thanks to several synthetic methods. They have an intense red colour due to their surface plasmon resonnance (SPR), collective electron charge oscillations that are excited by light. SPR induces an absorption peak in the visible range between 510 and 550 nm which shifts to a longer wavelength with increasing particle size. Moreover, AuNP are relatively stable in liquid and dried form, have low toxicity and a large body of protocols exists in the literature for its conjugation with detection bioreceptors [31] [50] [29].

In addition to optical reading, which is a qualitative measurement and user-dependent or semi-quantitative when a optical reader (camera or scanner) device is used to take a picture and treat it [51], it is also possible to use thermal methods with AuNP. The principle behind thermal contrast amplification (TCA) is pretty straight forward. After the test is run, the captured gold nanoparticles at the test line are excited by laser irradiation and show stronger photothermal effects than the background membrane, enabling the detection of subvisual positives and allowing to reach a semi-quantitative detection [52]. The main limitations of thermal contrast techniques are the need for both a laser and an IR camera [29].

Latex beads

Latex beads were the first labels used for lateral flow assay. They were appreciated due to their versatility, they can incorporate color dyes, fluorescent dyes and paramagnetic media. But also due to their conjugation ability to detection bioreceptors including simple adsorption and covalent coupling through the amino, carboxyl, and thiol groups and their low cost [31] [32]. However they tend to have higher limit of detection in comparison to AuNP. Moreover, the range of size used to be between 100nm to 300nm and its natural tendency to aggregate after binding to the ligands could result in problematic flow in strips. Lastly, high variability from batch to batch were reported [36].

Carbon nanoparticles

Carbon nanotubes and carbon nanoparticles were used as an alternative for AuNP. Although they do not have a plasmon resonance, like AuNP, that provides a strong signal but they are strongly dark colored nanoparticles and exhibit a high contrast with the background (often white/yellowish nitrocellulose) [29]. Moreover, carbon nanotubes are easy to prepare, possess more binding sites owing to their high specific surface area, available at low cost and stable in time [32]. However, the poor biocompatibility of CNTs limits their application in LFA. Particularly, carbon nanotubes (CNTs) cannot be dissolved in aqueous solvents due to the hydrophobic property of CNTs and strong Van der Waals attractions between the nanotubes. Surface functionalisation is required to promote their dispersion in aqueous solution. Both covalent modification of the CNTs surface and adsorption of surfactants have been shown to improve their biocompatibility [53].

Liposomes

Liposomes are vesicles formed by a lipid bilayer which is able to encapsulate very high concentrations of signal generating molecules within their cores. With sizes ranging from 50nm to 800nm, they can encapsulate visual dyes, fluorescent dyes, enzymes, or electroactive compounds. Once the test run and liposomes bounded to the test and control lines, they can be lysed to release the encapsulated material leading to detection [31]. Liposomes are quite easy to functionalize as different chemically active groups can be incorporated on the lipid surface but they have 3 main drawbacks that hinder their use in LFA. First, the drying and reconstitution of liposomes is not well covered in the literature leading to difficulties incorporate them in the conjugate pad [29]. Second, the synthesis of liposomes is often a long procedure and complex technique, with difficult size-control [29]. If the protocol is not well controlled it can lead to variation from batch to batch, which can impact the sensitivity of the test [50]. Lastly, liposomes are relatively unstable and susceptible to be lysed by detergent used in the buffers [31].

Quantum dots

Quantum dots are ideal fluorescent labels and have been widely used to improve the detection sensitivity of LFA. Quantum dots are nanocrystals or semiconductor nanocrystals that may be composed of CdSe, CdS, ZnSe, InP, or InAs, or a layer of AnS or CdS on a CdSe core. When a semiconductor absorbs a photon having energy greater than its bandgap, typically by exposing the material to a UV light, an electron is promoted from the valence band into the conduction band, leaving behind a positively charged hole. Recombination of the electron and the hole produces light whose wavelength is largely determined by the size of the quantum dot [31]. The light emitted can thus be tuned by changing the elemental composition and size of the quantum dot. The quantum dots are interesting as label for lateral flow assay due to their narrow emission spectra, high fluorescent quantum yields, their ease to be conjugated to detection bioreceptors, their good stability and higher resistance to photo-bleaching, lose of fluorescent properties, than organic dyes [29] [32]. These properties enable them to be detected and quantified sensitively with the use of an fluorescent reader. Moreover, the assays are as fast as with AuNP, regardless the time that fluorimetric analysis could take [50]. However, their elemental composition may be toxic, their cost is generally higher than AuNP and a UV lamp is required for excitation. The toxicity however could be overcome by the introduction of new carbon based quantum dots [54].

Upconverting phosphore nanoparticles (UCNPs)

Phosphorescence is the luminescence produced by certain substances after absorbing energy. It is distinguished from fluorescence in that the decay time of emission of phosphorescence light is longer (10^4 to 10^2 s) than the decay time of fluorescence emission. This implies that light emission continues even after the radiation causing the excitation has ceased [31]. Upconversion nanoparticles (UCNPs) can convert near-infrared (NIR) excitation into visible emissions, thus allowing great advances when used as signal reporters (e.g., avoiding background fluorescence (which can occur when illuminated with UV light), increasing photostability and improving signal-to-noise ratio and sensitivity in complex biological samples) [55]. Their strong emission in the visible region produces more-sensitive LFA than those obtained using QDs. However, the need for an expensive and bulky near-IR laser is not appropriate for many PoC applications, thus limiting the integration of UCNPs in LFA [29].

Magnetic and superparamagnetic nanoparticles (MNPs)

As we can see on the figure 2.23 here under, materials can be classed in 5 types depending on their reaction to an exposition to an external magnetic field: diamagnetic, paramagnetic, ferromagnetic, ferrimagnetic and antiferromagnetic. Diamagnetic are materials that do not show a residual magnetic field but when exposed to an external magnetic field, weak dipoles arise and oppose the external field. Paramagnetic material show randomly oriented dipoles due to the presence of unpaired dipoles, resulting in total null magnetic field. Those dipoles can be oriented under the influence of a external magnetic field, resulting in a non-zero magnetic field. Ferromagnetic materials are composed of oriented magnetic dipoles resulting in permanent magnetisation. In ferrimagnetic magnetic material dipoles of different amplitude point in opposite direction resulting, as in ferromagnetic material, in a remanent magnetic field. Lastly, antiferromagnetic materials contains anti-parallel dipoles of same amplitude resulting in a null global magnetic field. The magnetic properties of nano- and micron-sized magnetic materials may differ from those of the corresponding bulk magnetic materials. Indeed for sufficiently small particles, the particle becomes monodomain resulting in a behavior comparable to the paramagnetic materials, this is called superparamagnetism. For most magnetic materials, the single domain size usually falls in the range of 10–50 nm and is related with their intrinsic properties (such as magnetization saturation, magnetic anisotropy constant, and the exchange stiffness) [47] [56]. Superparamagnetic material is a material of choice in the framework of LFA because they do not present remanent magnetic field which prevents aggregation and precipitation and have high magnetic moment under exposure to an external magnetic field which is an important property to measure the quantity of particles with an external reader [32].

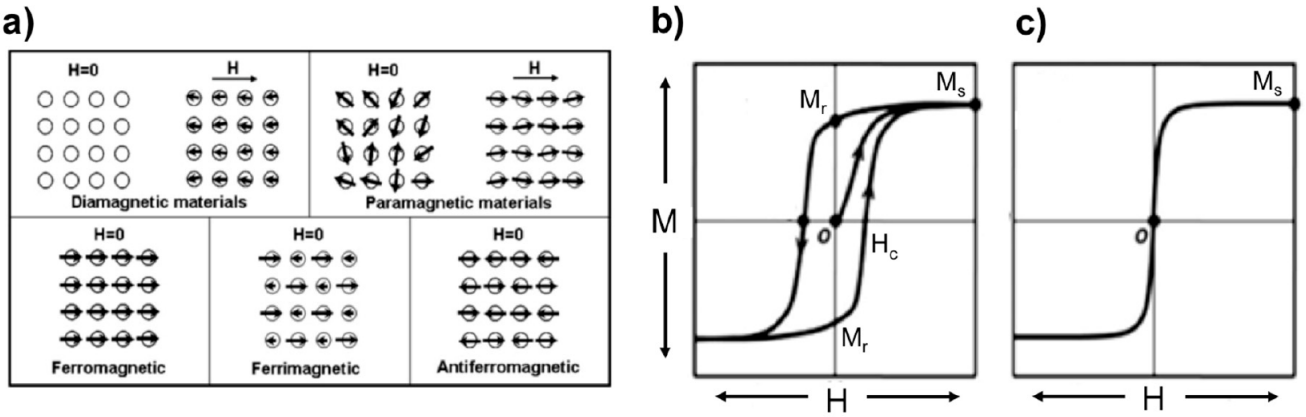

Figure 2.23: a) 5 types of magentic materials b) hysteresis curve of a magnetic material with H being the applied magnetic field, M the magnetisation, Mr the remanent magnetisation, Ms the saturation magnetization c) magnetisation curve of a superparamagnetic material, note the absence of hysteresis [47]

There are several magnetic material that can be used for LFA among which, iron oxide , such as magnetite (Fe_3O_4), maghemite (γ-Fe_2O_3) and hematite (α-Fe_2O_3)., metallic magnetic particles either monometallic (e.g., Fe, Co, or Ni) or bimetallic (e.g., FePt and FeCo), dopped metallic oxide,... . Metallic nanoparticles are generally less stable, more prone to oxidise and show higher

toxicity [47]. Because of their high saturation magnetisation, high magnetic susceptibility and chemical stability iron oxide nanoparticles are broadly used [56]. We will focus in this work on magnetite (Fe_3O_4) and maghemite (γ-Fe_2O_3).

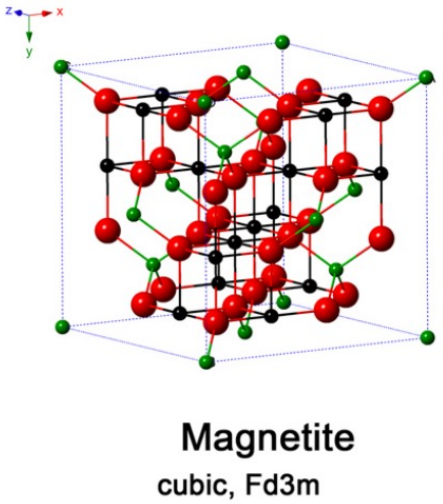

Figure 2.24: Crystal structure of magnetite (Fe_3O_4), image from [57]

Magnetite is also often deduced as iron (III) oxide due to its possession of ferric (Fe^{3+}) and ferrous (Fe^{2+}) iron elements. Maghemite (γ-Fe_2O_3) is a phase that is formed upon the oxidation of magnetite (Fe_3O_4). We can see on figure 2.24, the cristal structure of magnetite: the green balls are ferric ions, the red balls are oxygen and the black balls are ferrous ions. Bulk magnetite has ferrimagnetic properties but bellow a certain size (20-50 nm), nanoparticles exhibit superparamagnetic behavior [56] [47].

MNPs are versatile labels for LFAs, since they provide both an optical and a magnetic signal. Iron oxide nanoparticles are well-known and there are several possible ways to synthesize them, as we will quickly see, to coat them and to functionalize them with capture bioreceptors. Aside from magnetic detection, their magnetic properties can also be put into profit for easier functionalization (e.g. removing unbound bioreceptors without the need of centrifugation) [29]. These iron oxide colloids can be coated, enabling adsorption or covalent linking of capture bioreceptors. The conjugated nanoparticles particles can be used in lateral flow assays in the same way as latex or colloidal gold conjugates. The magnetic detection, which requires a device to generate a magnetic field and measure the magnetic response, enables quantitative detection. Moreover, it can achieve high signal to noise ratio. Firstly because the magnetic material does not exist usually in the environment or in the tested samples [32] whereas optical measurement of analytes in biological fluids can be difficult due to interfering substances, specular reflection, scattering, self-absorption, and quenching of signal (in fluorescence-based tests) [31]. Secondly because measuring the magnetic field allows for the use of all the labels accumulated on the analytical region [29]. Indeed, in a "conventional" LFA, the test and control lines are detected visually or by an optical instrument that measures reflectance, contrast, color change, thermal contrast or fluorescence. Such observations of the accumulation of particles at the test and control lines measure at most the top 10 μm of the substrate membrane [31].

We can see on the figure 2.25 the zones on the membrane where the nanoparticles detected visually can contribute to the signal. The nanoparticles on the bottom are generally non accessible because of the backing. To give an order of magnitude, on a CN95 membrane from Satorius which has a thickness of 240μm, optically we have access to 10μm i.e. about 4% of the nanoparticles at the test and control lines (if we assume a uniform distribution along the height) are used to induce the signal.

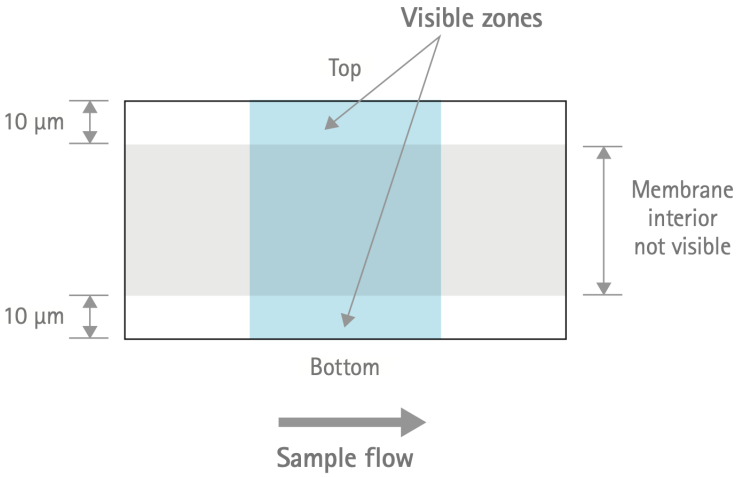

Figure 2.25: Zones generating optical signal, image from [34]

As we will see bellow, some type of magnetic reader are able to determine the amount of magnetic particles in the entire depth of the analytical zone of the membrane, which is beneficial because the strength of the magnetic signal increases directly with the mass of the magnetic label [31].

Magnetic readers There exist several methods to produce and/or measure a signal using MNPs but some are not transposable to LFA context due to their cost or the heavy or bulky equipment required e.g. Superconducting Quantum Interference Device (SQUID) which require cryogenics [47]. We will quickly discuss here the magnetic assay reader (MAR), Giant Magnetoresistance (GMR) and tunneling magnetoresistance (TMR). Commercial Magnetic assay readers (MARs), developed by Magna Biosciences LLC, generate a magnetic field as we can see on the figure 2.26. It excites the MNPs that simultaneously will produce their own magnetic field, detectable using the sensing coils of the device. With the use of MARs, wide working ranges, high selectivity, robust assays, good sensitivity and lower limits of detection than standard AuNPs LFAs were obtained [50]. Assays with MARs demonstrated that the intensity of the signal increase with the size (although this can impact the flow, bigger nanoparticles are slower) and the amount of MNPs [50]. Besides the reader model of MAR, another detection strategy is to measure magnetization saturation generated by magnetic nanoparticless (NPs) through magnetic sensors. It is the idea behind the giant magnetoresistance (GMR). GMR signaling is produced when the electrical resistance of the sensor is reduced by the effect of an external magnetic field derived from the MNPs [49] [50].With GMR, Ryu et al. detected a cardiac marker with a sensitivity of 0.01ng/mL [58] Last but not least, tunneling magnetoresistance (TMR) sensors are based, as their name indicates, on the tunnel magnetoresistance of a magnetic tunnel junction. It consists of a sandwich of two magnetic layers separated by an insulating layer (commonly MgO). TMR sensors offer a higher magnetoresistance ratio compared to GMR sensors and might provide higher sensitivity at low magnetic fields[47].

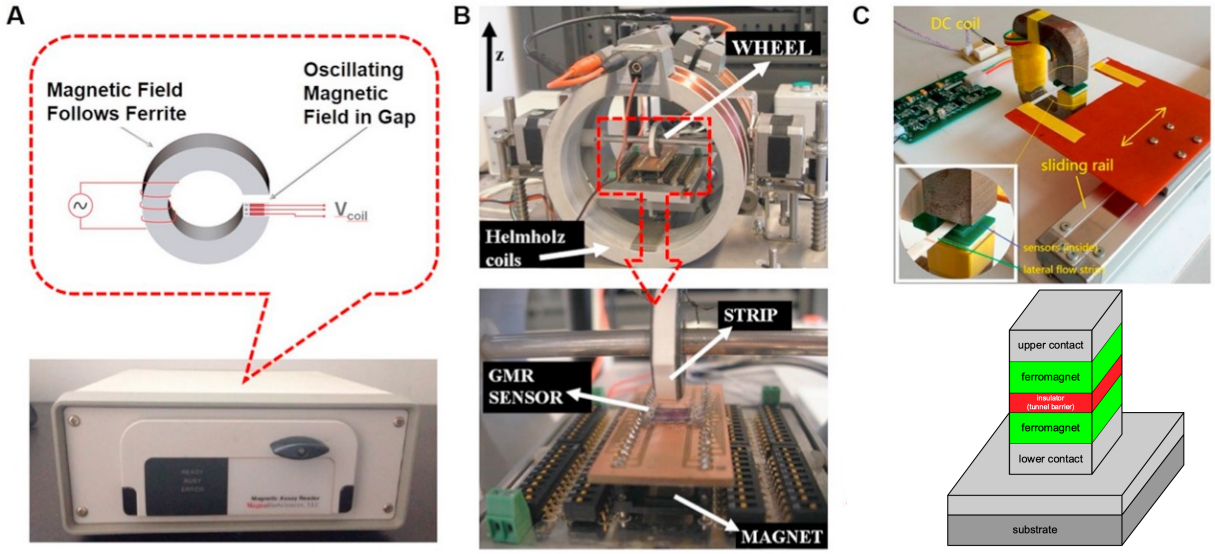

Figure 2.26: Depiction of 3 types of magnetic reader devices: A) Magnetic assay reader (MAR), B) Giant magnetoresistance (GMR) and C) Tunneling magnetoresistance(TMR), image from [49] and [59]

The above mentioned detection devices come with limitations. Indeed, MAR is not able to detect positioning and required manual correction of position. In the GMR method, the structure of the test strips may be damaged when placed on the detection wheel. The TMR sensor is bulky and the distance between the two side-by-side sensor chips is about 1 cm; thus, it was not capable of detecting multiple test lines simultaneously [49]. Moreover none of these device is designed to be transported on site, losing a big advantage of lateral flow assay. Miniaturization of those devices or the design of other is required to use LFAs to their entire potential. Last but not least, although the device is normally not heavily influenced by other magnetic material than the MNPs, electromagnetic interference from the external environment should be taken into account [49].

Synthesis of MNP As said previously, iron oxide nanoparticles are well-known and there are several methods mastered to synthesise them. A good synthesis process should be able, to result in size controlled NPs with a narrow distribution for a relatively low cost and short time while maximizing the amount of magnetite as the signal relies on it (some techniques uses core of other material or bulky coating). There are 2 main approach to obtain: top down, size reduction to nanometer range and dispersing solid phase, and bottom-up , condensation of precursors, approach. Generally, it is more difficult to design and control the process to produce the desired particle size and shape with top-down approach [60] [57]. You can find on table 2.8 a quick summary of the specificity of some bottom-up synthesis procedures.

Method	Achievable size[nm]	Size distribution	Shape control	Reaction (Difficulty and time)
Co-precipitation	4-43	Relatively narrow	Not good	Very simple, minutes
Thermal decomposition	1-150	Narrow	Very good	Simple, hours-days
Micro emulsion	2-200	Narrow	Good	Complicated, hours
Sonolysis	20-50	Narrow	Bad	Simple, minutes
Green method (Biosynthesis)	4-40	Broad	Bad	Complicated, hours-days

Table 2.8: Characteristics of different synthesis methods for iron oxide nanoparticle, based on information found in [47], [56] and [60].

2.2.6 Optimisation of LFA

Beside the milestones in the design of a lateral flow assay previously described that are important to optimize in order to reach a better sensitivity, there are possibilities to tune some parameters or add new features to the LFA to improve the results achievable. Some techniques encountered in the literature are rapidly exposed here under.

2.2.6.1 Influence on the flow

As the flow speed have a determinant impact on the sensitivity some manipulations to impact the flow were tempted. The goal here is to slow down the flow in order to increase recognition time which contributes to improved sensitivity. To this end Alam and al. in [61] added a hydrolyzed polyvinyl alcohol (PVA) dam into the nitrocellulose membrane before the test line zone as we can see on the figure 2.27. When the aqueous sample reach the PVA dam it will gradually dissolve it. At the end of the assay, the PVA dam will be totally dissolved but we would have slower the flow enough to increase the sensitivity. Using this PVA dam Alam and al. obtain a 20-fold sensitivity improvement.

In the same idea, Rivas and al. in [62] printed wax pillar into the nitrocellulose as we can see on the right part of the figure 2.27. These pillars act as obstacles delaying the regular flow on the strip and as for PVA dam it let more binding time between the analyte and the labeled antibody and therefore allowing an effective formation of the immunocomplex of the sandwich assay. This modification led to a 3-fold sensitivity increase. This idea of making modification to increase the time with label and the analyte together seems quite popular as some other experiments were done that way. In '*Development a stacking pad design for enhancing the sensitivity of lateral flow immunoassay*' [63] Tsai and al. add a stacking pad to the stick between the conjugate pad and the membrane. The stacking pad were tested with 3 materials: cellulose, polyester and glass fiber. They obtain a 2 fold improvement of the sensitivity because the stacking pad allow to extend the analyte/detection bioreceptor interactions.

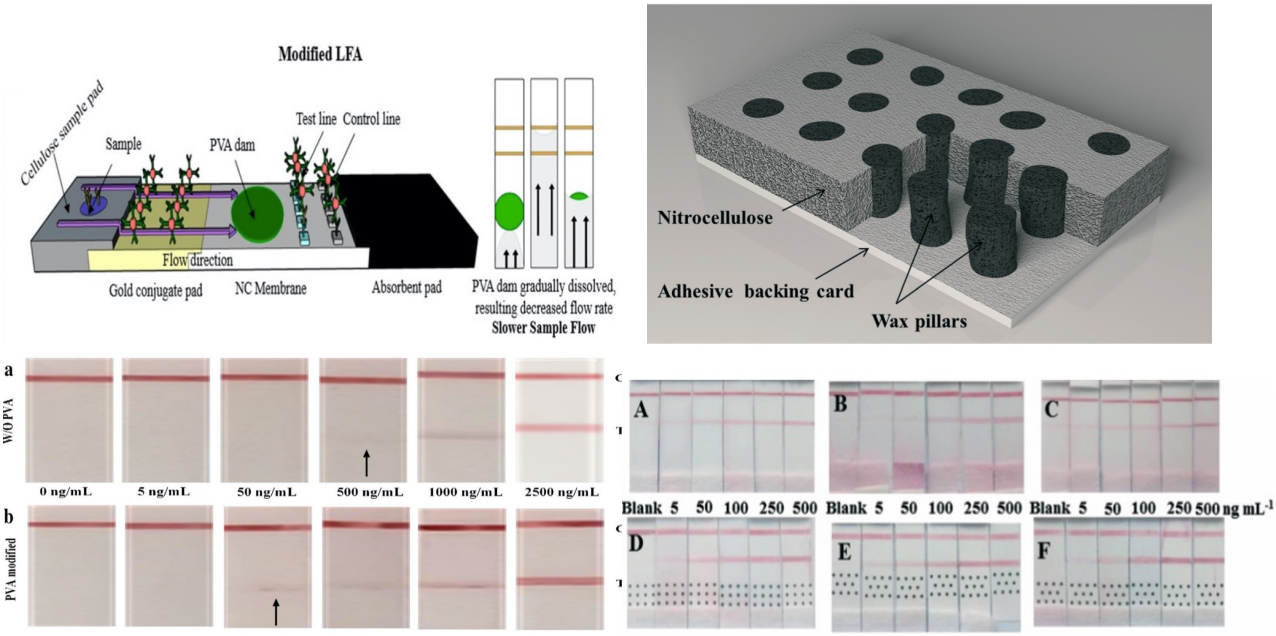

Figure 2.27: *Left:* Scheme of the LFA with PVA dam and result of the test, image from [61]. *Right:* Scheme of the wax pillar and result of the tests done with different configuration of wax pillars, image from [62]

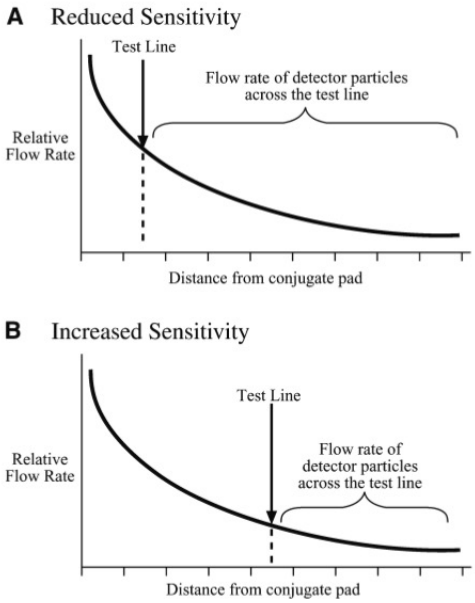

Another parameter related to the flow speed of the sample and which does not require change in the design is the emplacement of the test and control line. Indeed as we can see on the figure 2.28 the relative flow speed (flow speed of the sample) decreases as the distance from the conjugate pad increases. Placing the test line further can therefore lead to a better sensitivity as there is more time for the binding between the capture bioreceptor and the analyte.

Figure 2.28: Flow rate in function of the distance on the membrane, image from [36]

2.2.6.2 Use of a reader

Beside the increasing of the sensitivity of the stick itself it is possible to use some tools to better assess the outcome of a lateral flow assay. In '*Development of a smartphone-based lateral-flow imaging system using machine-learning classifiers for detection of Salmonella spp.*'[64] Min and al. took with a smartphone standardized pictures of LFA after test. Those photo were processed and used to train several machine learning algorithms (support vector machine (SVM), K-nearest neigh-

bor weighted and unweighted (KNN) and a decision tree). The SVM and weighted KNN reached accuracy of 95.56% and provide a better and consistent interpretation. Besides the interpretation, machine-learning classification improved sensitivity near the limit of detection, compared to visual inspection. With a likewise approach LFA lose a bit of its friendliness to the end user because it add steps: taking the picture in the small smartphone support they designed but it let no place for interpretation when the result is not clear enough. Beside, the smartphone could then be use to transmit the outcome of the test automatically which would be a step toward the real-time connectivity of the device.

Chapter 3

Objectives

In order to overcome the quantification problem inherent to an optically based lateral flow assay and, in the bigger frame, to achieve an ASSURED (Affordable, Sensitive, Specific, User-friendly, Rapid and robust, Equipment-free (or simple), and Deliverable to end-users) [8] water quality monitoring device, the lab would like to switch from gold nanoparticles to a magnetic nanoparticles based LFA. Those magnetic nanoparticles should be detectable by a magnetic reader which could lower the limit of detection (LOD) and achieve quantitative measurements.

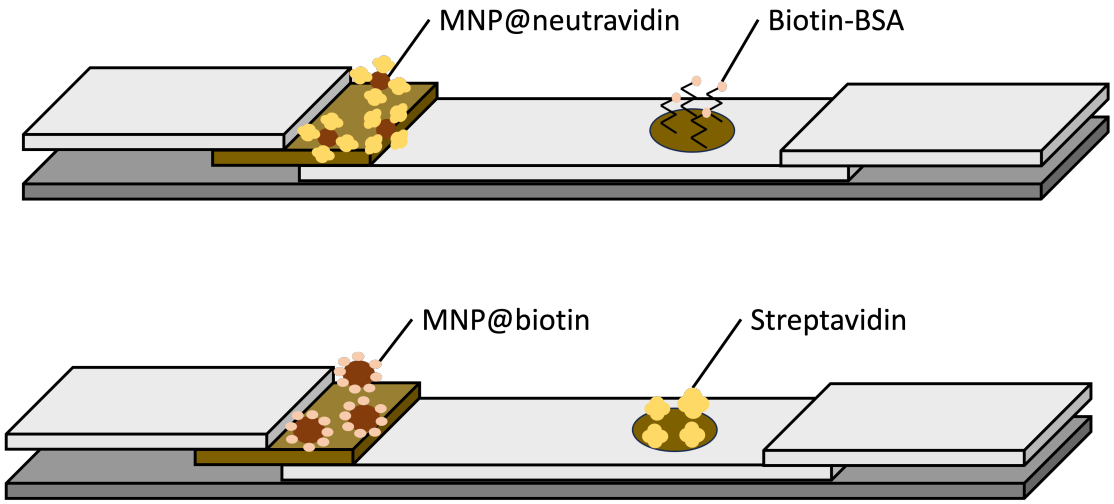

Figure 3.1: Scheme of the lateral flow assay prototypes with Neutravidin coated nanoparticles (up) and biotin coated nanoparticles (down)

My purpose is to design a lateral flow prototype using commercial functionalized iron oxide particles. It will not be used to detect an analyte in solution, hence the absence of a test line, but will be used to test and assess the performances of a magnetic reader which will be developed later. For the detection and capture receptors the complex biotin/avidin will be used because of the high affinity and specificity between those two molecules. Two types of iron oxide nanoparticles with different coating and size will be used, the first one is Neutravidin coated magnetic (nano)particle with a diameter of 1μm and the second one is biotin coated magnetic nanoparticle with a diameter of 10nm. As we can see on the scheme on figure 3.1, the control line will thus be composed of biotin for the Neutravidin coated nanoparticles and streptavidin for the biotin coated nanoparticles (see

section 4.2.2 for the differences between avidin, streptavidin and Neutravidin).

We will proceed experimentally as explained by Parolo and al. in "Tutorial: design and fabrication of nanoparticle- based lateral-flow immunoassays" [29]. The workflow divides the lateral flow stick in several parts, the goal being to proceed step by step in order to control the number of parameters and gradually increase the complexity of the lateral flow assay. The lateral flow assay hence designed could be used to test in a situation closer to real application the magnetic reader developed in parallel.

Chapter 4

Material and methods

In this chapter the process followed to achieve the LFA prototypes and the equipment used are detailed. The first part is dedicated to the formation, where after doing the all process with Grégoire Le Brun, Richard Ekoue Kouvahey and I tried on our own to adapt the protocol for 40 nm AuNP. Then elements to achieve the MNP based LFA prototypes are exposed and finally different techniques used to characterize the magnetic nanoparticles are explained.

4.1 Training on LFA with gold nanoparticles

The process to obtain a working LFA was mastered by Grégoire inside the lab. Richard and I followed a training with him in order to familiar ourselves with known LFA and discover the whole process, including functionalization of the NPs, an important step that I will not do with MNPs hence there were bought already functionalized. Beside familiarising with the process and the equipment, the goal of this formation is to adapt the process to use 40 nm diameter citrate coated AuNPs commercialised by Unisensor instead of the 20 nm previously used that were synthesized by Turketich method by Grégoire. The workflow to achieve LFA prototype follows the procedure described in "Tutorial: design and fabrication of nanoparticle-based lateral-flow immunoassays" by Parolo and al [29]. We can see on figure 4.1 a depiction of the LFA obtained by Parolo and al. Sample containing human IgG, the target analyte, is poured onto sample pad. It will flow through the conjugate pad where anti-human IgG antibody coated AuNPs in a conjugate pad buffer (see table 4.1 for composition) were previously dried. The sample then continue flowing through the membrane previously stripped with goat anti-human IgG antibodies (for the test line) and chicken anti-goat IgG antibodies (for the control line) and the flow ends in the absorbent pad.

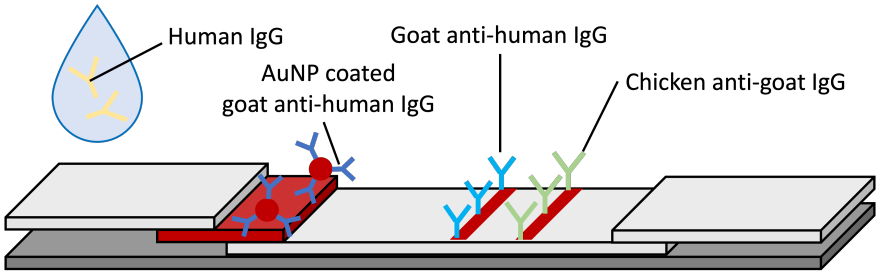

Figure 4.1: Scheme of LFA detecting Human IgG as manufacture by Parolo and al. in [29]

In our version, we used human IgG as target analyte and capture bioreceptor at the control line. Polyclonal goat anti-human IgG (Sigma aldrich I1886) as detection bioreceptor and capture bioreceptor at the test line.For the LFA stick we used cellulose (CFSP001700 EMD Milipore) for sample and absorbent pad, glass fiber (Merck Milipore GFDX001000) for conjugate pad and nitrocellulose membrane (CN95 from Satorius) for the membrane. We can see on figure 4.2 the big steps of the process.

The **gold aggregation test (GAT)** is to be done only once to determine the best concentration of detection bioreceptors to conjugate with the AuNPs. The conjugation is done with different solution of pH and antibodies concentration, then NaCl at 10% (wt/vol) is added to induce aggregation. Indeed the addition of salt will interfere with the repulsive charges between the gold particles, resulting in flocculation. If the surface of the colloidal gold is sufficiently covered by adsorbed molecules, the addition of high concentrations of salts will have no effect on the colloid. [65]. The spectra of the solution is measured thanks to a UV-vis spectrometer (see section 4.3.3), determining optimal conditions for the conjugation i.e. pH and antibody concentration that allowed to prevent aggregation. The spectrometer allows to detect aggregation of gold nanoparticles because they present a strong peak of absorbance (typically at 520 nm for 20 nm AuNP) that will become wider in case of aggregation.

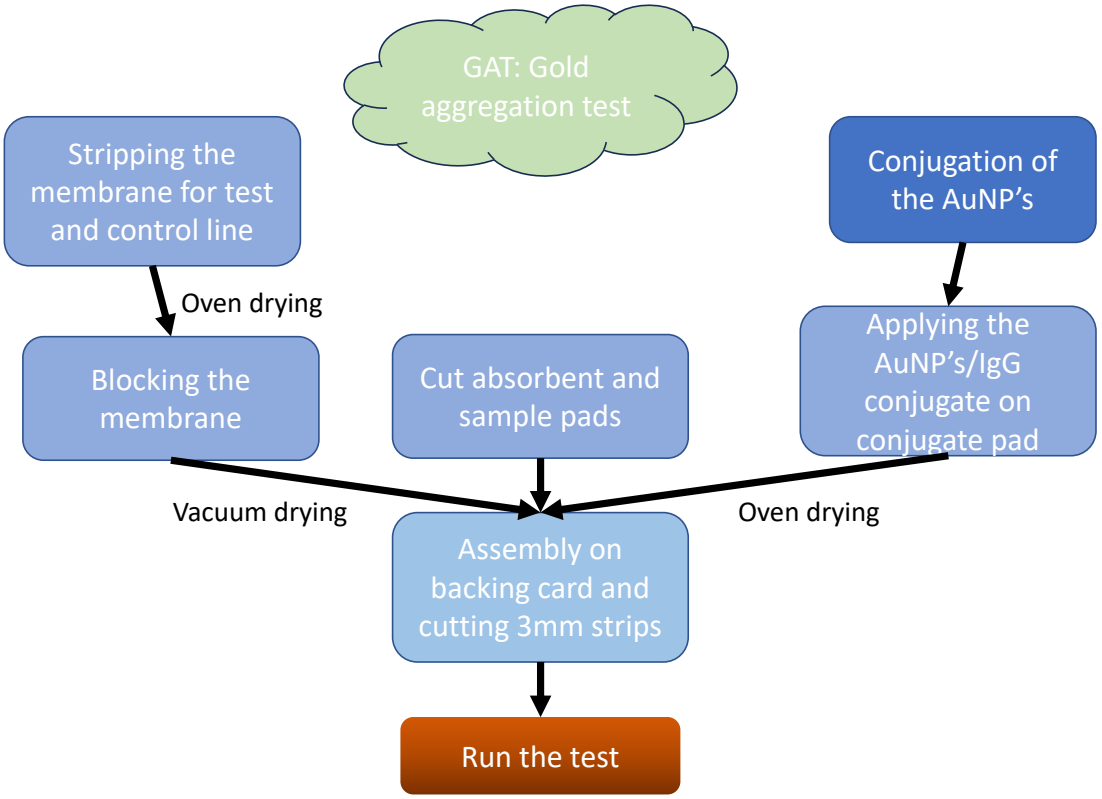

Figure 4.2: Workflow as done by Parolo and al. that was reproduced for the training

Conjugation of the AuNPs is thus done with the pH and antibody concentration defined previously i.e. the AuNPs are incubated with the defined amount of antibodies and pH for 20 min at 650 rpm at room temperature. Bovine serum albumin (BSA) can be add after to cover surface area not filled in with the antibody, to help with stability and to prevent nonspecific adsorption.

Then the solution is centrifugated 14,000 rpm for 20 min at 4 °C to segregate the nanoparticles and the media. The media is removed to withdraw the free antibodies that may interfere with the sensitivity of LFA. The conjugated AuNPs are then resuspended in conjugate pad buffer (see composition in table 4.1).

Once the conjugated nanoparticles have been obtained, they can be loaded onto the conjugated pad and dried for 2 hours in a vacuum chamber. The antibodies (1mg/mL) can be loaded on the membrane to form the **test and control lines** then dried in oven (20 to 30 minutes at 37°C) to fix the antibodies. Except once, the control and test lines were done by dropping 0.8μL with a micropipette. This results in a "control dot" more than a control line as the control line appear as a coloured round. The other pads can also be treated if needed: soak the sample pad in sample pad buffer (see composition on table 4.1) and then dry it 2 hours at 37°C. We did not treat the sample pad as this is an optional step aiming more to render the samples uniform in real applications. The membrane, after the fixation of the antibodies, can be **blocked** i.e. soaked 20 min in the blocking buffer then soaked 2 at least times in washing buffer with a gentle shake for 20 min. Finally, the membrane is dried 37 °C for 2 h.
Once all the pads fully dried, they can be **assembled** on the backing card. The membrane is first applied to be underneath, the conjugate pad is then put in place then the absorbent and sample pads are added. Each pad added must recover the neighboring pad on, at least, 3 mm in order to promote a good contact hence a good flow between the different parts. The mounted cards can finally be cut (typically 3 or 5 mm wide) and tested.

Buffer	Composition	Goal
Conjugate pad buffer	5% (wt/vol) sucrose, 1% (wt/vol) BSA and 0.5% (vol/vol) Tween-20 in PBS (0.01 M, pH 7.4).	Promote the release and flow of the conjugated AuNPs along the nitrocellulose strip.
Sample pad buffer	0.5% (wt/vol) BSA and 0.05% (vol/vol) Tween-20 in PBS (0.01 M, pH 7.4).	Control the pH, minimize the non specific binding and promote the flow
Blocking buffer	2%(wt/vol)BSA in 0.01M PBS at pH7.4	BSA covers the nitrocellulose to prevent nonspecific adsorption
Washing buffer	0.05% (wt/vol) SDS in 0.005 M PBS, pH 7.4	Remove excess BSA preventing clogging of the pores

Table 4.1: Buffer used for the training [29]. The references of all reagents used are displayed in the annexes (table A.1)

4.2 Experimental strategy to achieve MNP based LFA

To achieve a working lateral flow assay, workflows as presented in figure 4.3 have been formulated. The goal is to have an incremental strategy, starting with few components and low complexity then increase and optimize step-by-step.

The firsts steps are to chose the principal components of the LFA depending on the use context. The capture and detection bioreceptors, the mean of detection and the type of nanoparticle have to be chosen prior with respect to the target analyte. This a crucial step because if, for example, the capture bioreceptors show low affinity for the target there will be little to do to achieve a high sensitivity. The first tests with the stick are in half-stick format, consisting of only the membrane and the absorbent pad. Because the absence of sample, the tests are thus run by dipping the end of the membrane into the sample. The flow of the nanoparticles is tested and optimized iteratively and once a satisfying result is obtained another component is added (e.g. control line). As shown on figure 4.3, different components will be incorporated as the process will go on. In the end a hopefully functional full stick LFA will be obtained.

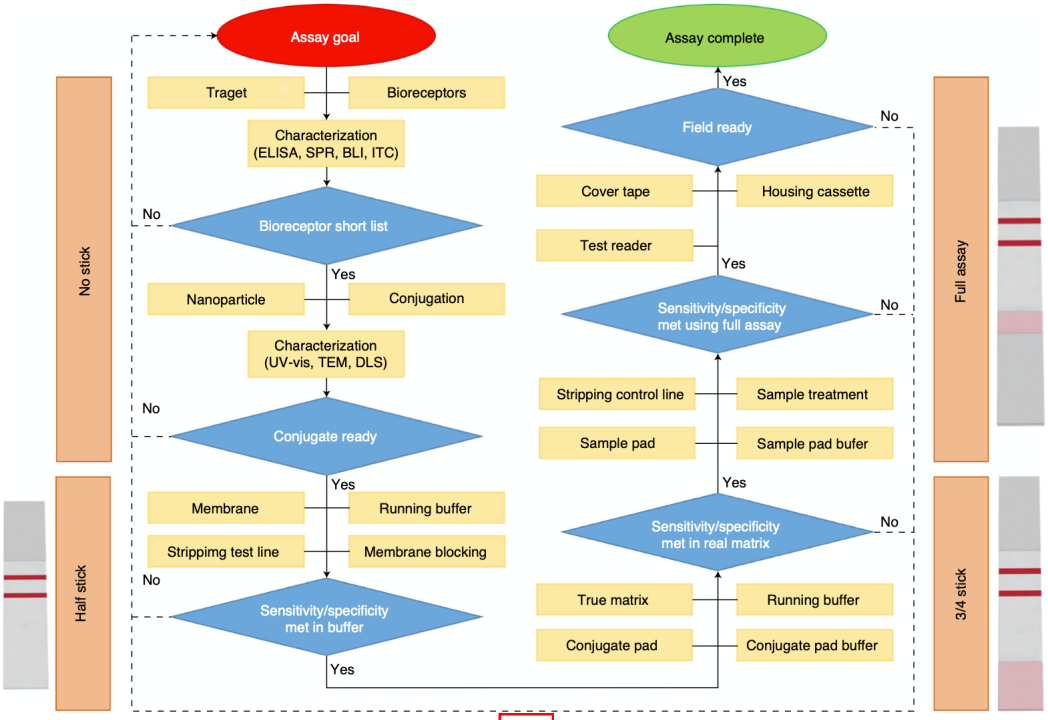

Figure 4.3: Flow chart for designing and optimizing LFA. Abbreviations: NC, nitrocellulose; NSB, nonspecific binding; RB, running buffer, image from [29]

Obviously, in this work, I won't go through all the steps depicted on the figure because the bioreceptors and functionalized nanoparticles were already chosen and my objective is to obtain a prototype and not a "field ready" assay. Which mean that the LFA obtained will not detect an analyte (so there is no need of control line), I will not consider a housing cassette, reader device, true matrix, long term preservation,...
Now that we went through the way of proceeding we will have a word on the central components used in this work.

4.2.1 Nanoparticles

In this work 2 types of iron oxide nanoparticles will be used: Neutravidin coated magnetic nanoparticle (MNP@Neutravidine) and Biotin coated magnetic nanoparticle (MNP@biotin).

The MNP@Neutravidine are the Cytiva's GE78152104010150 5mL (10 mg/mL) SpeedBeads Magnetic Neutravidin Coated particles with a diameter of 1μm. According to the packaging, the nanoparticles are suspended in 0.05% azide. After contact with the producer, it appears that they are suspended in: 50 mM Tris pH 8, with 150 mM sodium chloride, and 0.05 % sodium azide. It also includes a detergent (Tween20) at 0.1% concentration. It is presented as superparamagnetic despite its big size because of the structure of the nanoparticle [66].

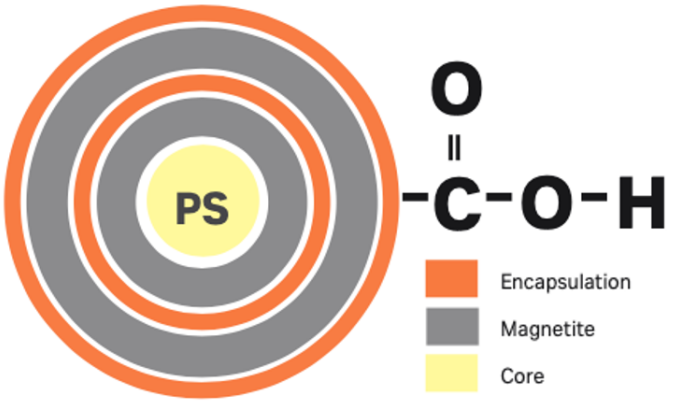

Figure 4.4: Structure of MNP@Neutravidine from [66]

As we can see on the figure 4.4, during the manufacturing process a first layer of magnetite is formed on a polystyrene core then encapsulated by polymers then a second layer of magnetite is encapsulated with carboxylated polymer. Those carboxyl groups enable a covalent coupling with NeutrAvidin during the conjugation process.

The MNP@biotin are iron oxide(II,III), biotin functionalized magnetic nanoparticles of 10 nm diameter dispersed in H_2O (1 mg/mL) 747424-1mL from Sigma-Aldrich. I have little information on those about their structure or suspension media, SEM imagery tends to confirm the size of approximatively 10nm.

Both nanoparticles visually appear quite brownish. This can rise question because the pure colloidal magnetite (Fe_3O_4) solutions are archetypally distinguished by jet-black colour. However when magnetite oxidises it gives maghemite ($\gamma-Fe_2O_3$), which is quintessentially denoted in brownish colour [56]. This brownish color is therefore due to the content of maghemite and could be influenced by the coating.

4.2.2 Bioreceptors

As we have just seen, the nanoparticles used in this work are coated with biotin and Neutravidin. It was decided to use those functionalized nanoparticles because in this way the complex biotin/avidin could be exploited. The links between avidin, stretptavidin and Neutravidin is explained here under but the 2 later are derived from avidin and keep its binding affinity for biotin. The biotin/avidin complex is well known and extensively used because of the strong affinity between those 2 molecules. Indeed with a dissociation constant (Kd) of 10^{-15} M, it is the strongest known non-covalent interaction between a protein and ligand. The binding between biotin and avidin is very rapid and difficult to unbound. Moreover, the biotin, also known as Vitamin B7, whose

chemical structure is displayed in figure 4.5, is a quite small molecule (244.3 Daltons) that can be conjugated to many proteins and other molecules without significantly altering their biological activity [67]. Biotin is thus ideal to be used as a tag in numerous applications.

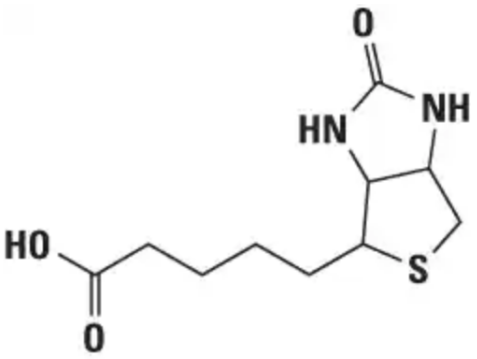

Figure 4.5: Chemical structure of biotin, image from [67]

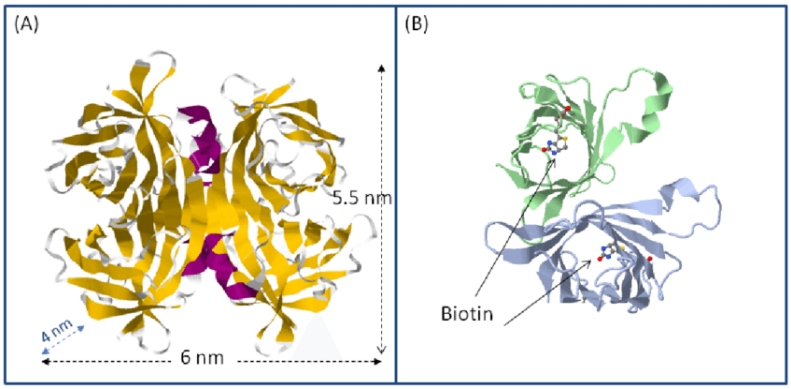

Figure 4.6: (A) Three dimensional structure of Neutravidin (B) Two subunits of the Neutravidin showing the binding pockets with the biotin molecules from [68]

Avidin Avidin/biotin has a dissociation constant of about 10^{-15} M. Avidin is a tetrameric protein with four biotin-binding sites which can be readily isolated from hen egg white at relatively low cost. Chicken avidin has a mass of 67-68 kiloDaltons [67]. Besides the high affinity to biotin, avidin has a big limitation. Because it is highly glycosylated, with about 10 % of its total mass being carbohydrate, contributing to its basic isoelectric point (pI) of 10-10.5, the avidin has a low specificity for biotin leading to non specific binding i.e. binding with other reagents than biotin [69]. Research has thus been done to obtain a molecule which keeps the affinity for biotin but grants better specificity.

Streptavidin Streptavidin is a 60 kDa tetrameric biotin-binding protein that is isolated from Streptomyces avidinii bacteria. While Avidin and Streptavidin have very little amino acid homology, their structures are very similar which grant a similar affinity towards biotin [67]. Moreover streptavidin is not glycosylated and has a relatively neutral isoelectric point (pI 5–6). It shows higher specificity although it is not entirely free of non-specific interactions. Streptavidin has however the disadvantage of being more expensive to produce than avidin [69]. Streptavidin (S4762 Sigma-Aldrich and 189730 Merck Milipore) will be used in this work as a capture bioreceptor placed on the membrane to attach the biotin coated nanoparticles.

Neutravidin Neutravidin, whose structure is displayed on figure 4.6, is a commercial variant of avidin designed to overcome its limitations. It is a deglycosylated form of the avidin. With a mass of 60kDa it retains the high biotin-binding affinity while lowering the isoelectric point (IEP=6.3), effectively reducing the non-specific interactions [67] [69]. In this work Neutravidin will be used as detection bioreceptor and will bind to biotinylated bovine serum albumin (biotin-BSA, Sigma Aldrich A8549) bound to the membrane.

4.2.3 Lateral flow assay manufacturing

For the manufacturing of the stick, cellulose (Merck Milipore CFSP001700) was used for sample and absorbant pad, glass fiber (Merck Milipore GFDX001000) was used for conjugate pad (and in a minor extend tested for sample pad). Finally 2 nitrocellulose membrane were used : CN95 from Satorius with nominal pore size between 10 to 12μm and CN140 from Satorius with nominal pore size about 8 μm. We can see on the figure 4.7 scanning electron microscopic images of those nitrocellulose membranes made by Grégoire Le Brun in the framework of his PhD thesis [70]. He assessed the size of the pore by measuring the pores visible at the surface. We can see that the mean size matches the size given by the manufacturer but the pore size have a log normal distribution.

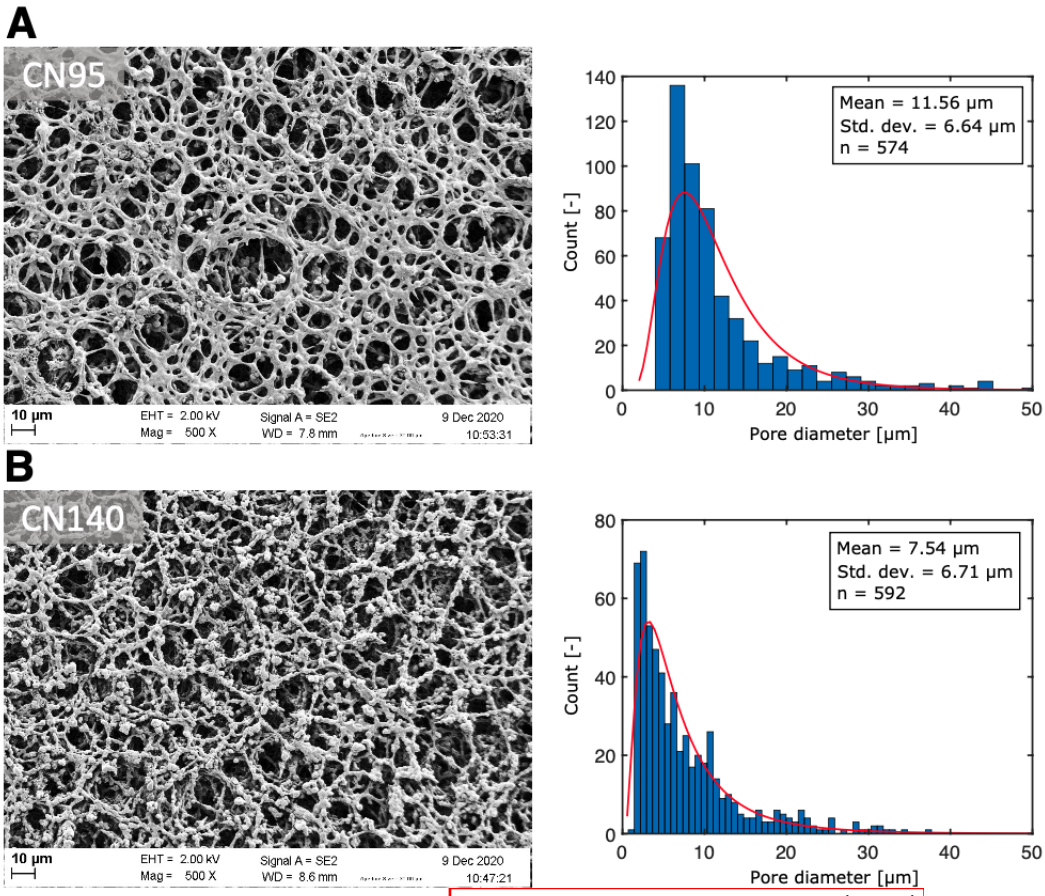

Figure 4.7: Analysis of pore size made from Scanning Electron Microscopy (SEM) image on metallized nitrocellulose, image from [70]

The manufacturing process is similar to the process followed during the training (see figure 4.2) or to the process showed in the state-of-the-art chapter (see figure 2.17), i.e., depending on the state of development and on the parameter tested, prepare the (already functionalized) nanoparticles (resolubilisation in different buffers, sonication or not,...), prepare the different pads (treatment, applying the conjugate pad buffer, applying the control line with a micropipette), once the pads dried assemble them on the backing card (Kenosha KN-PS1060.45) and cut the cards into strips. In half-stick format (only sample pad and membrane) the strips were cut with a width 3 mm

while full-stick (all the pads) were 5 mm wide. The LFAs hence manufactured were usually run immediately. A standard protocol of manufacturing full stick LFA with MNP@Neutravidine is available in the annexes A.

During the manufacturing process some equipment were used. In order to sonicate the nanoparticles, I used a bath **ultrasonic cleaner** (VWR USC200TH). Eppendorfs containing the nanoparticles in the conjugate pad buffer were partly immersed into tap water filled device and sonicated 20 minutes before applying onto the conjugate pad. The sonication or ultra sonication, refers to the application of sound energy at frequencies largely inaudible to the human ear (higher than 20 kHz), in order to facilitate the disruption of particle agglomerates through a process known as cavitation. During the process of ultrasonic disruption, sound waves propagate through the liquid medium in alternating high and low pressure cycles at frequencies typically in the 20–40 kHz range. During this alternation of low and high pressure, microscopic bubbles form and collapse producing local shock waves [71]. Aside from the ultrasonic bath, a **shaker** (Heidolph titramax 100) was used for the blocking and the retention tests (see chapter on toxicity). In order to dry the membrane I used a **oven** (Memmert UF30). Once the pads assembled on the backing card, the strips were cut with the **Programmable Strip Cutter** ZQ2002 depicted on figure 4.8 from Shanghai Kinbio Tech.Co., Ltd which can cut with a precision of about 0.05mm. A control and test **line dispenser** arrived in the lab during the year (ZX1010™ Dispense System Biodot). It was used once to make the final test during the formation but was not used for the manufacturing of the LFA prototypes with iron oxide nanoparticle because of the small number of sticks that were done each time to test the influence of some parameters.

Figure 4.8: Some equipement used, *Left:* Strip cutter (image from KjnBi manufacturer), *Middle:* ultrosonic bath, *Right:* shaker (image from Heidolph manufacturer)

A list of the parameters tested is available at the table 4.2 for the MNP@Neutravidine and at the table 4.3 for the MNP@biotin. A table with the references of the reagents used is available in the annexes A.1. For each parameter tested, triplicates, 3 lateral flow assay sticks with the exact same manufacture process, have been made to avoid drawing wrong conclusion based on one stick that could be flawed. The dots of capture bioreceptors were usually placed at 1cm from the beginning of the membrane.

It is relatively difficult to give a clear view of the exact process followed to manufacture each stick as the parameters tested led to many variations. A standard protocol for reach at the end of the development is available in annex A. Unless explicitly stated, the MNP@Neutravidine based

sticks were made with CN95 nitrocellulose for the membrane, glass fiber for the conjugate pad and cellulose for the sample and absorbent pads. Per triplicate (15mm of conjugate pad) 10μg of MNP@Neutravidine in 90 μL de conjugate pad buffer (5% (w/v) sucrose, 1% (w/v)BSA and 0.5% (v/v) Tween20 in 0.01M PBS) were vacuum dried for 2 hours after soaking the conjugate pad. The control line was formed by laying 0.8muL dot of 1mg/mL biotin-BSA on the membrane and then dried 20 to 30 minutes at 37 °C in the oven. A standard protocol is available in the annex A.

Those basis specifications are, except otherwise specified, also true for the MNP@biotin based lateral flow assays sticks. Due to problems to see the apparition of a control line however, the control line was formed by laying 3 times 0.8muL dot of 1mg/mL streptavidin with 30 minutes intervals while drying 37 °C in the oven then dried 1 hour in the same conditions.

Last but not least, once a prototype with MNP@biotin was achieved, I did an attempt to go a step further and to detect an analyte in solution. This way with the LFA prototype an optical limit of detection could be assessed in a more realistic way. Once the reader designed the prototypes could be used to see if the reader allows to achieve a better limit of detection (LOD). As we can see on the figure 4.9, the configuration retained for this "detecting prototype" is to use the MNP@biotin as label, biotin-BSA as test line capture receptor and streptavidin as analyte and control line bioreceptor. The stick was composed of CN140 nitrocellulose for the membrane, glass fiber for the conjugate pad and cellulose for the sample and absorbent pads. For 2 cm of conjugate pad 15μg of MNP@biotin in 110 μL de conjugate pad buffer (5% (w/v) sucrose, 1% (w/v)BSA and 0.5% (v/v) Tween20 in 0.01M PBS) were vacuum dried for 2 hours after soaking the conjugate pad. One 0.8μL drop of 1mg/mL biotin-BSA was applied to form the test line and dried during 2 hours and the same protocol described in the preceding paragraph was applied for the control line. The streptavidin analyte was dissolved in miliQ water at different concentrations.

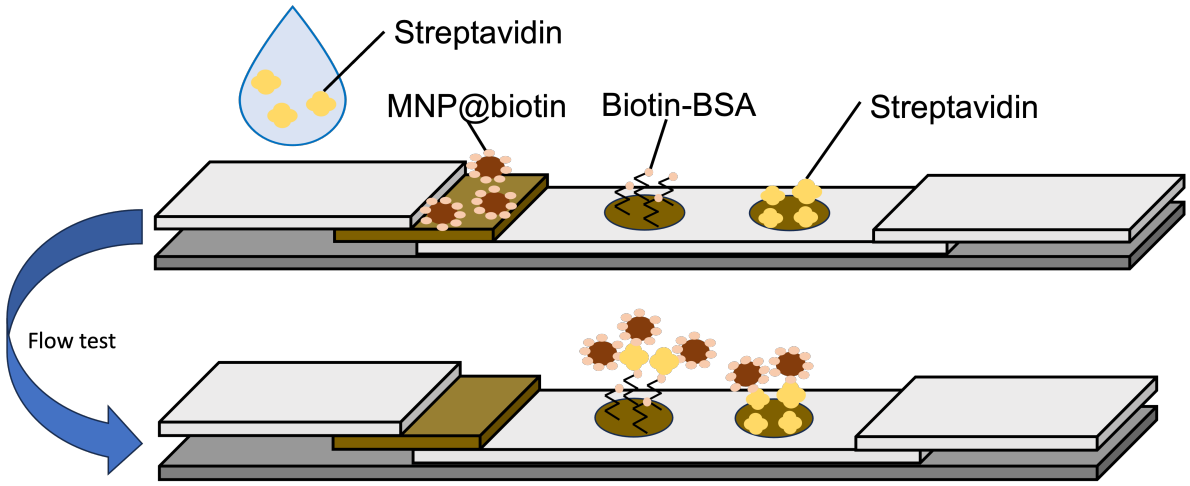

Figure 4.9: Scheme of LFA detecting streptavidin in solution.

The detection was done with the MNP@biotin because the analyte is a tetrameric protein of 60kDa with four biotin binding sites. Sandwich LFA is thus feasible. The alternative, with the components at my disposal, would have been to use biotin as analyte. However biotin is too small (0.24 kDa) to be detected in sandwich format [29]. To detect biotin, a competitive format is required but I had no suitable capture bioreceptor at hand to make the control line.

Type of parameter	Parameter/composition	Goal
Running buffer (half-stick only)	10 mM PBS pH 7.4 with 0.5% Tween-20 and 1% BSA	Obtaining a flow of the nanoparticles
Running buffer (half-stick only)	10 mM PBS pH 7.4 with **0.5** or **1** or **2**% Tween-20	Assessing the impact of Tween20 on the flow
Running buffer (half-stick only)	BSA 1%	Assessing the impact of BSA on the flow
Running buffer (half-stick only)	10 mM PBS	Obtaining a flow of the nanoparticles
Blocking the membrane and running buffer	Blocking and washing buffer as depicted in Table 4.1	Improving the flow
Adding a sample pad in glass fiber	Glass fiber	Promote regular flow at the intrance of membrane + impact of horizontal
Blocking (passivation) of the membrane	Blocking and washing buffer as depicted in Table 4.1	Improving the flow by reducing non-specific interactions
Re-suspension of the nanoparticles	In **miliQ water** (purified/ deionised water with a resistivity of 18,2 MΩcm) or in **PBS** 10mM or in BSA 1% or in running buffer (10 mM PBS pH 7.4 with 0.5% Tween-20 and 1% BSA)	Prevent aggregation of the nanoparticles
Sonication	20 minutes sonication in conjugate pad buffer or other suspension media	Promote monosipersion of the nanoparticles
"Washing" the nanoparticles	Resuspend them 3 times in PBS or miliQ water by removing the media with magnetic separation	Assess the impact of unknown components in the commercial suspension media
Membrane	**CN95** or **CN140**	Assessing the influence of pore size
Drying method	Oven or under vacuum drying	Assess the influence of the drying method
Capture bioreceptor concentration (biotin-BSA)	0.25mg/mL, 0.5mg/mL, 1mg/mL and 1.5mg/mL	Assess the influence of biotin-BSA concentration on the perceived signal
Concentration of nanoparticles in the conjugate pad	10, 20 and 40 μg per triplicate (respectively 3.33, 6.67 and 13.33 μg per LFA stick)	Obtain a maximal signal at the control line

Table 4.2: Parameter tested for MNP@Neutravidine, % in (v/v) or (w/v). The reference of the reagents used are available at table A.1 in the annexes

Type of parameter	Parameter/composition	Goal
Running buffer (half-stick only)	10mM PBS	Obtaining a flow of the nanoparticles
Running buffer (half-stick only)	10 mM PBS pH 7.4 with 0.5% Tween-20 and 1% BSA	Obtaining a flow of the nanoparticles
Concentration of the capture bioreceptor (Streptavidin)	0.25mg/mL, 0.5mg/mL, 1mg/mL, 2mg/mL, 5mg/mL, 10 mg/mL	Assess the influence of capture bioreceptor concentration on the perceived signal
Sonication	20 minutes sonication of the nanoparticles in conjugate pad buffer	Promote monodispersion of the nanoparticles
Membrane	**CN95** or **CN140**	Assessing the influence of pore size

Table 4.3: Parameter tested for MNP@biotin, the reference of the reagents used are available at table A.1 in the annexes

4.3 Characterisation of the nanoparticles

In order to characterise the MNP@Neutravidine and MNP@biotin that were bought, 3 techniques were used to have a better perception of their characteristics and to assess the consequences of treatments (e.g. sonication, "washing" or different suspension media) that were applied to the nanoparticles. We can find in the following sections the explanations of those techniques.

4.3.1 Scanning electron microscopy (SEM)

SEM is a microscopic technique which is able to reach 200,000 times magnification. As its name indicates, images are obtained by scanning an electron beam of high energy on the sample surface. Electrons are able to resolve finer features/details of materials observed to a much greater extent compared to optical light microscopy thanks to their smaller wavelength, for comparison the wavelengths are displayed in figure 4.10. In SEM the electrons are accelerated between 5 to 30 keV.

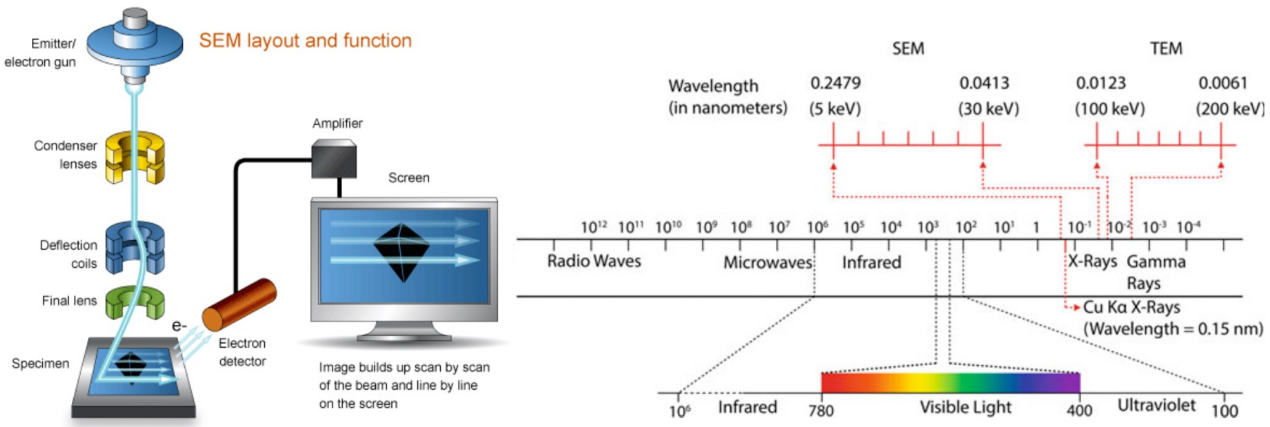

Figure 4.10: *Left:* Components of a scanning electron microscope, image from [72]. *Right:* Electromagnetic spectrum showing the size of the wavelength used in the light, scanning (SEM), and transmission electron microscope (TEM),image from [73]

As we can see on the figure 4.10, the electrons originating from the emitter travel, in vacuum (less than 10^{-3} Pa), through electromagnetic lenses which focus these electrons on the surface of the sample. Electron-sample interaction results in information emanating from the specimen which is passed through detectors and reconstituted as an image. [73]. Scanning electron microscopy is thus able to reach nanometer scale resolution on bulk sample, is globally nondestructive although some beam damage may result on the surface of the sample especially if the sample is low conductive.Scanning electron microscope can sometimes also be used for microchemical analysis, the x-rays resulting from interactions between the sample and the electrons are detected and analysed. However this require specific detector and more intense vacuum (less than 10^{-6} Pa). The non conductive samples however need to be covered with conductive coating, only still samples are observable and the analysis has to be done under vacuum [73]. The scanning electron microscope used in this work is a Crossbeam 550 Gemini 2 from Zeiss.

4.3.2 Dynamic Light Scattering (DLS)

Dynamic light scatering (DLS) is a spectroscopic measurement technique which relies on a numerical transformation of spectral measurement signals of sample into size distributions with accurate analysis from nano up to micrometer scale. As we can see on the figure 4.11, the DLS measure high-frequency fluctuations in scattered light most frequently due to Brownian motion.

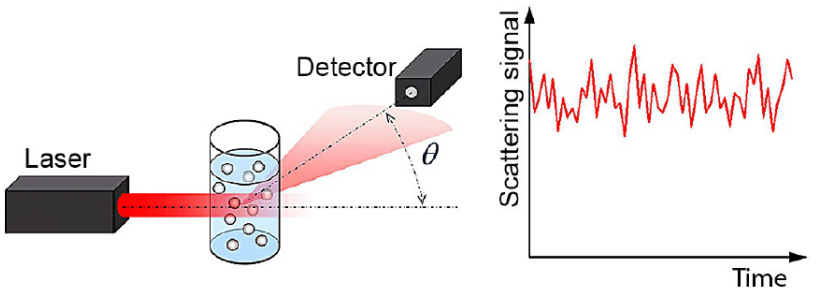

Figure 4.11: DLS working principle: Laser illuminates particles in solution which scatters the light. The fluctuation of scattering indicates the size of the particle, smaller particles moving faster. Image from [74]

The Brownian motion of particles in solution causes a permanent spatial rearrangement, thus affects the interference of the individual scattering signals and consequently results in a fluctuating signal at the detector [74]. The Stokes-Einstein equation here under gives the particle diffusion coefficient D_p which determines the dynamics of the rearrangement of the particle:

$$D_p = \frac{k_B T}{3\pi\eta x_{h,t}}$$

with k_B the Boltzman's constant, T the temperature, η the dynamic viscosity of the fluid and $x_{h,t}$ the hydrodynamic diameter of translational motion [74]. The hydrodynamic diameter is the diameter of a theoretical sphere which would have the same diffusion coefficient as the particle measured. The hydrodynamic diameter refers to individually moving components, that is, monodispersed particles and aggregated particles. It typically reflects the outer dimensions, but it is virtually not related to the size of constituent particles within an aggregate or agglomerate. So that it is a good indicator of the aggregation of particles in solution. Ideally, DLS measurements

should be performed at lowest possible concentrations and at constant temperature. Low particle concentration ensures that the viscous interactions between neighbouring particles are negligible and that multiple scattering can be excluded [74].

Due to the computation process, there is a factor 10^6 in the distribution of the size. A particle A being 10 times larger than a particle B, particle A will be represented as 10^6 more numerous than particle B. There are ways to attenuate this effect by weighting the distribution integrated in the software of the DLS used but choice has been made not to use it in this work as we do not have a clue of in which extend it works. Therefore it will be important to keep in mind this 10^6 factor when looking at DLS based graphs.

4.3.3 Spectrometer UV-vis

UltraViolet-visible spectrometer or UV-vis spectrophotometer is used to measure the reflectance or the absorbance of a sample with UV and visible light (wavelength ranging from 200 to 900 nm [75]). It is a well known technique, since first commercial UV-Visible spectrophotometer were sold in the 1940's, and a low cost method of analysis. As we can see in figure 4.12, the principle behind UV-vis spectrometer is quite straightforwards. A light source illuminate a sample at different wavelengths and a detector placed behind the sample to record the light passing through the sample. The transmittance, i.e. the intensity measured (I) divided by the incident intensity (I_0), is then known and the absorbance defined by $A = \log_{10}(\frac{I_0}{I})$ can be obtained. The absorbance of the sample is usually obtained by subtracting the absorbance of a blank measure [76].

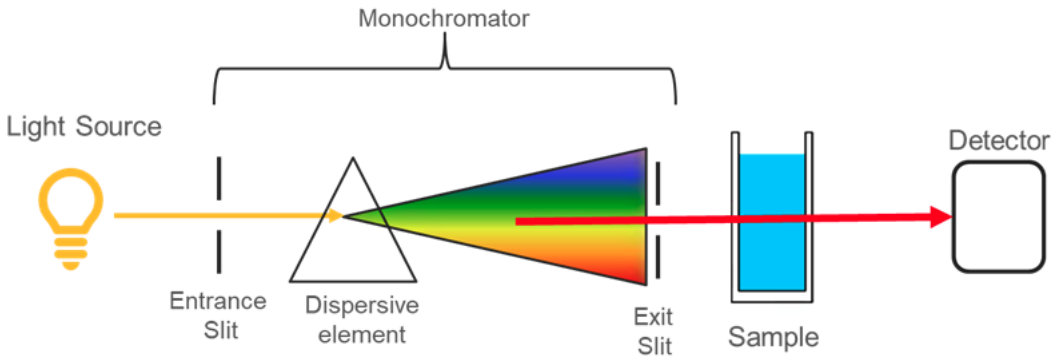

Figure 4.12: Illustration of spectrometer principle, image from [77]

UV-vis spectrometer (Ultrospec 8000/PC from Biochrom) was used in this work for the gold aggregation test during the training, as gold usually demonstrate a strong absorbance peak at 520nm a sagging or disappearance of this peak indicates an aggregation of the gold nanoparticles. Absorbance measurements were also done to quantify the amount of MNP@Neutravidine in solution for the retention tests (see toxicity chapter 7.3).

4.4 Recording and processing of the results

During the training and the first stages of the development of the LFA with iron oxide nanoparticles the results were assessed optically and pictures with smartphone were taken right after the flow test (10 minutes after for the CN95 membrane and 15 minutes for the CN140 membrane due to the difference of flow speed). Once control line was obtained, optical assessment became insufficient. To better perceive the improvement or degradation of the flow due to the parameters tested, a more quantitative method was required. This way, I began use Fiji, the mac version of imageJ. ImageJ is a free access image analysis software developed by the US's National Institutes of Health (NIH). It was used to assess the gray value of the pixels along a line on the middle of the lateral flow stick, as we can see on the figure 4.13. High gray values correspond to white and inversely lower values correspond to darker area, where nanoparticles are visible. It appeared afterwards that the use of Fiji on the pictures taken with smartphones were not useable to do a quantitative analysis because it was too influenced by artefacts like change in light exposure, shadows, bad focusing, different distances and blurring due to movement. To avoid those problems, I tried to scan the LFA sticks but due to a too strong light, the LFA were over exposed resulting in not representative images. To obtain images with less of these artefacts, a paperboard box (length:14cm, width:10.5cm, height:13.5cm) was used. A hole was made in the middle of the top face, big enough for the camera and the flash but small enough to not let light passes when the smartphone is placed. The pictures were taken with the flash of the smartphone (Samsung Galaxy A6) which was laid on the top of the box at the emplacement and the LFA was laid on the same place with a white background (white paper). This way light exposure and distance were constant across the different pictures and shadows, bad focusing blurring due to movement were diminished.

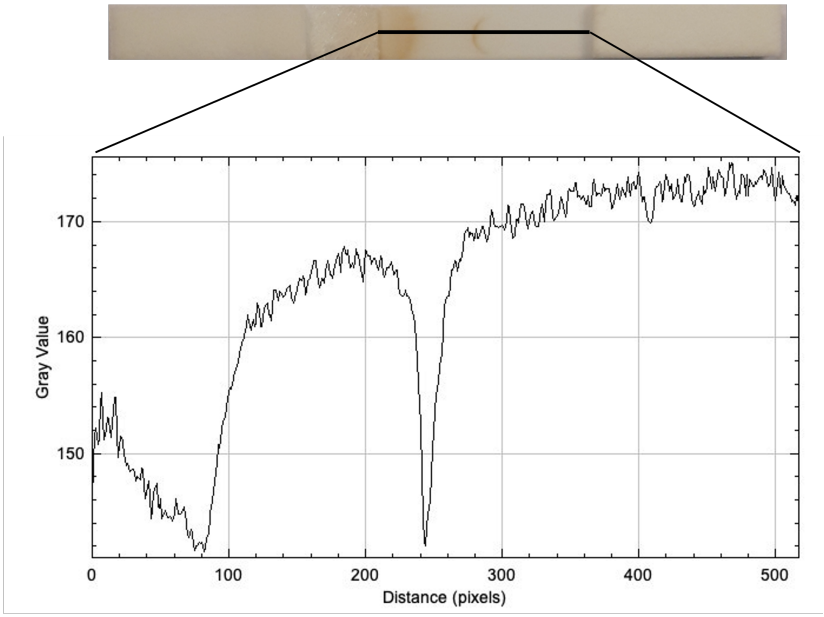

Figure 4.13: ImageJ analysis of a lateral flow assay. We can see agglomeration of the nanoparticles on the left of the graph and the middle peak corresponding to the control line.

We can see on the figure 4.13, a typical gray value curve along the membrane. As we can see here, the dot of the control line is not fully coloured, it appears like a quarter moon. The gray values

are measured along a line which is taken each time at the centre of the membrane. Several line widths were tested with imageJ and the analysis is made with 5 pixels wide lines because it is a compromise between too much variation due to a pixel and too wide line that would be too much influenced by the shape of the dot. There are generally 2 interesting features on the gray value curve. The peak and the beginning of the stick. The peak here correspond to the control line and the left of the graph, the beginning of the membrane where bad flow of the nanoparticles prevent a part of them to advance coloring the beginning of the membrane. The coloration of the beginning of the membrane was compared qualitatively. The size or depth of the peak was computed to make quantitative comparisons by subtracting the lowest point of the peak to the mean of the gray values of the area behind the control line. To assess the precision and repeatability obtained with this technique, I made this analysis on 15 pictures of the same LFA stick. I obtain a mean peak depth value of about 44 with a standard deviation of 5.7. Because of those variations between optical measures and because the pictures taken with the box were taken sometimes long after the flow test (To avoid comparing stick that would have aged differently, the comparison with semi quantitative measurement are done on sticks made on the same day.) with dry stick (which let agglomeration of NP on the stick less apparent than when wet), we have to keep in mind that the analysis of the results in this work can thus only be semi quantitative, but this process still enables to perceive the tendencies.

Chapter 5

Results

In this section the significant results obtained during the formation, where we adapted the LFA with 20nm diameter gold nanoparticles to 40nm AuNP, and during the conception of lateral flow assay with 2 kinds of iron oxide nanoprticles (1μm diameter MNP@Neutravidine and 10nm diameter MNP@biotin) are presented.

The outcome of the formation is presented first, with an emphasis on the functionalization step. As we will see this step can have big repercussion on the flow once the nanoparticles loaded on the LFA stick and those results allows to make a broader picture of a LFA manufacturing. Then the parameters tested to obtain a good flow with the MNP@Neutravidine are exposed. Finally the outcome of the development of MNP@biotin based lateral flow assay prototype and the detection of streptavidin in solution is presented.

5.1 Training on AuNP's

To ensure the stability and determine the best conditions of pH and antibody concentration for the functionalization of the 40 nm AuNP, we performed the gold aggregation test (GAT).

We can see on figure 5.1 the measures taken with the UV-vis spectrometer. Monodisperse gold nanoparticles of 40 nm diameter show strong absorbance at a wavelength of 520 nm. An absorbance peak which is enlarged (wider), lowered or absent is denoting of the aggregation of the AuNPs. Aggregation of the nanoparticles could impede the good running of a lateral flow test, those conditions of conjugation are thus discarded. In the end, pH 9 with a concentration of 6.25 μg/mL anti human IgG antibodies were the conditions retained for the functionalization.

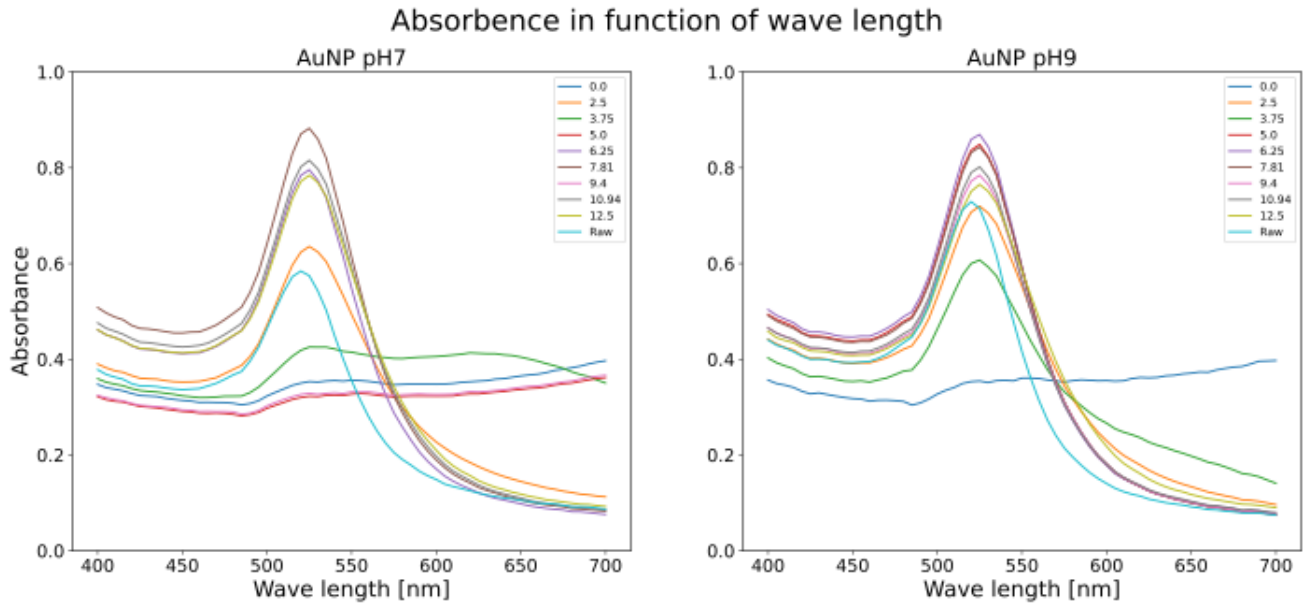

Figure 5.1: Spectrometer measurements for the gold aggregation test. Aggregation is indicated by low or no absorbance peak. The up-right legend is the concentration of antibodies (in μg/mL) for the functionalization.

After firsts tests in half-stick format it appeared that, compared to 20 nanometers, the 40 nm AuNPs were colouring the membrane. This indicates that nanoparticles or agglomerates are stuck or bound non-specifically to the membrane. To counter this effect, we tried to "block" or passivate the membrane, as described in the state of the art, and to diminish the concentration of antibodies. Indeed, as explained by Parolo and al. [29], it is sometimes indicated to use a antibody concentration lower than the one defined by the GAT to provide a lower background signal. We therefore used a concentration of 6.25 (for comparison), 4.69 and 2.5 μg/mL. The outcome of half-stick tests for the different concentration of antibodies during the conjugation is visible at figure 5.2. We can notice that the dots are not fully coloured unlike the control line normally obtained with 20nm AuNP.

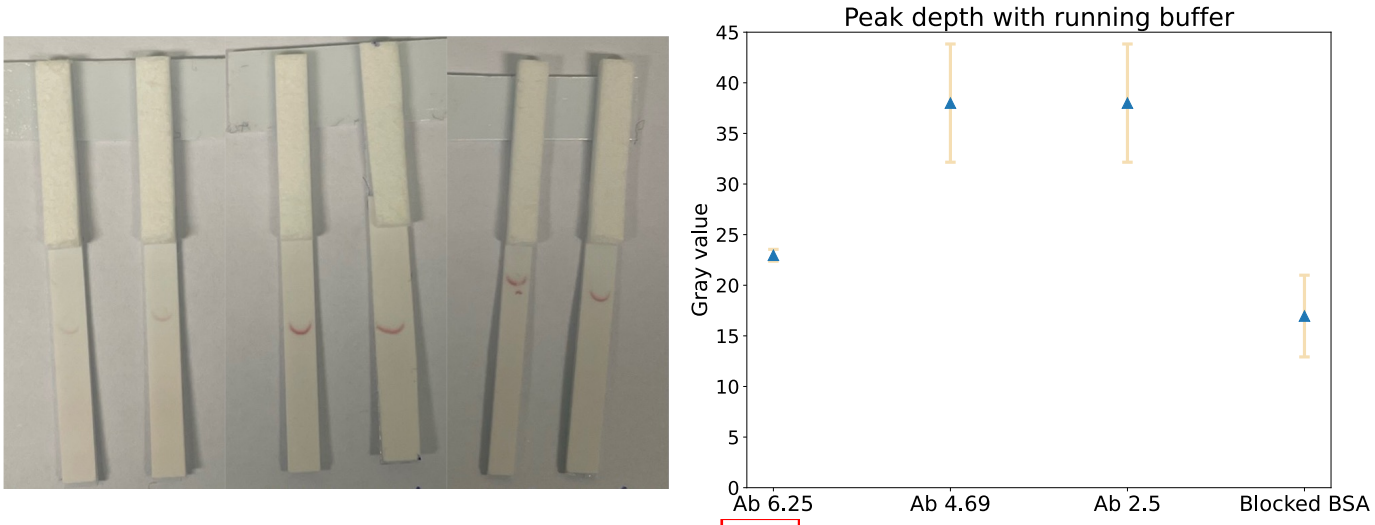

Figure 5.2: *Left:* Half-stick with different conjugation of AuNP (from left to right 6.25μg/mL, 4.69μg/mL and 2.5 μg/mL). *Right:* Peak depth at the control line for blocked half-stick and different conjugation with mean and standard deviation.

As we can see on the figure 5.2, the coloration of the membrane was less pronounced for concentration of 4.69 and 2.5 μg/mL and darker control lines were obtained, meaning that more nanoparticles were able to reach and bind at the control line. We can notice that the dots for the control line were not placed at the same distance on the membrane. This is to be avoided because, as we saw in the state of the art chapter, the placement of the control line can influence the sensitivity of the test. The consequences of the blocking of the membrane were less obvious, the colouring of the membrane seemed to be slightly attenuated and as we can see on figure 5.2 (*left*) the peak depth is slightly diminished.

To assess the improvement we did functional full sticks with 20nm (figure 5.3 and figure 40nm 5.4) gold nanoparticles detecting concentration of 1000, 300, 100, 30, 10, 3, 1 and 0 ng/mL of human IgG (from left to right on the picture). We can clearly see that the membranes with 40 nm AuNPs retained some of the nanoparticles colouring the stick. We can notice that the test and control lines are actual lines because of the used of the dispenser. It will not be used further in this work because tests were made in small quantities which render the use of the dispenser difficult and capture bioreceptor consuming.

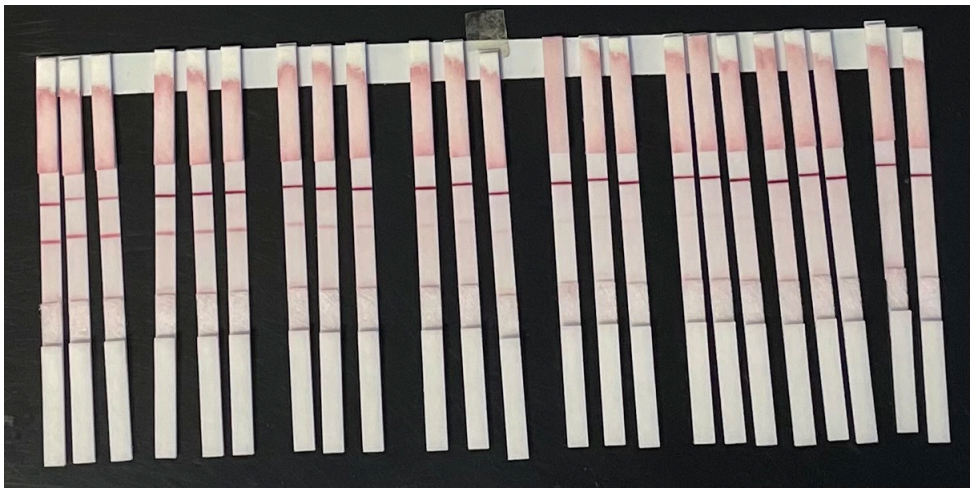

Figure 5.3: Sticks with the 20 nm gold nanoparticles

Figure 5.4: Sticks with the 40 nm gold nanoparticles

As we can see on the pictures, the membrane is much more coloured with the 40nm nanoparticles. The figure 5.4 shows the 40 nm AuNP with a concentration of 6.25 μ/mL of antibodies during the conjugation. The ones with 4.69 and 2.5 μ/mL led to similar results. More surprisingly, test line is visible for all the concentrations of human IgG, even the blank sample on the right. This should not happen and is revealing that something went wrong while manufacturing the LFA or during the experiment.

5.2 Developpement of LFA with Neutravidin coated MNP

As explained previously, the purpose of this work is to switch from gold nanoparticles to iron oxide nanoparticles whose concentration could be assessed by a magnetic reader thanks to their magnetic properties. Two kinds of iron oxide nanoparticles are tested to be used in LFA, the MNP@Neutravidine and the MNP@biotin. In the iterative process to achieve a lateral flow assay with MNP@Neutravidine (nanoparticles of 1μm of diameter coated with neutravidin), some difficulties were encountered at various stages. In this section are explained the parameters that were tested to overcome those problems.

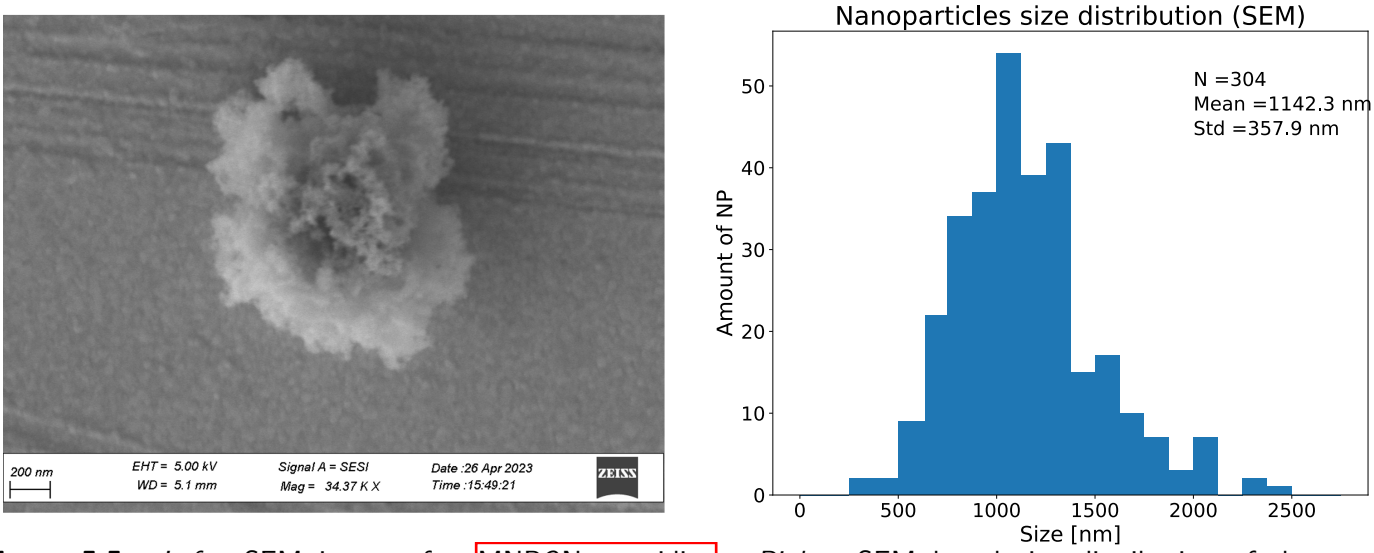

Figure 5.5: *Left:* SEM image of a MNP@Neutravidine. *Right:* SEM based size distribution of the MNP@Neutravidine

We can see on the figure 5.5 a MNP@Neutravidine observed with scanning electron microscope. These nanoparticles were always observed with the fluffy/cloudy material that recovers it. I first thought it was neutravidin but the manufacturer did not think so although they were not able to tell what it was, maybe something in the buffer that is aggregating around the bead. Nevertheless based on the SEM images I was able to measure the size of 304 nanoparticles, the distribution hence obtained is visible on the left of the figure 5.5.

5.2.1 Running buffer

The first tests in half-stick were done to assess the flow of nanoparticles diluted at different concentration in miliQ water. As you can see on figure 5.6, the MNP@Neutravidine were not able to flow properly across the membrane. Indeed a colour line is visible at the beginning (lower end) of the membrane indicating that the nanoparticles stopped flowing nearly immediately after they get to the membrane. Some tests were made to allow the flow of the nanoparticles among which sonicating the NPs right before the test to prevent aggregation, adding a sample pad of glass fiber to promote a more regular flow as done in by Wang and al in [78] or lowering the concentration of the NPs to avoid congestion. Contrary to the use of a running buffer, none of these attempts made it possible to obtain a flow of the NPs.

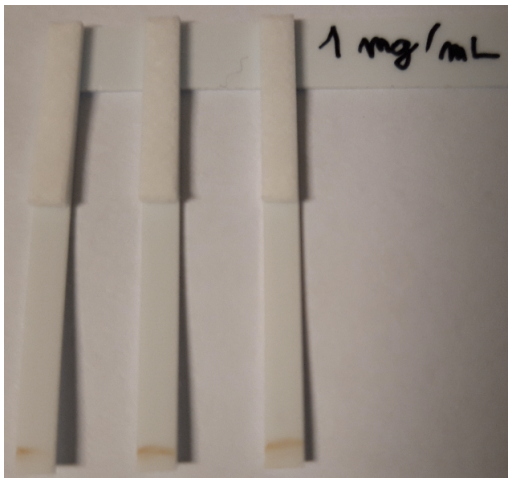

Figure 5.6: Agglomeration at the beginning of the membrane

The running buffer found in the literature ([79]) consists in 10 mM PBS pH7.4, 0.5%(v/v) Tween-20 and 1% (w/v) BSA. The desired amount of nanoparticles were resuspended in the the running buffer right before the test and it allowed to prevent the agglomeration at the entrance of the membrane. This improvement of the flow allowed to pass to the next step and fix biotin-BSA on the membrane to have a control line. We can see on the figure 5.7 the result obtained with the running buffer and dotting the biotin-BSA.

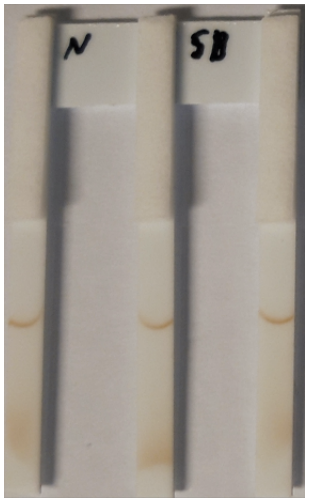

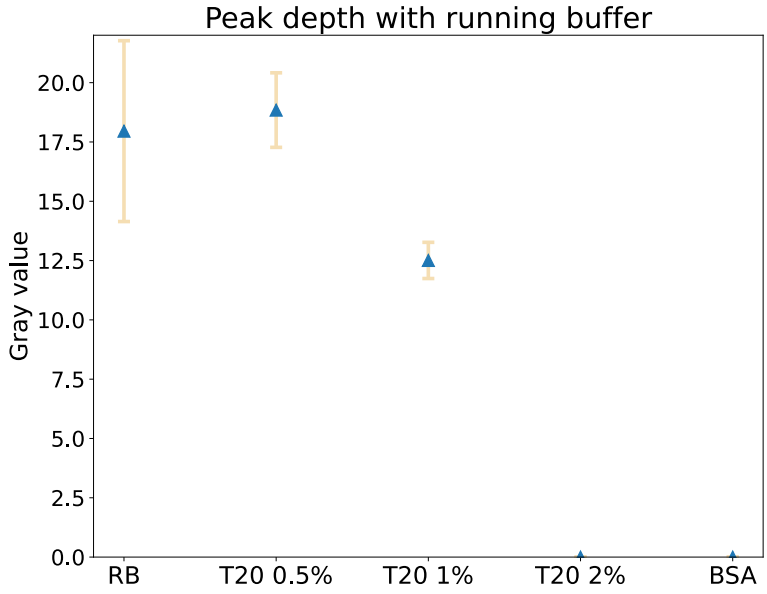

Figure 5.7: *Left:* Control line with MNP@Neutravidine in running buffer *Right:* Peak depth obtained with different running buffer. RB:initial running buffer, T20:Tween 20. As we can see running buffer composed of only BSA and Tween 20 2% did not enable the appearance of a control line.

Later, the components of the running buffer were tested individually to optimize the flow and determines which component allow nanoparticles to flow. The depth of the peak achieved with the

full running buffer and its components independently tested (1% (w/v) BSA, 0.5%(v/v) Tween 20, 1%(v/v) Tween 20 and 2%(v/v) Tween 20 all in 10 mM PBS) is displayed on the right of the figure 5.7. On the graph the blue triangle is the mean of the 3 LFAs (triplicate) and the bars denote the standard deviation. As we can see running buffer with only 1% BSA did not allowed to obtain a visible control line. Similarly, too high concentration of Tween 20 (2% (v/v)) did not allowed to obtain a control line although no agglomeration at the begging of the membrane was observed. Indeed, we can note that even if we have a flow that allow to obtain a control line, we have an unwanted feature on the sticks. The membrane is coloured before the test line as we can see on the left part of the figure 5.7. It is indicative of nanoparticles that stop flowing and stay on the membrane.

5.2.2 Blocking the membrane

The blocking (or passivating) of the membrane was also tempted as a solution to obtain a flow and diminish the non specific bindings leading to colouration of the membrane. The same blocking procedure than for the AuNPs was thus done. Without running buffer it seemed to improve the flow as the agglomeration was more spread than without as we can see on figure 5.8. However it did not allowed to obtain a control line. Worst, with the use of a running buffer and later a conjugate pad, no control line was obtained. With the MNP@Neutravidine the blocking of the membrane, as done for the AuNPs, prevented the appearance of a control line.

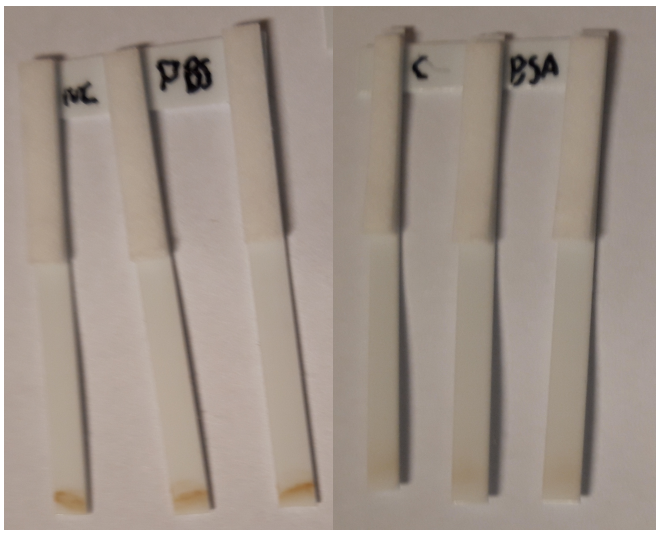

Figure 5.8: Nanoparticle flow test in 0.01M PBS without (*left*) and with (*right*) blocking the the membrane.

5.2.3 Conjugate pad buffer

After obtaining a control line the glass fiber conjugate pad and cellulose sample pad were added to the stick. The conjugate pad buffer used was the same than the one used for the formation with gold nanoparticles (5% (w/v) sucrose, 1% (w/v) BSA and 0.5% (v/v) Tween 20). As we can see on the figure 5.9 it ensures a good rewetting of the nanoparticles and the MNP@Neutravidine leave the conjugate pad without visible problem. Because the conjugate pad buffer also contains the components of the running buffer, the running buffer was not needed anymore. Indeed,Tests were made with the previously used running buffer (1% BSA, 0.5% Tween20 in 0.01M PBS) and

with PBS 0.01M. No solution proved to be better than the other so the following tests were made by applying 140 μL of 0.01M PBS onto the sample pad.

Figure 5.9: 1st full stick ou SB

Unfortunately a defect in the flow remained as we can see on the figure 5.9. Indeed, although being less pronounced than with half stick, the colouring at the beginning of the membrane due to bad flowing of some nanoparticles is still visible. In the next sections, parameters are changed or tested in the aim to reduce this artefact.
Two other variants of the conjugate pad buffer were tested. To assess the importance of the bovine serum albumin (BSA) a version without BSA was tried. Similarly instead of drying the conjugate pad in vacuum for 2 hours I tested to dry it in the oven at 37°C. We can see the gray value peak depth corresponding to the control line in figure 5.10. These two changes deteriorated the signal at the control line in a comparable manner. The first conjugate pad was thus kept for further experiments.

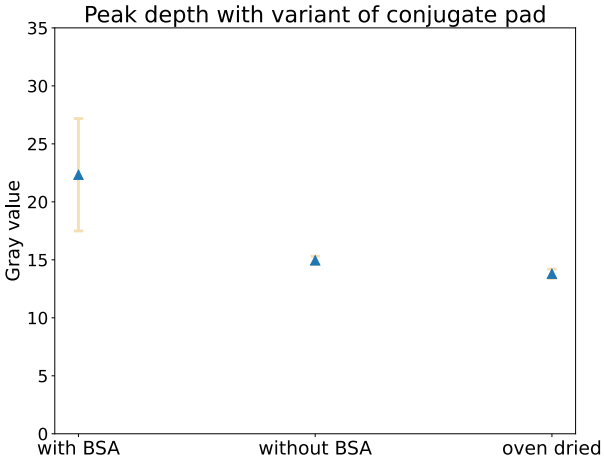

Figure 5.10: Colorimetric peak depth obtained with variants of the conjugate pad buffer

5.2.4 Resuspension

In order to avoid the colouring of the membrane different suspension media were tested. The goal is to have a solution that promote monodispersion of the nanoparticles and avoid the formation of aggregates that can hinder the flow, leading to colouration of the membrane. Two suspension media were investigated in depth, miliQ and 0.01M PBS and two other (running buffer and 1% (w/v) BSA in miliQ water) were discarded after showing downgrade of performance in the test. Before any tests or measurements, it was assessed optically that the MNP@Neutravidine tend to

sediment faster in the miliQ suspension than in the PBS media. The depth of peak reached with the different resuspensions in half-stick lateral flow assay is visible in figure 5.11.

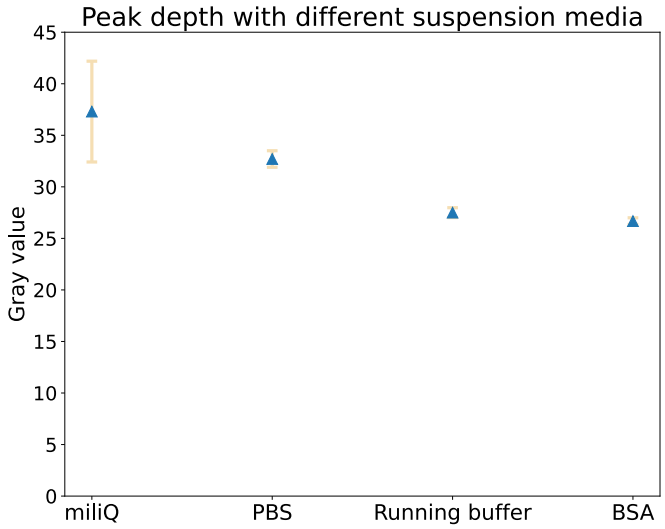

Figure 5.11: Depth of peak reached with miliQ, PBS, running buffer and BSA 1% suspension media

DLS measurements

We can see on figure 5.12 and 5.13 the mean of the 4 measurements done with the dynamic light scattering. DLS report the intensity (amount in arbitrary unit (a.u.)) in function of the hydrodynamic diameter. When looking at those graphs we need to keep in mind that there is a factor 10^6, particles 10 times larger will appear 10^6 more numerous. Even if the DLS is less accurate for particles above 1μm, we have an indication on the size of the nanoparticles in solution. We can easily observe that the MNP@Neutravidine in miliQ suspension have a broader size distribution with a curve that is increasing at 3000nm revealing the presence of agglomerates. The PBS suspension on the contrary seems to present less aggregation.

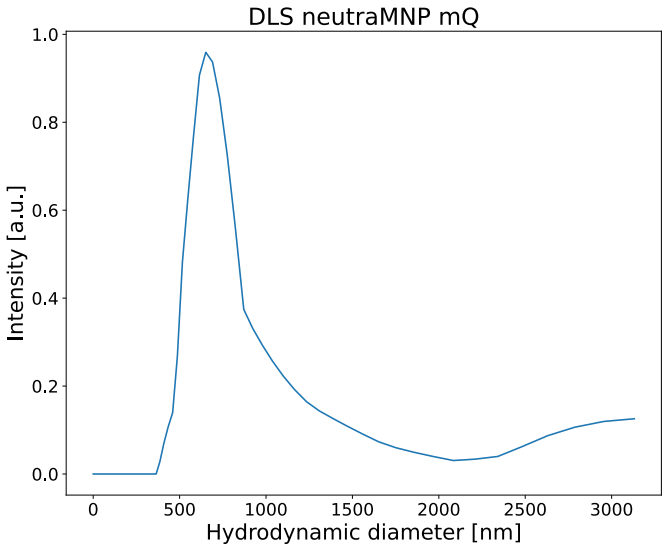

Figure 5.12: DLS: miliQ suspension

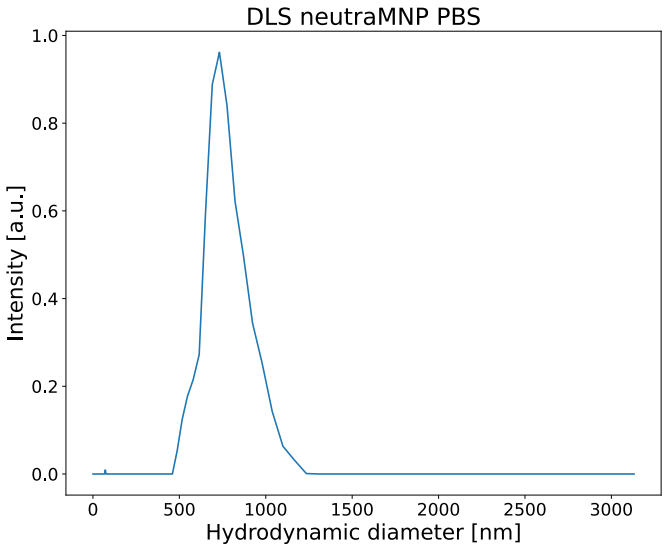

Figure 5.13: DLS: PBS suspension

5.2.5 "Washing"

To characterize the nanoparticles, images of dried MNP@Neutravidine diluted in miliQ water were made with SEM and their sizes were measured as we have seen in figure 5.5. On these images unidentified components were observed. We can see it on figure 5.14 (some circled in blue), beside the "cloudy" structure recovering the nanoparticles that some white more or less rectangle shape material is present.

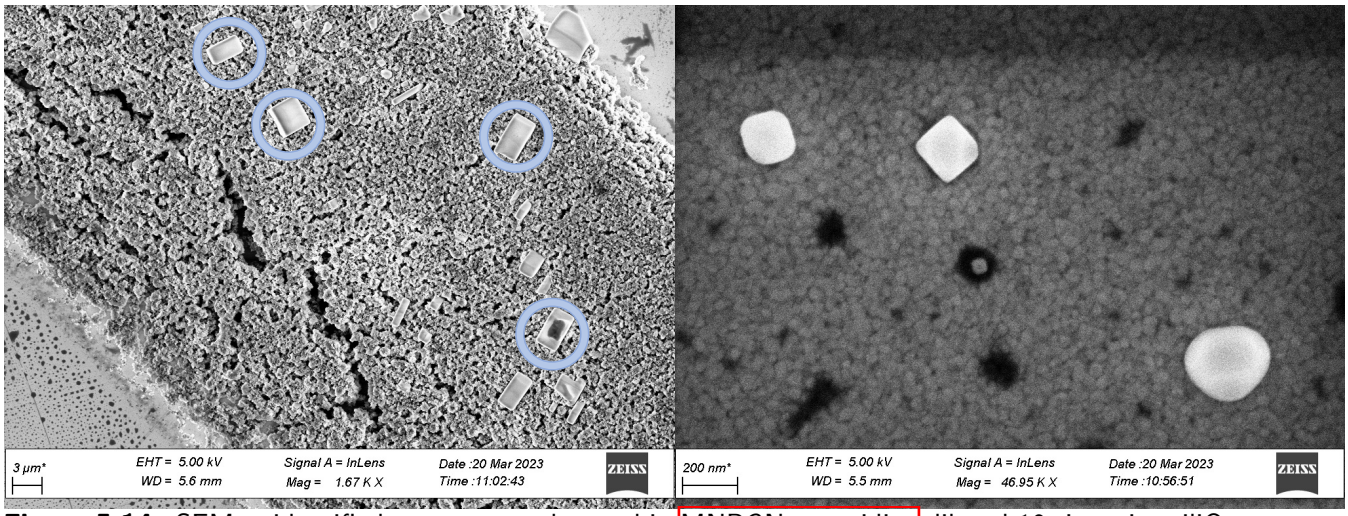

Figure 5.14: SEM unidentified component observed in MNP@Neutravidine diluted 10 times in miliQ water at different scales

After questioning the manufacturer, they were not able to identify precisely these unknown components. Moreover they do not think that the cloudy structure surrounding the nanoparticles was neutravidin, as I previously thought, but "perhaps something in the buffer that is aggregating around the bead". In order to assess the impact of those component on the flow, I washed the nanoparticles. This step consisted in retaining the nanoparticles with magnets, removing the media and re-suspending in 0.01M PBS or miliQ water. The operation was repeated 3 times to ensure that a very low amount of the initial solution remains. On the SEM images taken after the washing the bright rectangular shaped unidentified component was not observed anymore, assessing that it was successfully removed.

The results of the test with PBS suspension and PBS washing is displayed on the figure 5.15 and the peak depth obtain with nanoparticles washed in PBS and miliQ water are displayed on the graph of the figure 5.15. We can observe that the washed particles allow to obtain slightly less concentrated control line. This could be due to losses of nanoparticles during the washing process. Indeed, after submitting the removed media to a magnet all night long, a small amount of nanoparticles was observed. However, washing did not allowed to avoid the colouring/agglomeration on the beginning of the membrane.

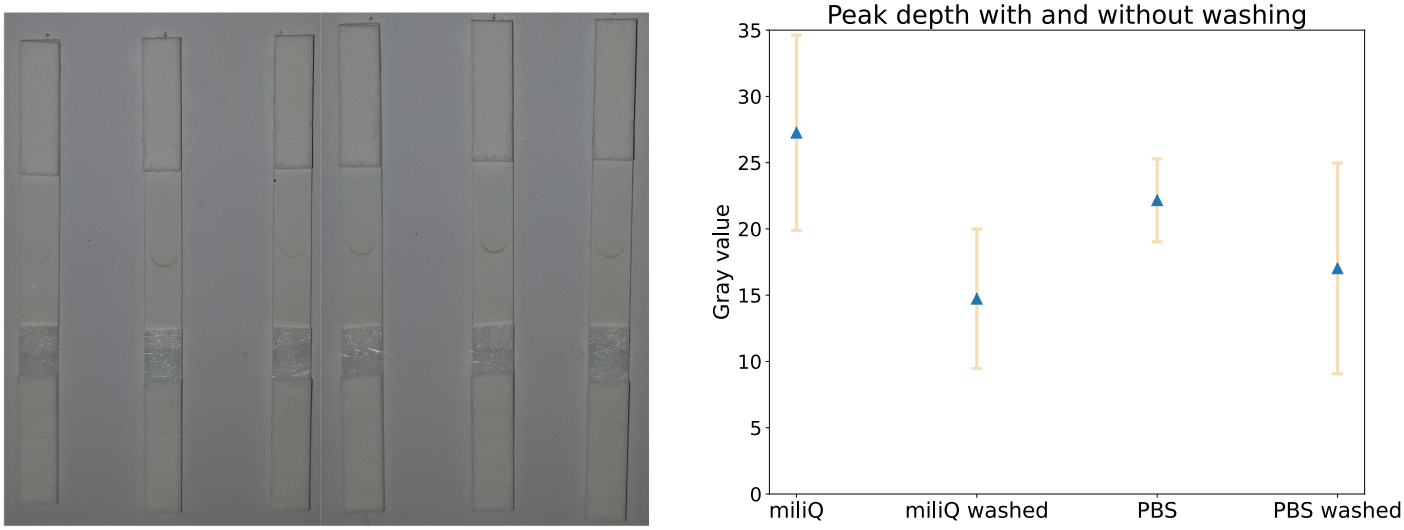

Figure 5.15: On the photo we see the triplicate with washed MNP@Neutravidine in miliQ (left) and diluted in miliQ (right). The graph presents the peak depth of the nanoparticle in 0.01M PBS andin miliQ water with and without washing

5.2.6 Sonication

Following the detection of bigger aggregates in DLS measurements sonication of the nanoparticles was done before applying the conjugate pad buffer to the conjugate pad. DLS was used to assess the impact of the sonication on 0.01M PBS and miliQ water diluted nanoparticles, we can see the outcome on the figure 5.16. We can see the distribution is a bit more sharp, less agglomerates are detected. We can also notice the appearance of small peaks around 100-200nm. This could correspond to some coating that is detached from the nanoparticles. As we can see the figure 5.17 which shows a SEM image of sonicated miliQ water suspension MNP@Neutravidine dried, that some "cloudy" material was found separated from the nanoparticles. This was also the case with non-sonicated nanoparticles but those depots were generally bigger and less numerous.

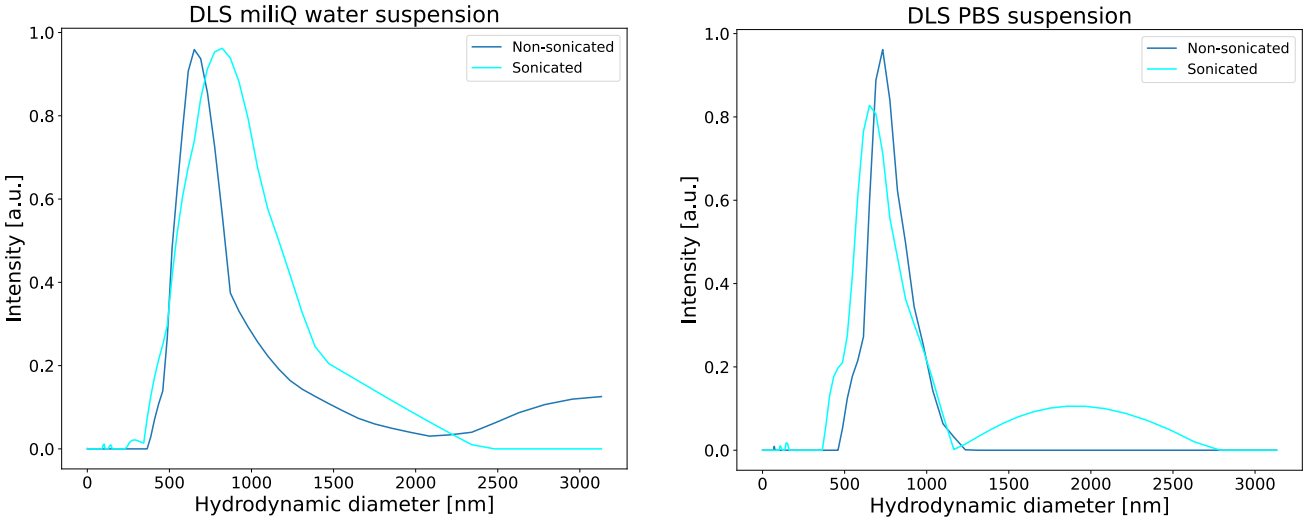

(a) Nanoparticles suspended in miliQ water **(b)** Nanoparticles suspended in 0.01M PBS

Figure 5.16: Hydrodynamic size of sonicated versus non sonicated nanoparticles

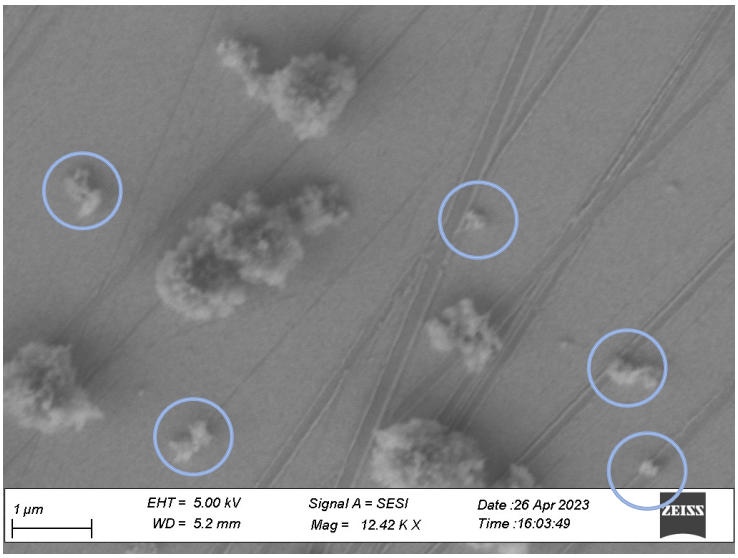

Figure 5.17: "Cloudy" material detached from the nanoparticles highlighted by blue circles

The results achieved with the sonicated nanoparticles are displayed here under 5.18. We can observe that the sonication seems to have deleterious effects on the ability to have a high concentration of nanoparticles at the control line when done to the miliQ water suspended MNP@Neutravidine. On the other hand, sonication of the PBS suspended MNP@Neutravidine led to no major improvement or downgrade of the peak depth.

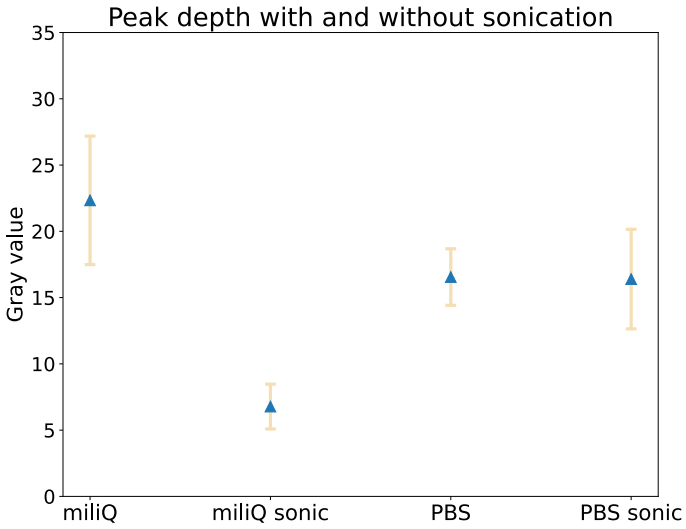

Figure 5.18: Gray value peak depth of control line with sonicated nanopaticles

5.2.7 Membrane pore size

Ideally, testing with a membrane having bigger pores would have been interesting to assess the importance of this parameter, the MNP@Neutravidine being quite large compared to the nominal pore size of the membrane (10-12 μm). Unfortunately the membrane with bigger pore size arrived

too late to be tested but test were made with smaller pore size (CN140, 8μm) [1]. The results are visible at the figure 5.20. As we can see the use of a membrane with smaller pore size greatly diminishes the amount of nanoparticles able to reach the control line and the colouration of the membrane is more marked.

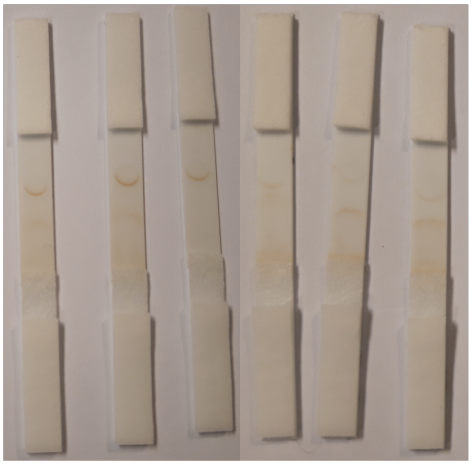

Figure 5.19: Triplicate on the left is CN95 and the right triplicate is CN140

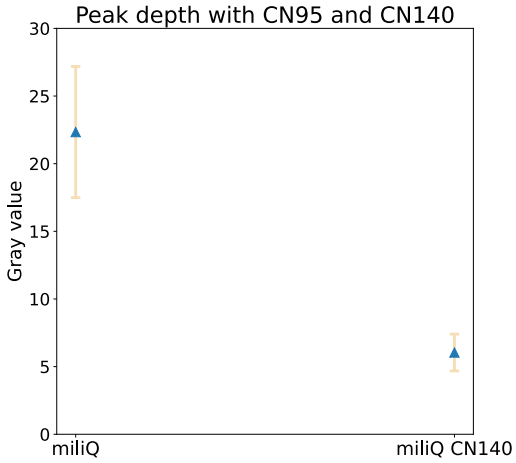

Figure 5.20: NMNPCN140

5.2.8 Maximum achievable signal

In order to maximise the amount of nanoparticles at the control line 3 concentrations of MNP@Neutravidine were tested: 3.33μg, 6.67μg and 13.33 μg per stick (5mm wide). For each of these nanoparticles concentration, 4 concentrations of biotin-BSA were dropped (0.8μL) at the control line: 0.25μg/mL, 0.5 μg/mL, 1μg/mL and 2μg/mL. The results are displayed at the figure 5.21

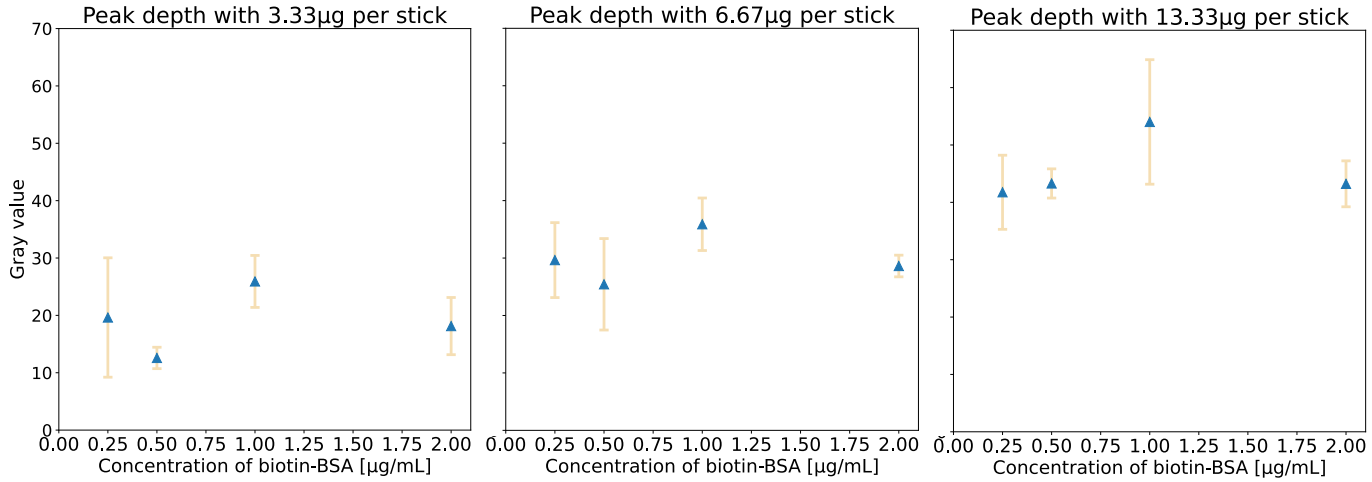

Figure 5.21: Peak depth at the control line for different concentration of MNP@Neutravidine and capture bioreceptor (biotin-BSA).

[1] Another membrane (HF75 with bigger pores from 12 to 17μm) arrived during the week preceding the submission of this work. The result is displayed in the annexes B

We can observe that increasing the amount of nanoparticle increases the signal at the control line. However bigger concentration of nanoparticles also led to a more pronounced colouration of the membrane (more non specific binding visible). More surprisingly, concerning the amount of biotin-BSA it follows the same pattern for all the concentration: The first concentration (0.25μg/mL) seems to lead to slightly better or equivalent result than 0.5μg/mL. The better signal is obtain with 1 μg/mL at the control line. Finally the concentration of the nanoparticle at the test line seems to be sensibly the same for 0.25 and 2 μg/mL.

5.3 Developpement of LFA with biotin coated MNP

The second type of nanoparticles tested are the MNP@biotin, biotin coated iron oxide nanoparticles of 10nm diameter. The same designing workflow was followed. Based on my experience with MNP@Neutravidine I tested with the same running buffer (a running buffer of 0.01M PBSr also tested confirming that it does not work as we can see on the figure 5.22). We can notice than the result of the flow test is better in comparison with the MNP@Neutravidine because very light coloration of the membrane is observable with the MNP@biotin when the running buffer is used. On the figure 5.23, you can see the white dots that are supposed to be the MNP@biotin but as we approach the limit of resolution of the scanning electron microscope, the nanoparticles measuring 10nm, they are a bit difficult to perceive. The parameters tested to achieve a LFA are explained in the next sections.

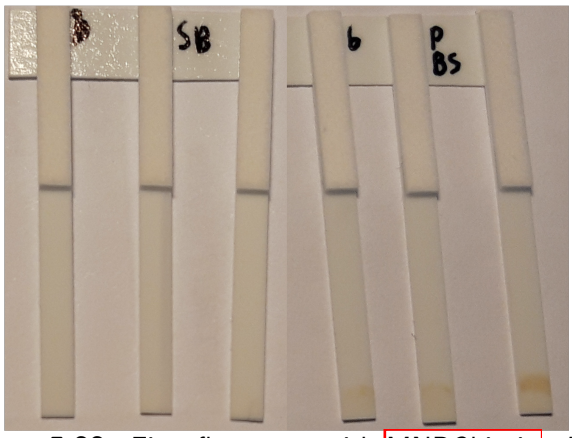

Figure 5.22: First flow tests with MNP@biotin. *Left:* with running buffer, *right:* without running buffer

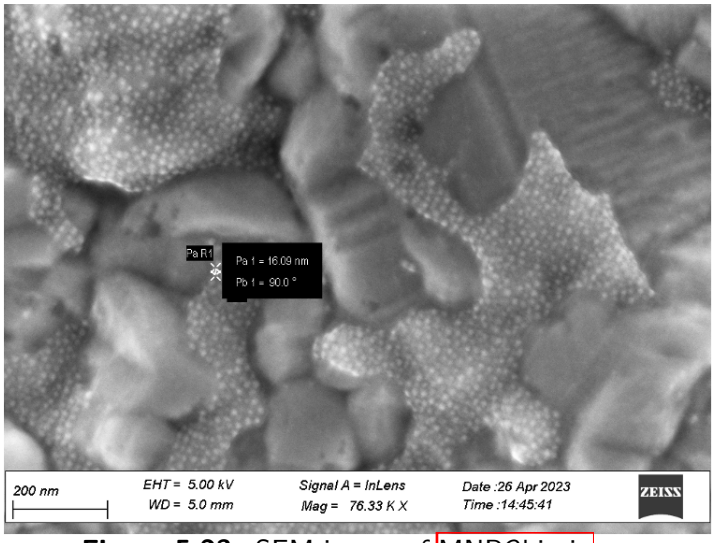

Figure 5.23: SEM image of MNP@biotin

5.3.1 Control line

In order to fix the streptavidin for the control line first tests were made as for the MNP@Neutravidine, i.e. the streptavidin was drop casted onto the nitrocellulose membrane (0.8 μL at 1mg/mL in miliQ water) and oven dried at 37 °C for 20 minutes, this was inspired from the literature [80] although they let the stick for 2 hours in the oven. Contrary to the biotin-BSA used as capture bioreceptor for the MNP@Neutravidine, this process was not able to lead to the appearance of a control line. Several attempts have been made to obtain a control line including: changing the running buffer to 0.5% Tween 20 to avoid BSA to impede the biotin/streptavidin interaction, vacuum drying

and ambient temperature drying. None of these enabled the appearance of a control line during the flow test. In the literature another way to make a control line with streptavidin was found where they increase the concentration up to 5mg/mL and let it 2 hours in the oven at 37°[81]. Increasing the concentration of streptavidin at the control line was firstly done by applying 3 dots of 0.8μL instead of one (with an interval of 20 minutes to allow to put the dots at the same place, if it is still wet the dot just spread more) because at the time I had only this solution of 1mg/mL of streptavidin. The sticks were scrupulously dried 2 hours in the oven at 37 °C. This way a control line was obtained as we can see on the figure 5.24. We can observe that contrary to the control lines obtained with MNP@Neutravidine the entire dot here is coloured. It is a good sign because it is revealing of a uniform distribution of the capture bioreceptor and also that the MNP@biotin are flowing through the all dot. The front of nanoparticles was observed to flow across all the membrane and to end in the absorbent pad, colouring it, which was not observed for the MNP@Neutravidine.

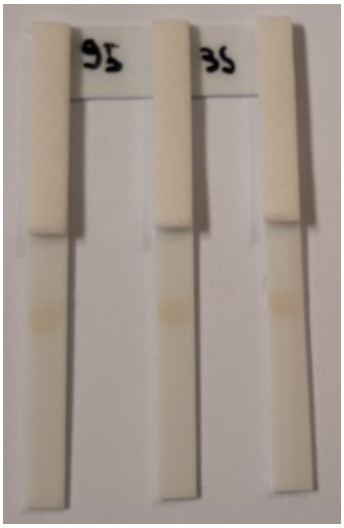

Figure 5.24: Control line of streptavidin with MNP@biotin

5.3.2 Sonication

Due to "strange" flow of the nanoparticles, formation of very deformed front of nanoparticles (as we can see on figure 5.25) and to a residual colouration of the membrane, sonication was tested to disperse the aggregates that formed in solution. Unlike for MNP@Neutravidine, the sonication induced visible change during the tests. The flow proved to be much more uniform with sonicated nanoparticles. It was thus decided to sonicated the MNP@biotin before running a test or spreading it onto the conjugate pas buffer. We can see on the following figures (5.26a) the mean of the 3 measures taken with the DLS to assess the impact of sonication. The sonicated nanoparticles seem to have a narrower distribution .

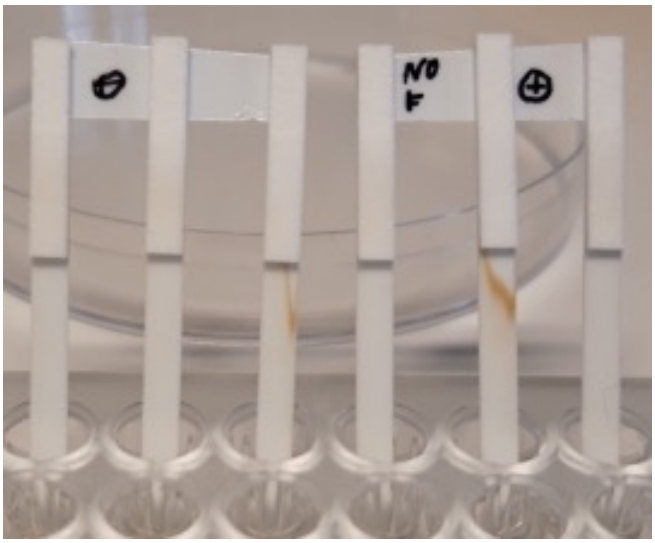

Figure 5.25: "Strange" flow of nanoparticles, deformed front

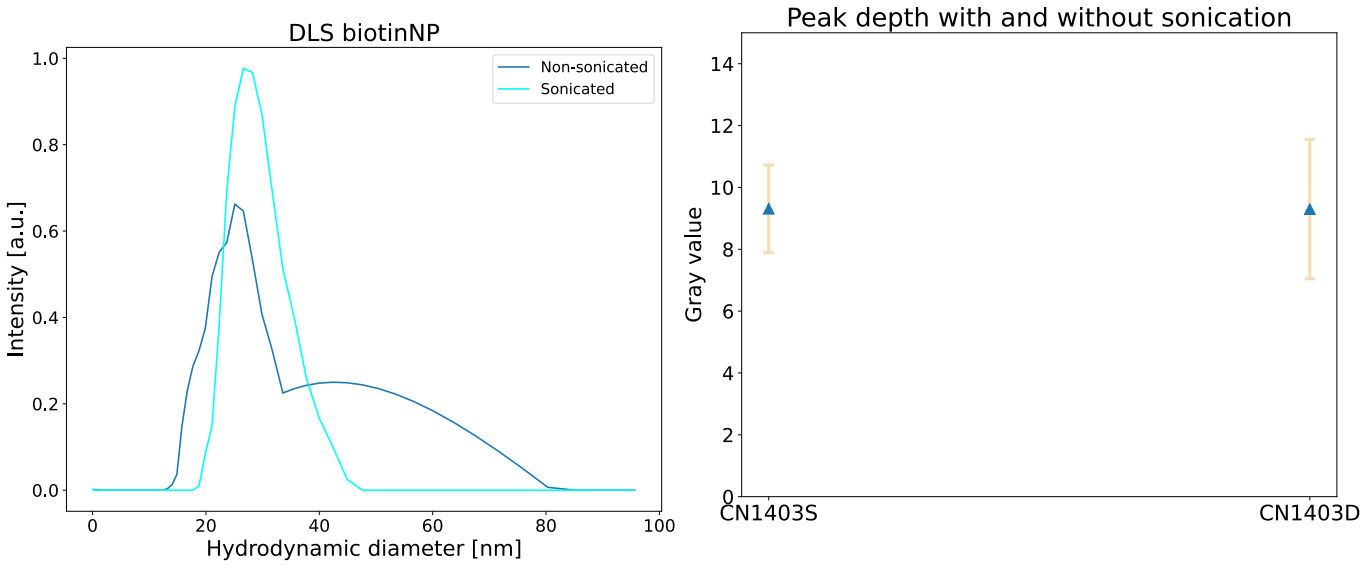

(a) DLS measures of sonicated and non-sonicated MNP@biotin in miliQ water (dilution 100, 10ng/mL)

(b) Peak depth of the control line for sonicated (CN1403S) and non sonicated (CN1403D)MNP@biotin, the membrane is CN140(8 μm pore size)

Figure 5.26: Sonication of the MNP@biotin

On the figure 5.26a, we can see that the peak depth obtained for sonicated and non-sonicated MNP@biotin is similar. This test was done with CN140 membrane, because as we will see, CN140 allows to have more visible control line. We can notice on figure 5.26b that the values obtained are lower than for MNP@Neutravidine this can is due to the fact that all the dot is coloured, diminishing the intensity of the signal. After obtaining the control line, the conjugate pad and absorbent pad were added. The conjugate pad buffer used is the same than for MNP@Neutravidine: 10 μg of MNP@biotin (1mg/mL, initial solution) in 90μL of 1% BSA, 0.5% Tween 20 in 0.01M PBS for a triplicate (15mm of conjugate pad). This buffer promote a good resolubilisation, nanoparticles were observed leaving the conjugate pad without aggregates formation.

5.3.3 Maximum achievable signal

As for the MNP@Neutravidine I tried to obtain a strong signal at the control line in order to have a maximum of nanoparticles to test with the magnetic reader device. For the MNP@biotin the concentration of nanoparticles was increased to 15 μg per triplicate (5 μg per stick of 5 mm width) but only one concentration was tested because in previous tests a significant part of the nanoparticles were observed to go to the absorbent pad and for concerns about having enough MNP@biotin for all the conditions. 6 streptavidin concentrations were tested (0.25, 0.5, 1, 2, 5, 10 μg/mL) on 2 nitrocellulose membranes CN95 and CN140. The streptavidin (0.8μL dot of the second streptavidin (189730 Streptavidin Merck Milipore)) was loaded only once then dried in oven at 37°C for 2 hours. We can see the results on figure 5.27 and 5.28. First we can note that the results obtained with this streptavidin are better than with the previous one where 3 dots at

1mg/mL were required to clearly see the control line. In addition, we can see that the CN140, membrane having smaller pores (8μm compared to 10-12μm for CN95), achieve higher peak depth, meaning more visible dots. Finally we can notice that after a certain concentration of streptavidin the signal seems to stop increasing, 2 μg/mL for the CN95 and 5 μg/mL for the CN140 membrane.

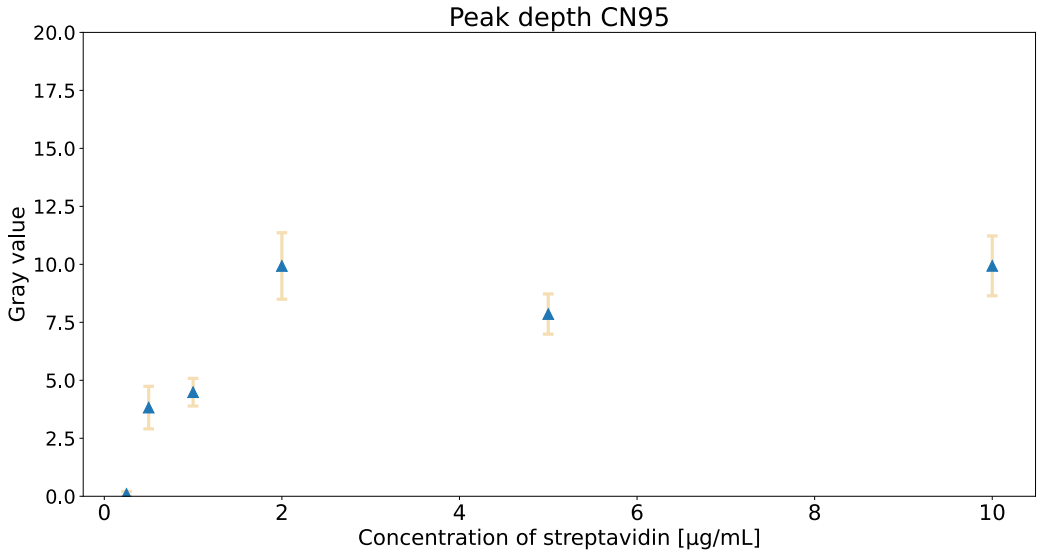

Figure 5.27: Gray value peak depth at control line with CN95

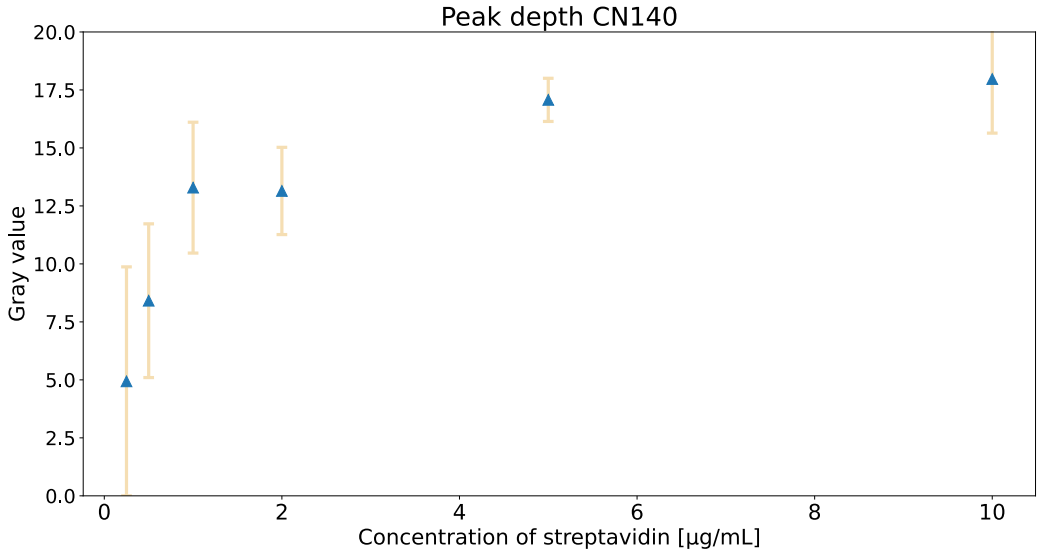

Figure 5.28: Gray value peak depth at control line with CN140

5.4 Functional LFA detecting streptavidin in solution

In order to go a step further and to see if the prototype of lateral obtained was able to detect an analyte in solution, an attempt was made to achieve a "functional" LFA. At test line of biotin-BSA was thus added and 140μL with concentrations of 0, 50, 100 and 500μg/mL of streptavidin were poured onto the sample pad. Those concentrations are quite important especially regarding the concentration used for the test at end of the formation with the AuNP. We can see the result on the figure 5.29. Although we can observe some features indicative of some problems like the dot of the control line of the blank stick which is not filled or the line in the middle of the membrane on the right stick which reveals an aggregation or an overflow problem, we can see that the streptavidin was successfully detected for the different concentrations. The lateral flow stick hence obtained thus able is able to detect the streptavidin in solution with a limit of detection of 50 μg/mL.

Figure 5.29: Functional LFA with from left to right: blank witness, 50μg/mL, 100μg/mL and 500μg/mL

Chapter 6

Discussion

In this chapter are discussed the factors influencing the design of a lateral flow assay with magnetic nanoparticles highlighted by results previously presented. In a first time the specificity and the outcome of the experiments AuNPs in comparison to the MNPs. Then a comparison is drawn between the MNP@Neutravidine and the MNP@biotin based lateral flow assay. Finally the limitations of this work and future perspectives are addressed.

6.1 Comparison MNP's/AuNP's

Besides familiarising with the process, the equipment and good manufacturing practises and even if it ended on bad note with results that were not expected, several points can be highlighted and points of comparison can be made between the training on AuNPs and the design of lateral flow assay with MNP@Neutravidine.

6.1.1 Blocking the membrane

Although the same process was applied to block the membrane with bovine serum albumin, i.e. passivate/block the membrane to reduce non-specific binding, different outcomes were obtained with the 40nm AuNPs and the 1μm MNP@Neutravidine. Evidence of the BSA reducing non-specific binding was observed. Without running buffer the agglomeration/colouration of the membrane was more spread than without blocking indicating a slightly better flow as we have seen on figure 5.8. But when tested with a suitable running buffer or in full stick, blocked membrane did not enable a flow good enough to obtain a control line. Whereas for AuNP the blocking of the membrane did not led to an significant improvement but did not led to a downgrade either as we saw in figure 5.2. According to Parolo and al.[29], BSA given its high molecular weight (66kDa) should no be used when the capture bioreceptor have a molecular weight under 50 kDa. With the AuNP this is not a problem since the human IgG antibodies used for the control line have a molecular weight of approximately 150 kDa [82]. The capture bioreceptor of MNP@Neutravidine should not cause problem because it is biotinylated BSA with a molecular weight of 66 kDa. The main hypothesis is linked to the size of the neutravidin coated nanoparticles. When blocking the membrane, if the washing step is not efficient enough some excess BSA can stay in the membrane and even clog the pores. This might have append to a certain extend letting enough space for the small 40 nm gold nanoparticles and not enough, hindering the flow too much, for the 1 micrometer

MNP@Neutravidine. Unfortunately, the blocking was not tested with the 10 nm diameter biotin coated magnetic nanoparticles to corroborate this assumption. Another way to reduce the non-specific binding would be to put blocking agent in other parts of the stick (sample pad or conjugate pad) or to multiply the number of blocking agent. Some articles state that it is generally better to use low concentrations of several different blocking reagents rather than one reagent at a high concentration [65].

6.1.2 Conjugation of the nanoparticles

Although I did not conjugate the iron oxide nanoparticles, the training on AuNP highlighted the significance of this step for the proper operation of a lateral flow assay. Changing the concentration of bioreceptors can lower the non-specific bindings during the tests. Besides optimizing the detection bioreceptor concentration can also improve the sensitivity by increasing the capture efficiency as described by Poonlapdechaa and al. in "*Antibody-conjugated ferromagnetic nanoparticles with lateral flow test strip T assay for rapid detection of Campylobacter jejuni in poultry samples*" [83].

6.2 Iron oxide nanoparticles

6.2.1 Suspension media

Beside the coating, the stability of the nanoparticles can be affected by the ionic strength and pH of the solubilisation media. Different media were assessed to see if one could lead to better results with LFA by preventing or impeding the aggregation of nanoparticles. The MNP@Neutravidine was diluted in different storage buffer: miliQ water, in phosphate buffer saline (PBS) 0.01M (to have fix 7.4 pH and some ions in solution to interfere with the interaction between surface charges of the nanoparticles as done in several work [84] [85]), in 1%(w/v) BSA as done in [86] and in the running buffer (10 mM PBS pH7.4, 0.5%(v/v) Tween-20 and 1% (w/v) BSA). We have to keep in mind that the when it was diluted (generally by a factor 10), a fraction of the initial commercial suspension was also present in the solution.(For MNP@Neutravidine it contained 50 mM Tris pH 8 as buffering agent, with 150 mM sodium chloride (NaCl), 0.05 % sodium azide (NaN_3) as preservative and 0.1%Tween20 as detergent. The only information I have for the suspension of MNP@biotin is water but it is unlikely that it is the only component.) To assess the influence of those, some nanoparticles were "washed", in miliQ water and in PBS 0.01M. In short, the storing buffer did not showed tremendous effects. The miliQ water gives slightly better results overall although it seems to present bigger aggregates on DLS measurements and it was visually assessed that MNP@Neutravidine tend to sediment faster in miliQ water suspension. This could be explain by the small number of those bigger aggregates who would not have a great impact on the flow. Besides the sonication in the sample pad buffer could shuffle the cards.

6.2.2 Buffer

Apart from the blocking buffer already discussed, 2 buffers were used with the lateral flow assay: the running buffer (0.5%(v/v) Tween-20, 1% (w/v) BSA in 0.01M PBS pH7.4,) in half-stick

format and the conjugate pad buffer (5% (w/v) sucrose, 1% (w/v) BSA and 0.5% (v/v) Tween 20 in miliQ water) in the full-stick format. The tests made with those buffers and their variants allowed to highlight the importance of certain components.

Tween 20 Tween 20 is the commercial name for polyoxyethylenesorbitan monolaurate. As we saw in the results (see 5.2.1), the Tween 20 proved to be crucial to obtain an adequate flow of nanoparticles allowing to get a control line. Without Tween 20 no control line was obtained. The experiments also demonstrated that increasing the concentration of Tween 20 led to less visible aggregation on the stick but also diminished (or prevent for 2%(v/v) Tween 20) the binding of MNP@Neutravidine at the control line. The Tween 20 is a detergent, amphiphilic chemical component composed of a hydrophilic polar and a hydrophobic apolar region as we can see on figure 6.1 [87]. Due to its chemical structure, it has surfactant properties: Tween 20 is able to reduce the interfacial tension. As a chaotropic agent, the Tween 20 can also interfere or break non-covalent interactions (hydrogen bonds, dipole-dipole interactions, hydrophobic interactions) [34]. Those properties are put into profit to prevent aggregation, and reduce non-specific binding and adsorption on the membrane by preventing the proteins from coming into contact with the nitrocellulose at the molecular level [36]. However Tween 20 may also affect the affinity of bioreceptors, so their use must be carefully considered [65]. It is probably what happened with the 2% Tween 20. This too high concentration prevented non specific binding, resulting in visibly less coloured membrane but its chaotropic effect may have impeded the formation of a control line, either by preventing the neutravidin/biotin binding or by breaking the bounds between the biotin-BSA and the membrane.

Bovine serum albumin (BSA) BSA is a stable, moderately non-reactive protein which is used in the LFA framework to bind on active site and prevent non-specific interaction. The impact of BSA is less evident in this work. The blocking of the membrane was already discussed, it did reduced the non specific interactions but did not allowed to obtain a control line for the MNP@Neutravidine. When it is not used in the running buffer (half-stick format) the peak depth at the control line does not seems impacted (or is slightly bigger). In the conjugate pad buffer however the control line obtained was darker when including BSA. This can enter in contradiction with "*Consideration for product development*" from Merck Milipore [34] which states that it is not advisable to dry the detector reagent into the conjugate pad in the presence of blocking proteins or detergents especially if the detection bioreceptor is not covalently attached to the nanoparticle. The reason is that exogenous proteins could displace the detection bioreceptor from the nanoparticle during a prolonged storage. This is why they prefer putting those agents in the sample pad, which could be tested on this prototype. They do not mention however the stabilizing agent (such as succrose) which is supposed to protect the capture bioreceptor.

Sucrose Sucrose (sometimes called saccharose) is a sugar formed by a glucose and a fructose molecule as we can see on figure 6.1. It forms a hydrated glaze, which is solved easily and quickly when aqueous sample enters the conjugate pad [32]. It has proved to be an essential component for the proper resolubilization of the functinalized nanoparticles dried in the conjugate pad. Indeed during the training we mistakenly took glucose instead of sucrose and it led to an aggregation of the AuNPs nanoparticles on the beginning of the membrane. The same conjugate pad buffer was successfully used for the 3 types of nanoparticles (AuNP 20 and 40nm, MNP@Neutravidine

and MNP@biotin). When properly (and completly) vacuum dried it enabled the release of the conjugated nanoparticles.

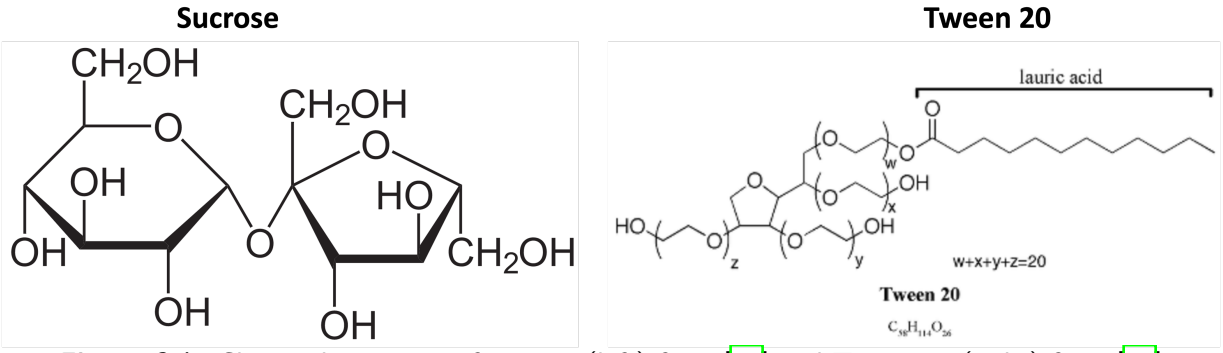

Figure 6.1: Chemical structure of sucrose (left) from [88] and Tween 20 (right) from [87]

6.2.3 Sonication

Both MNP@Neutravidine and MNP@biotin were sonicated to promote monodispersion of the nanoparticles avoiding putting aggregates onto the conjugate pad buffer. Optically the consequences of sonication was not observe on the flow of MNP@Neutravidine but it greatly improved the flow of MNP@biotin, the front of nanoparticles being more uniform and their flow more constant. When observed with dynamic light scattering (DLS), the sonicated nanoparticles seem to have globally a more tight hydrodynamic size distribution with less bigger size aggregates than without sonication as we can see on figures 5.26a and 5.16. However the impact seems to be less obvious for the neutravidin coated nanoparticles especially in PBS suspension. This could be due to some impurities in the solution or to the time between the sonication and the DLS measurements. Indeed, the firsts measurements were done about 20 minutes after the sonication, the time get to the lab with the DLS equipment and beginning the analysis. We can notice on the figures presenting the impact of the sonication on MNP@Neutravidine (5.16) some small peaks around 100-200 nm. If this is not an artefact it could be revealing of damage induce to the coating especially if we have in mind the factor 10^6 due to the processing to obtain the hydrodynamic size explained in the section 4.3.2, the phenomenon could more important that it seems at first sight. The ultrasonication can indeed have deleterious effects on chemicals. In "Ultrasonic dispersion of nanoparticles for environmental, health and safety assessment: issues and recommendations" by Taurozzi and al. [71], it is reported that sonication is able to induce damage on proteins and enzymes, e.g. ultrasonication was shown to damage the BSA structure, and even to impact surface coating of nanoparticles (loss of the coating was sometimes reported). In other work the sonication slightly increased the metal release from the nanoparticles, although this is for bare nanoparticles [89]. We have therefore to be cautious with sonication, but in this work its impact was globally positive: lighter colouration of the membrane, better flow of the MNP@biotin. However it did not lead to a more visible control line for MNP@Neutravidine in PBS buffer and forMNP@biotin and it led to a decline of the signal for the MNP@Neutravidine in miliQ water suspension which may resume from the impact on the coating.

6.2.4 Membrane type (CN95 or CN140)

In this work 2 types of nitrocellulose membrane were tested, CN95 with nominal pore size of 10 to 12 μm and CN140 with nominal pore size of 8 μm. Their impact on the flow is obvious hence assays with CN140 membrane took longer to be completed (absorbent pad fully wet).

The comparison between the membrane with the MNP@Neutravidine (1μm diameter) highlight the problem linked to the size of these (nano)particles. Indeed the flow of those 1 micron large particles on the CN95 proved to be a bit poor because of the large colouration on the membrane outside the detection zone. Those non specific bindings increased substantially with the use of CN140 having smaller pores. This demonstrate the significance of the size of the pore and the flow speed. A membrane with bigger pore size (Merck's HI-Flow Plus HF075 with pores of 12 - 17 μm) was ordered but arrived too late to conduct experiments [1].

With the MNP@biotin the 2 membranes allowed good flow of the nanoparticles, no difference was observed in the flow of nanoparticle depending on the membrane. However the control dots are more visible/coloured on the CN140 membrane. This can be due to 2 factors. The first one is that having a slower flow speed, the MNP@biotin had more time to bind to the streptravidin fixed on the membrane. This effect should though be minor due to the high affinity between biotin and streptavdin. The second factor is that smaller pore size grants higher surface to volume ration hence more surface to fix capture bioreceptor [90].

6.2.5 Fixing the control line

The stripping of the control line, i.e. the good adsorption of the capture bioreceptors on the nitrocellulose membrane, did not cause problem at first sight for the training with antibodies (IgG and anti-IgG) or the biotin-BSA that bind to MNP@Neutravidine. The hypothesis that the dots are not fully coloured (quarter moon dots) because of a non-uniform distribution of the biotin-BSA can be discarded because, as we saw with the prototype detecting streptavidin in solution with MNP@biotin (figure 5.29), the test line is not quarter moon shaped even though it is also biotin-BSA loaded in a similar manner. A more likely explanation is related to the size or aggregation of the nanoparticles as we will see in the next section.

Problem arose with the streptavidin control line for the MNP@biotin. After following the process done by Mohammed and al. in "*Lateral flow aptasensor for progesterone: Competitive target recognition and T displacement of short complementary sequences*" [80] which consisted in applying streptavidin at 1 mg/mL dissolved in miliQ water no control line was obtained (on CN95 with streptavidin S4762 from Sigma Aldrich), the membrane was dried 20 minutes at 37 °C. It is only letting dry in the oven for 2 hours at 37 °C that a coloured dot became slightly perceivable. To see the dot more clearly, I then increased the concentration of streptavidin to about 5mg/mL as done in "*A strip of lateral flow gene assay using gold nanoparticles for point-of-care diagnosis of African swine fever virus in limited environment*" [81] by Wang and al.

[1] The HF75 finally arrived the week before submitting this report. The result obtained with this membrane having a bit bigger pore size is available B. It does not change the elements presented in the discussion.

In this way I was able to obtain coloured dots for the control line and even for the test line with the functional prototype detecting streptavidin. We saw that the type of membrane influenced the colouration of the dot, smaller pore size allowing more capture bioreceptors to bind. Another parameter could have increased the amount of bioreceptors able to be adsorbed on the membrane, improving the result obtained. The adsorption of proteins on the nitrocellulose governed by noncovalent interactions. It is not clear if it is due to hydrophobic interaction between the nitrocellulose and hydrophobic portion of the protein or to electrostatic interaction between the dipoles of the nitrocellulose nitrate groups and dipoles within the protein [91] although the later one is thought the be preponderant. That being said, if the bioreceptor is loaded on the membrane in a buffer with a pH close to its isoelctric point, pH at which the total charge of the molecule is null, it can increase the adsorption to the membrane for 2 reasons. Firstly, the proteins are strongly hydrophobic at their isoelectric point so the hydrophobic interaction with the nitrocellulose can be favored. Secondly, at the isoelectric point the electrostatic repulsion between capture bioreceptor is very low allowing to form densely packed protein layers on the membrane [90]. A way to improve the results obtained in this work would thus be to load the biotin-BSA in a 4.7 pH buffer and the streptavidin in a pH buffer about 5, their isoelectric point, more bioreceptors should be able to fix to the membrane leading to more nanoparticle able to bind at the control or test lines.

6.2.6 Size of the nanoparticles

The two types of nanoparticles used in this worked had very different diameter size, 1 000 nm for the MNP@Neutravidine and 10 nm for the MNP@biotin. As a matter of fact, the word 'nanoparticle' usually defines particles with a diameter smaller than 100 nm, its use to define the MNP@Neutravidine in this work is thus an abuse of language. As we saw in this work, their sizes strongly influenced the LFA prototype.

Impact on the flow As the diameter increases, physical resistance to flow in the porous membrane increases. That way, particles with a diameter of 0.5 μm or greater are restricted in their usage to medium- to fast-flowing membranes with bigger pore size. The same restriction apply to colloids that form larger aggregates [31]. This slower flow of big particles promotes the non-specific binding with the membrane which, beside the simple clogging of the pore and the better optical detection of bigger particles, may explain the colouration of the membrane observed with the LFA prototypes using MNP@Neutravidine.

Impact on the detection (optical) The size of the nanoparticles considered in a LFA can have repercussions on the detection whether optical or magnetic. Indeed bigger particles are usually more visible on nitrocellulose membrane. Khlebtsov and al. found the following relationship between the dot intensity (I_{dot}), the surface density of the nanoparticle (N_d) and the diameter of the particle (d) [92]:

$$I_{dot} = K \cdot N_d \cdot d^{3.1}$$

with K a constant. This relation can not be applied as such to this work because in their work, Khlebtsov and al. used AuNPs with size ranging from (16-115 nm) and that the size of the gold nanoparticle influence their surface plasmon resonance. However it highlights a tendency which

is also reported for iron oxide nanoparticles as in Liu and al. "*Lateral Flow Immunochromatographic Assay for Sensitive Pesticide Detection by Using Fe3O4 Nanoparticle Aggregates as Color Reagents*" [93] where bigger size aggregate were reported to lead to great improvement of the visual detection limit both because of slower flow and better visibility. This goes into explaining why membrane colouration was more pronounced with MNP@Neutravidine (alongside the membrane type and fixation of the control line already discussed) and why the gray value peak depth reached (for same concentration of the capture bioreceptor and nanoparticles) was bigger with those.

Shape of the dots An very important parameter to explain the bigger gray value peak depth reached is the shape of the coloured dots. Indeed for the MNP@Neutravidine the dots were not fully coloured but 'quarter moon coloured' whereas such patterns was not observed for MNP@biotin for which the signal was less localized and coloured all the dot. During the training such colouration was also observed with AuNP in some experiments. The main hypothesis is linked to the size of the particles or agglomerates. Due to their big size with respect to the pore size, the first particles (or aggregates) that bind at the control line clog the pores sufficiently to block the following particles which pile up and bind non-specifically. If this hypothesis is verified, it would mean that aggregation occurred during the training when such pattern was observed. We can also take it into consideration while assessing the impact of sonication. The results of sonication were less good for MNP@Neutravidine than for MNP@biotin, if sonication did reduce the aggregation of MNP@Neutravidine it could have led to a less localized clogging of the pore. More particles able to go through the dot limi before it becomes too clogged, spreading a bit the quarter moon shape leading to less localized signal and smaller gray value peak depth. This however seems a bit unlikely because of the short time of appearance of the the quarter moon. Indeed the control line is becomes visible some dozens of seconds after the front of water goes through the dot. This clogging of the pores by the nanoparticles would render a detecting LFA inoperative, the nanoparticles will stop only at the first control or test line depending on the format of the lateral flow assay.

Impact on the detection (magnetic) Although I did not investigate the magnetic properties of the iron oxide nanoparticles used in this work, we should not lose sight of the magnetic detection goal. Indeed the size of the nanoparticles can have an impact. First bulk iron oxide is a ferrimagnetic material, i.e. it exhibits remnant magnetization when not exposed to external magnetic field. It is a properties that would lead to agglomeration of particles in colloidal suspension. The iron oxides nanoparticles are interesting because they are superparamagnetic when their size is close to the one of magnetic domains (below 50nm) [60]. It is difficult to say if the MNP@Neutravidine used are completely superparamagnetic, they have a big size but the proportions of magnetite, polystyrene core and polymer coating are not known. If it is not due to their big size, a small remnant magnetic field could be at the origin of their fast sedimentation. Beside those considerations, one of the key factors in magnetic detection is magnetic susceptibility (ξ) for small fields and saturation magnetization (Ms) for large fields. A stronger magnetic moment (high Ms) offers higher sensitivity toward a magnetic reader [47]. The saturation magnetization increases with the size of the nanoparticles (and with the magnetic content) [94].
More over on the surface iron oxide nanoparticle there is dead layer, a part which has not the same magnetic properties than the bulk of the nanoparticle. This dead layers is approximately 0.9 nm width [95]. This is due to the crystalline structure that is perturbed by the close surface.

In nanoparticle of 5nm diameter, this represent a non negligible part of the nanoparticle volume that do not possess the magnetic properties expected. As for the the magnetic susceptibility it is normally constant for superparamagnetic but it also evolves with the size of the magnetite nanoparticle once bigger than 50 nm. The size is thus a parameter that should be optimized in regards to its other impacts on the superparamagnetism or flow speed. To have more magnetic nanoparticles on the test line an interesting way is to synthesize multi-core particles that have the advantages of superparamagnetism and a bigger magnetic content in a size controlled nanoparticle [60].

6.3 Limitations of the work

The purpose of this work was not to detect analyte of interest in real life application but to design lateral flow assay prototypes based on iron oxide (nano)particles to have a first experience with magnetic nanoparticles in the lab and to assess further the results obtained with the magnetic reader. To this end the complex biotin/streptavidin (and Neutravidin/bioin) was used. This is because of their high affinity that it was decided to use them, but, as we can see on the figure 6.2, those 2 molecules have a dissociation constant several orders of magnitude higher that the bioreceptors used in real-life applications. We should therefore keep in mind that in real life application the lower K_D could prevent the use of fast-flowing membrane with big pores.

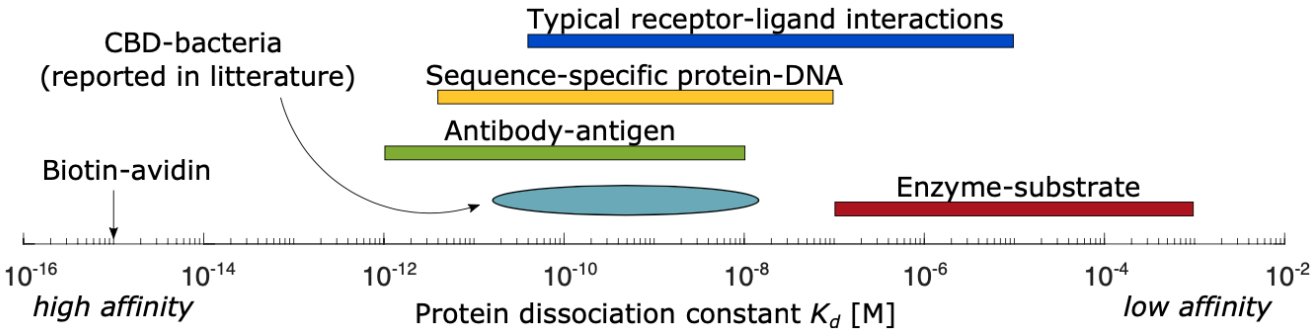

Figure 6.2: Dissociation constant of biotin-avidin compared to other molecules that are used for real application, CBD for cell binding domain (from phage protein), image from [70]

A major limitation in this work is the way to assess and treat the results obtained with LFA sticks. First the results were assessed optically, with the use of image processing software (imageJ) for the semi-quantitative measurements. It implies that the limitation of optical detection impact the way the results are assessed: we only have access to the 10 μm at the surface of the membrane so we have no insight of what happens in the bulk of the membrane (e.g. non uniform distribution of the bioreceptor along the depth), the optical limit of detection applies (not possible to detect non specific binding on the membrane below this limit), the appearance of the stick depends if it is wet or dry, ... Secondly, the semi-quantitative measurement were done on basis of photos taken sometimes a long time (2 months) after the the flow test on dry stick because the photos done at the time of the test flow were subjected to artefacts. It is only with the use of the black box described in section 4.4 that the artefacts were reduced enough to allow semi-quantitative measurements but as we saw this method is not perfect either, leading to (relatively small when

compared without the box) variations of the gray value peak depth obtained for a same stick.

On the outcome itself, prototypes of LFA strips using iron oxide nanoparticles were obtained and could be used to test a magnetic reader. However the sticks with MNP@Neutravidine with their high non-specific binding onto the membrane will increase the noise. The sticks using MNP@biotin will probably lead to less noise but also to less signal, the nanoparticles being smaller. A possible way to increase the signal would be to load the capture bioreceptor at their isoelectric point as previously explained. Lastly the functional LFA detecting streptavidin was tested with quite high concentration of streptavidin in solution as proof of concept. This functional LFA could be optimised (bioreceptors at their IEP, blocking, optimizing the amount of capture bioreceptor,...) in further experiments to lower its limit of detection (LOD). Once the visual limit of detection assessed, if the magnetic reader developed is able to have a lower limit of detection, it would be a nice achievement for the team and a step towards a water monitoring lateral flow assay based on magnetic nanoparticles.

6.4 Future concerns

Some observations made during the realisation of this work allowed to highlight some interesting points or concerns that will need to be considered in further steps of the development of lateral flow assay. Some are discussed in this section.

6.4.1 Size of the bacteria

The flow issues with the 1 μm large MNP@Neutravidine raise concerns to the ability to achieve a good flow with whole bacteria cells. Indeed bacteria are micron sized organisms, E.coli that is used as an indicator for water quality is a rod shaped bacteria that can measure up to 3 μm long and 0.5 μm large [13]. Such bacteria, especially if nanoparticles labels are attached, could suffer from slow flow which promotes non-specific binding or just clogs the pores of the membrane. Of course faster-flowing membrane with bigger pore could be used to prevent this effect but as we saw in this work, this choice have other repercussions such as reducing the membrane capture bioreceptor loading capacity which could reduce the limit of detection. In order to promote the flow of micron-sized bacteria it would surely be necessary to optimize the membrane pore size in combination with appropriate surface modification with regards to their impact on the other parameters [96].

6.4.2 Inter-sticks variation

Some variation between sticks that were manufactured the same way was observed by looking at the standard deviation of the triplicates on the graphs. Obviously any performance variation between sticks should be avoided, especially for quantitative detection. It will thus be needed to minimize the outcome differences that we can obtain. To do so, good manufacturing practices need to be followed: homogenize solutions, clean work space, avoid contamination, avoid inducing damage to the membrane,... Automation and manufacturing tools can be of great use to improve strip-to-strip reproducibility [31]. For example, in this work choice has been made not to use the control and test line dispenser device other than for the training because of the complexity, the

relative small number of LFA produced each time (usually 3 per parameter tested) and the waste of capture bioreceptor solution linked to the use of this device. Instead the test and control lines were dotted onto the membrane but this can lead to variation in position of the dot, size and shape of the dot or even induce damage of the membrane if the tip of the micropipette touches the surface. In quantitative lateral flow assay, the use of such tool would be of great interest. Aside from manufacturing the sticks caution can be given to the storage conditions and to the housing cassette which can prevent a flooding of the stick when the sample is applied [36].

6.4.3 LFA storage conditions and conservation

Usually the flow tests and the manufacture of the sticks was done the same day in this work. Once, the conjugate pad was done and dried a day before assembly of the LFA and stored into the fridge. It was either not well dried or the fridge was quite humid because the following day, the conjugate pad was partially wet rendering it unusable. This highlights the importance of the storing conditions (dry environment, no exposition to light) that could have deleterious effects on the membrane, capture bioreceptor or functionalized nanoparticles. Moreover, the possible variations of the outcome of the test due to long term conservation should be assessed and taken into account or prevented in the framework of quantitative LFA.

6.4.4 Global considerations for large scale use

It was not a part of this work but we should not lose sight on the framework in which lateral flow assays are to be used. It must be part of a more global management strategy. For example, for water quality monitoring LFA would be one tool among others and must be part of a plan that brings together several actors to ensure that monitoring is effective, results are reported, risks are assessed and that actions are done if necessary to ensure the safety of all the people relying on the incriminated water source. The world health organisation (WHO) issued guidelines that explain precisely the parameters to take into account for ensuring water quality, and what should be done in case problem is detected [2]. We can also take advantage from the return of experience of large scale use of LFA during the COVID-19 crisis. For example we know now that in low-, middle- and high-income regions, COVID-19 lateral flow assays self-tests have shown high acceptability from the public although some concerns about their wrong utilisation due to inadequate educational intervention were reported [27]. However generally a small percentage of the outcome of the tests were reported (e.g. 14% in the United-Kingdom) which increases the difficulty for the authorities to have a global view of the situation [25]. For qualitative lateral flow assay, a solution to remedy this problem would be to give to the reader the capacity to report the outcomes of the tests, maybe via the use of a smartphone, ensuring a real REASSURED device (Real-time connectivity, Ease of specimen collection, Affordable, Sensitive, Specific, User-friendly, Rapid and robust, Equipment-free or simple, and Deliverable to end-users [8]).

Chapter 7

Toxicity

Into the literature, concerns about the toxicity of Iron oxide nanoparticles (IONPs) are highlighted. At first sight the toxicity of iron oxide nanoparticles seems less straightforward or worrying that other types of nanoparticles like silver nanoparticles (that are well known and used for their bactericide properties) or other magnetic nanoparticles (Zn, Co, FePt, FeCo...). The use of iron oxide nanoparticles was even sometimes promoted because of their low toxicity compared to those other magnetic nanoparticles [47]. I found interesting to dig a bit into this subject in order to have a better perception of IONP related toxicity. The goal of this part is thus not to determine the toxicity of the particles used in this work but only to give an overview on the possible problems linked to the iron oxide nanoparticles usage in a lateral flow assay framework.

7.1 Toxicity of iron oxide nanoparticles

Some apparently contradictory information can be found in the literature. Iron oxide nanoparticles, due to their interesting properties, are being considered for numerous biomedical applications such as a contrast agent for magnetic resonance imagery (MRI), targeted drug delivery vehicles, hyperthermia treatment for cancer therapy (Strategy that use the higher sensitivity to temperature enhancement of cancerous cells. The injected nanoparticles link to cancerous cells and are heated by applying alternative electric field.),... [97] [98]. Several commercial magnetite-based nanoparticles have even been approved by the US Food and Drug Administration (FDA) for clinical use [99]. However, some in vivo and in vitro studies point out the toxicity of iron oxide nanoparticles. This could seems counter intuitive but as a matter of fact the definition "iron oxide nanoparticle" is too vague when talking about toxicity. The reported toxic effects of those particles indeed heavily rely on numerous factors such as their size, coating, shape, concentration, exposure (chronic or acute), roughness of the surface, intake mean, type of cells tested, age of the subjects,... So we cannot conclude on the toxicity of all IONPs but only on some with specific characteristics. Before explaining more in detail the impact of those factors, we will first discover how the nanoparticles are able to induce deleterious effect on living cells.

Cellular toxicity is thought to be mainly governed by reactive oxygen species (ROS) although IONPs might also interfere pore membrane transport or with electron transport processes once internalized [100]. Indeed nanoparticles may adhere to a cell and block essential pores and membrane functions but can also enter the cell by endocytosis, via diffusion through pores (with the

potential for pore stretching or damage), or via ion transport systems. Having entered the cell, the NP can potentially interfere with electron transport processes, or facilitate reactive oxygen species (ROS) production [100]. ROS are chemicals highly reactive which can be generated by IONPs from the nanoparticle surface, via leaching of iron molecules, via alteration of mitochondrial and other organelle functions, or via induction of cell signaling pathways. ROS, such as free radicals like hydroxyl radicals, superoxide anion, and the nonradical hydrogen peroxide, have the potential to affect the protein and lipid materials of the cell, and cellular organelles (mitochondria, nucleus, and endoplasmic reticulum) [99]. Cells have defense mechanisms against those, a low level of oxidative stress enhances transcription of defense genes, leading to increased expression of antioxidant enzymes to combat ROS. But as we can see on the figure 7.1, high ROS levels can damage cells by peroxidizing lipids, disrupting DNA, modulating gene transcription, altering proteins or cytoskeleton and resulting in decline in physiological function and finally to cell death either by necrosis or apoptosis. Aside from cellular death, it can also have a carcinogenic effect. The risk of cancer development increase if the high level of ROS induces damage to the DNA and if no apoptosis results [101] [102].

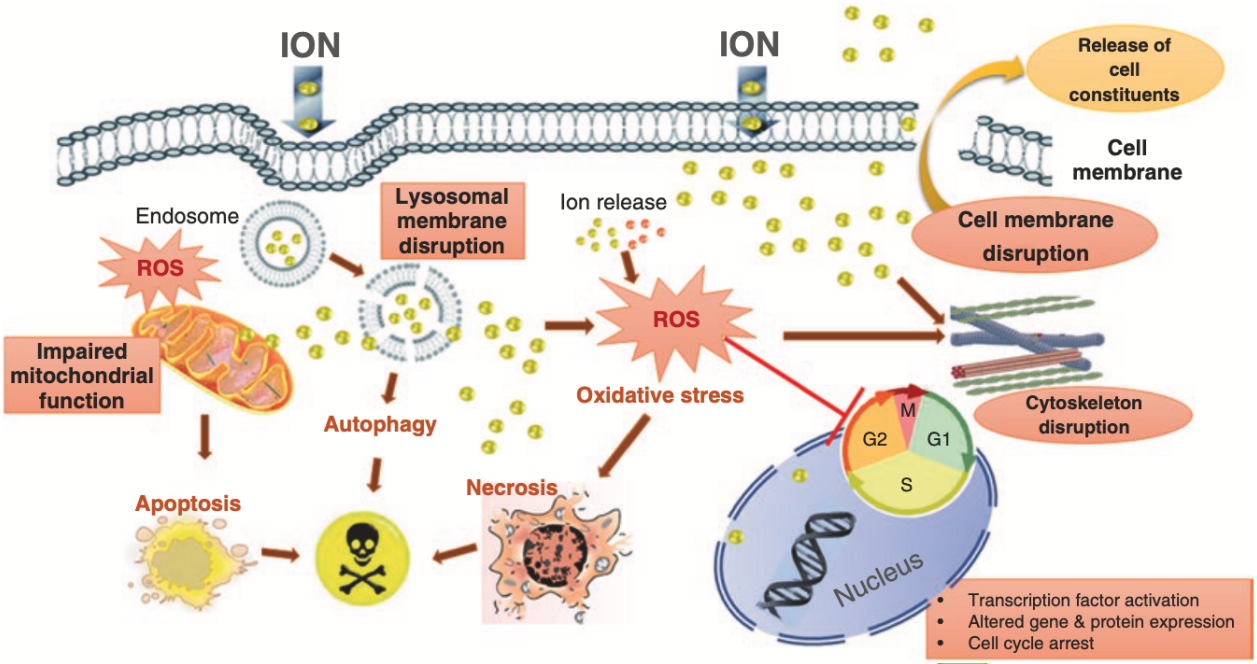

Figure 7.1: Cellular toxicity induced by iron oxide nanoparticle, image from [102]. NOM: natural organic matter

Knowing how cellular toxicity occurs, we can now focus on the characteristics of the iron oxides nanoparticles that affect their toxicity. The principal ones are the size, coating and concentration of the nanoparticles. The table 7.1 sum up characteristics that are related to high toxicity.
The **size** of the nanoparticle is of great significance for the toxic ability of nanoparticles in general. It can impact cellular and body intake, evidence showed that 5-10nm nanoparticle were able to enters through the skin [98]. Similarly the small sized nanoparticles were observed crossing the blood brain barrier (BBB) and blood testis barrier (BTB) [97]. The size can also impact the distribution inside the body. IONPs larger than 200 nm in diameter are rapidly trapped in the

liver and spleen through macrophage phagocytosis, whereas IONPs smaller than 10 nm in diameter are likely to be eliminated through renal clearance [103].
The nanoparticle's **shape** will also have an effect on toxicity in that it has an impact on the leaching/dissolution rate. Rods are reportedly more toxic than spheres due to fast dissolution from points, although a secondary toxicity may exist with sharp edges causing mechanical damage e.g. piercing cell membranes [100]
Beside the size and shape, the **coating** of the membrane plays a tremendously important role in the potential toxicity. The nanoparticles approved by the FDA have resistant coating that hinder their harmfulness abilities. The coating at the surface of the nanoparticle will interact with the cells and determine the cellular uptake, cytotoxicity, distribution and clearance of iron oxide nanoparticles [98]. Obviously a coating that is in itself toxic will worsen the toxicity of the coated nanoparticle. Proper surface coatings can stabilize iron oxide NPs and avoid agglomeration. It is also an efficient way of preventing the leaching of ions that will promote ROS production. The surface charge, charge of the coating, is determinant. Because cellular membrane and intracellular compartments are characterized by negative charge, the positively charged nanoparticles are more internalized than negative ones [99] [94]. Generally, neutral surfaces are the most biocompatible, whereas cationic surfaces are more likely to induce hemolysis, platelet aggregation or opsonisation and phagocytosis of the nanoparticle [101] [103].
The last predominant factor that influences the toxicity is the concentration to which subject or cells are exposed. It obviously depends on the previously highlighted characteristics. Higher concentrations usually lead to higher toxicity. It is important to make the distinction between the acute and chronic exposition, concentration leading to no observe effect on short time could reveal itself toxic on long-term exposition.

	Size	Shape	Coating	Concentration
Characteristics	10-100 nm	Sharp edges	Toxic in itself or positively charged	Mortality for rats at 1.5 mg/kg, zebrafish neurobehavioral toxicity at 10 ppm (14 days exposure)[97]

Table 7.1: Typical characteristics that were identified enhancing toxicity of iron oxide nanoparticles

As we have seen the iron oxide nanoparticles that would be used in lateral flow assay can be toxic regarding to their characteristics. The real effect of the use of IONPs is however difficult to assess, as we have seen it depends on the characteristics of the nanoparticle itself but other parameters are to be taken into account. First experiments done in the literature have limitations, short term in vitro test results cannot be used as a good prognostic indicator of long-term physiological effects. In vitro experiments are attractive because they are more cost-effective, faster, and easier without ethical problems. However cell cultures are extremely sensitive to changes in their environment such as fluctuations in temperature, pH, nutrient and waste concentrations and may not accurately reflect the actual toxicity of iron oxide nanoparticles as they do not adequately represent the functions of 3D tissues that have extensive cell-to-cell and cell-to-matrix interactions [101] [99]. Secondly, in the framework of lateral flow assay, the major possible issues linked to the nanoparticles would result from loss of nanoparticles that would spread into the environment either during the manufacturing process or from used LFA stick, which still contain nanoparticles, abandoned in the

environment. This means that we should take into account the possible transformation endured by the nanoparticle such as depicted in the figure 7.2. This can affect the coating or the aggregation (size of the particle), 2 factors that have a clear impact on the toxicity. Assessing the environmental risk linked to the iron oxide nanoparticles would require large amount of work, but as we will see in the next section processes have been put in place to standardize this type of analysis.

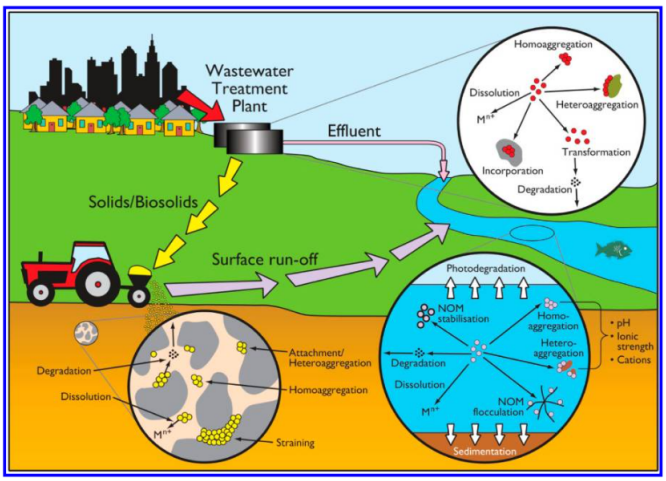

Figure 7.2: Scheme of possible pathways and transformation of nanoparticle in the environment, image from [104]

7.2 Environmental toxicity: risk assessment

In this section we discover more in detail how environmental risks can be characterized and assessed for chemical product (nanoparticles enter this category). The explanation of risk assessment is mainly based on risk assessment part of the course "*LBRTE2201 – Human and environmental toxicology* [105]" given at the UCL which present the REACH (Registration, Evaluation, Authorisation and restriction of CHemicals), risk assassement procedure from the European CHemical Agency (ECHA) European Union although some additional information have been found in "*Predictive Environmental Risk Assessment of Chemical Mixtures: A Conceptual Framework*" from Thomas Backhaus T. and Faust M. [106].

We will first begin by defining the basis, what is a risk. A risk is a hazard, something that can cause harm, and an exposure to this harm. Here the hazard is the toxicity of iron oxide nanoparticle. For risk characterization, we therefore need to identify the hazard and its effects upon exposure. The European Union put in place the REACH (Registration, Evaluation, Authorisation and restriction of CHemicals) which defines the procedures to standardize risk assessment. The risk is characterised by the Risk Characterisation Ratio which is defined as $RCR = \frac{PEC}{PNEC}$, the PEC (Predicted Environmental Concentration) divided by the PNEC (Predicted No Effect Concentration). The risk associated to the use of chemicals and nanoparticle thus increases with the Risk Characterisation Ratio. The assessment is performed for defined tonnage categories: 1-10 ton/year, 10-100 ton/year, 100-1000 ton/year or $>$ 1000 ton/year. The risk assessment is also done for various specific compartments: marine ecosystem, inland aquatic ecosystem, terrestrial ecosystem, atmosphere, microorganisms in sewage treatment systems,... To assess the RCR we

therefore need to assess the PEC and the PNEC. The predicted environmental concentration is thus assessed for specific scales and compartment at the relevant steps of the product life cycle. Several factors can enter in the evaluation of the predicted no effect concentration as we will see.

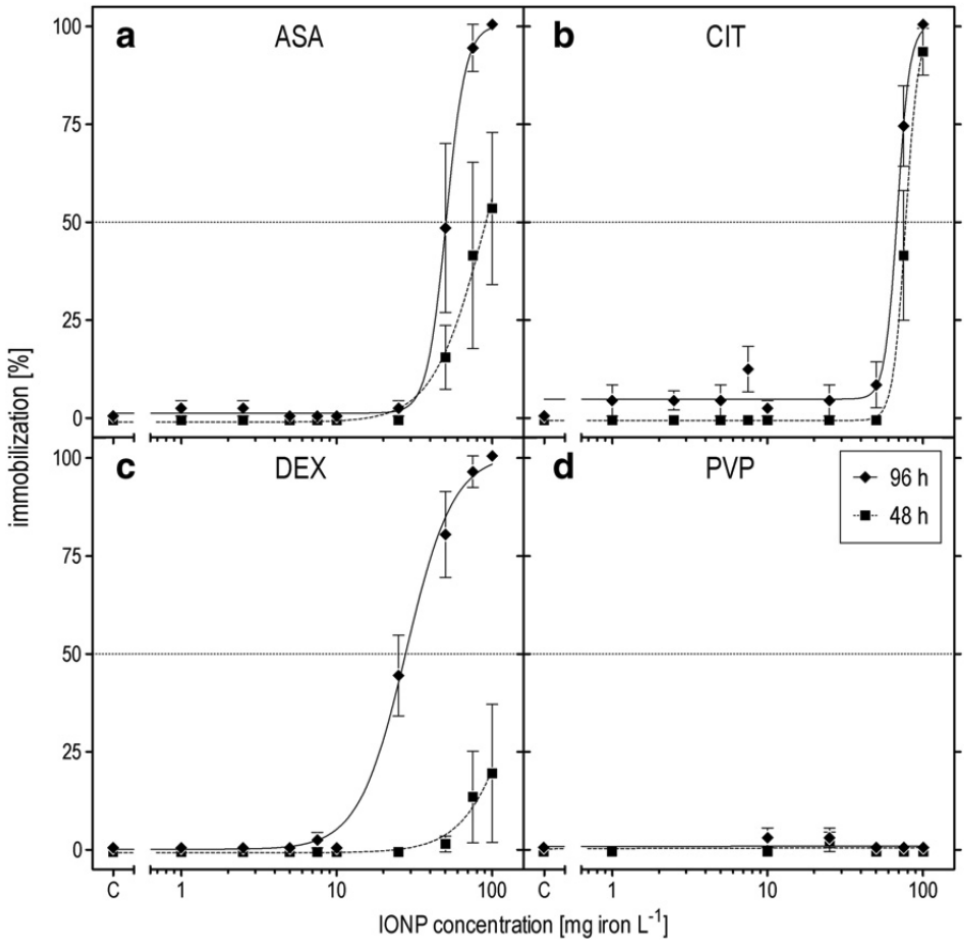

Figure 7.3: Effect concentration 50 for different nanoparticle (5 nm diameter) coatings (ASA: ascorbate, CIT: citrate, DEX: dextran, PVP: polyvinyl pyrrolidone) on daphnia magna crustacean zooplankton, image from [107]

In laboratory we can assess the effect of products on certain species as we can see on the figure 7.3. We can deduce the EC50 (Effect concentration 50), the concentration for which 50% of the subjects demonstrate an indicator (in the figure it is the mobility of *Daphnia magna*, invertebrates which have numerous predators). We can also deduce the no observed effect concentration (NOEC) for that specie in the experiment conditions. However, ecosystems more sensitive to chemicals than individual organisms in the laboratory. Besides, if the nanoparticles or chemicals tend to stay in the body, in real ecosystem there is trophic transfer which can lead to biomagnification, accumulation of products by an organism following consumption of another organism previously exposed [100]. To extrapolate the PNEC from the laboratory obtained data, there are 2 main methods, the SSD (Species sensitivity distribution) and the AF (Assessment factor). The SSD is the more advanced method but it supposes a substantial amount of ecotoxicological knowledge is at hand [106].

The assessment factor method will require tests on several trophic level (e.g. Algae (primary producer) , Invertebrates (primary consumer) , fish (secondary consumer)). The PNEC is defined by the concentration that affects the most sensitive species divided by the assessment factor (AF), an empirically established figure that varies in function of the amount of information available and the compartment/ecosystem considered. Indeed in marine ecosystem for example, there is higher biodiversity, more trophic levels, higher life expectancy of the top predators,... all that encourages greater caution because the effects are more difficult to predict. In this case, another criteria can be associated, the PBT (Persistence, Bioaccumulation and Toxicity) criteria.

We have now a broader view on how is assessed the risk related to the use of a substance for the environment. To achieve a full risk assessment of the use of a specific iron oxide nanoparticle (with its own size, coating,...) it would require large amount of work to assess the toxicity for the different living beings present in the compartment studied and to compute the possible environmental concentration. This is obviously not the goal of this chapter but what we could do is to make a experiment to have better knowledge on which extend the nanoparticles are able to spread into the environment as we will see in next section.

7.3 Retention test

As we have seen, the toxicity of iron oxide nanoparticles depend on several factors among which the concentration of these. The amount of IONPs that could end up in the environment is also of great importance for risk assessment. There are 2 main moments in the life cycle of lateral flow assays that could lead to release of nanoparticle in the environment: losses during the manufacturing or release from used LFA sticks poured into the environment. To gain information about the later one I performed an 'retention test', experience aiming at quantify how easily the nanoparticles could leave the stick and spread into the environment.

7.3.1 Material and methods

The idea of the test is straightforward, immersing used lateral flow assays for different amount of time and quantify the percentage of nanoparticle leaving the stick. To this end, full stick LFAs prototypes were manufactured with 6.67 μg of MNP@Neutravidine per stick in the conjugate pad (20μg/triplicate) as described in section 4.2.3. The test were ran leading to the appearance of a control line and colouration of the membrane and dried over night at ambient temperature. The day after they were immersed in 5mL Eppendorfs tubes (3 LFAs in 5mL 0.01M PBS pH 7.4 at ambient temperature) for several time period and with agitation or not (150 rpm on the shaker), the sum up of the condition is displayed at table 7.2. The 4 and 7 days immersion were not agitated because of convenience. After the indicated duration in immersion, the sticks were removed and a magnet was applied to each Eppendorf over night to attract the nanoparticles and to retain them while removing the media. The next day as just said 4mL were taken from the Eppendorfs and discarded to end up with the nanoparticles in 1mL. The absorbance was then measured with a UV-vis spectrometer, as described in the material and method chapter, to quantify the amount of nanoparticles in the solution. For each condition a blank sample, Eppendorf containing 3 lateral flow assay with no nanoparticle (the conjugate pas buffer was loaded but the nanoparticles were

not added), was done to have a blank measure for the absorbance. The blanks were however forgotten for 4 days and 1 week duration.

	10 min.	30 min.	1 hour	2 hours	6 hours	4 days	1 week
Still water	Yes	Yes	Yes	Yes	Yes	Yes	Yes
Agitated water	Yes	Yes	Yes	Yes	Yes	NO	NO

Table 7.2: Duration of the retention tests performed.

To quantify the amount of iron oxide nanoparticles released from the LFA sticks 2 means were employed. Firstly as for the rest of the work the gray value peak depth at the control line was computed and the difference before and after immersion was to be assessed. Unfortunately the photos taken before immersion are not good enough to do a semi quantitative analysis (not taken in the box to reduce light artefacts). The gray value peak depths at the control line after the immersion are displayed anyway to show the tendency. Secondly, the absorbance of the solutions were measured to assess the concentration of MNP@Neutravidine in solution. To do it several measures of MNP@Neutravidine in solution were taken to find the relation between the absorbance and the concentration. In the spectrum of the MNP@Neutravidine a bump is visible around 420nm as we can see on figure 7.4 and is specific to those nanoparticles. It was decided to take it as reference point. Measures have been taken from solution at 1 μg/mL to 75 μg/mL and then via python an 1D interpolation was computed to convert the absorbance measures obtained with the retention test into concentration of nanoparticles. The reference curve is displayed at figure 7.5

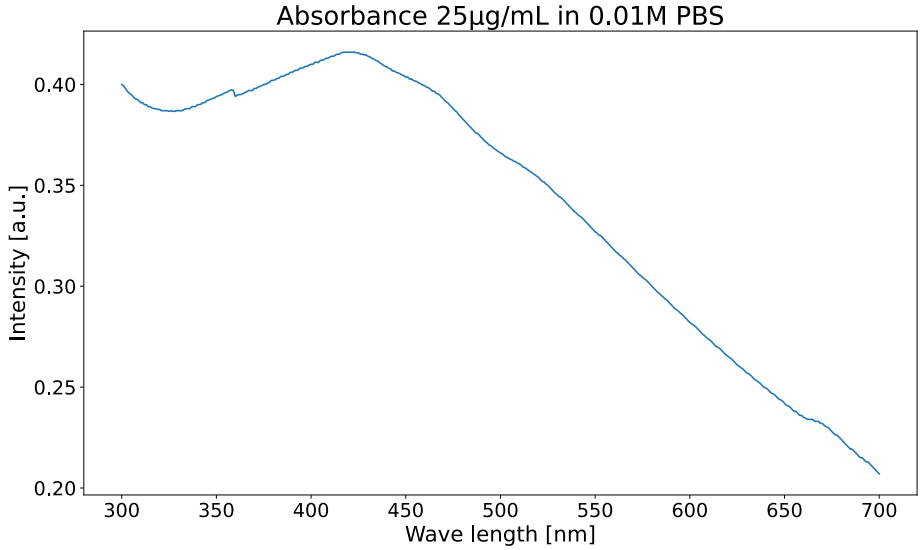

Figure 7.4: Absorbance spectrum of MNP@Neutravidine in 0.01M PBS at 25μg/mL

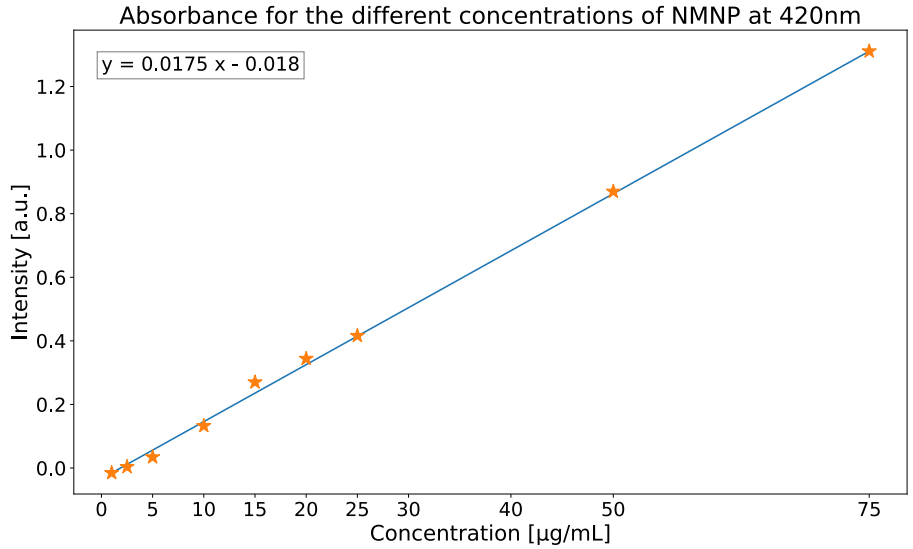

Figure 7.5: Absorbance at 420nm wavelength for different concentrations of MNP@Neutravidine in PBS 0.01M (stars). The blue line is the interpolation.

7.3.2 Results

First we can notice that when removing the surplus media from the 5mL Eppendorfs no (or very little) accumulation of nanoparticles was visible in front of the magnet. All the sample corresponding to sticks immersed less than one day (with or without agitation) had lower absorbance (all nearly identical, close to zero) than the one corresponding to 1 μg/mL so they could not be interpolated. It means that after spending 6 hours under mild agitation, the sticks released less than 5% of their MNP@Neutravidine content. For the sticks which spend 4 days and 1 week the same result was acheive: 2.79 μg/mL.

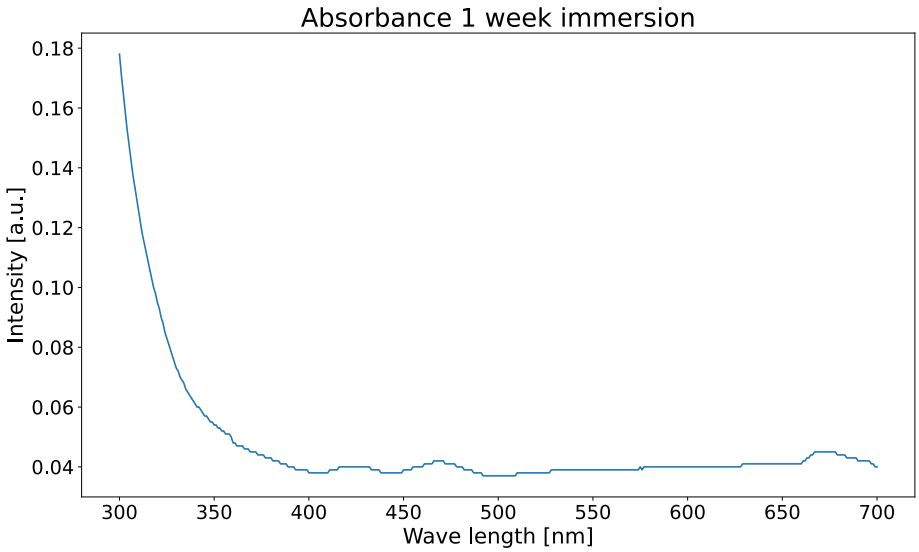

Figure 7.6: Absorbance spectrum of the media after stick immersion for 1 week (without blank measure)

It is important to note however that no blank measure was subtracted for those because they were forgotten, the blank measure used for those was thus the 6 hours blank. This mean that this amount is probably over-evaluated because debris from the stick (cellulose) was more important for those. However we can see on the absorbance curve corresponding to the 1 week immersed sticks in figure 7.6 that a small bump at 420nm is seeable which could indicate the presence of MNP@Neutravidine.

On the figure 7.7 we can observe the mean colourimetric peak depth at the control line after the sticks were immersed and dried at ambient temperature. We can notice that there is some variation between the sticks but we cannot observe a clear tendency. It might be revealing that very few nanoparticle left the sticks or that the nanoparticles that left the sticks were essentially coming from other parts like the glass fiber, the absorbent pad or other place on the membrane (non-specific binding).

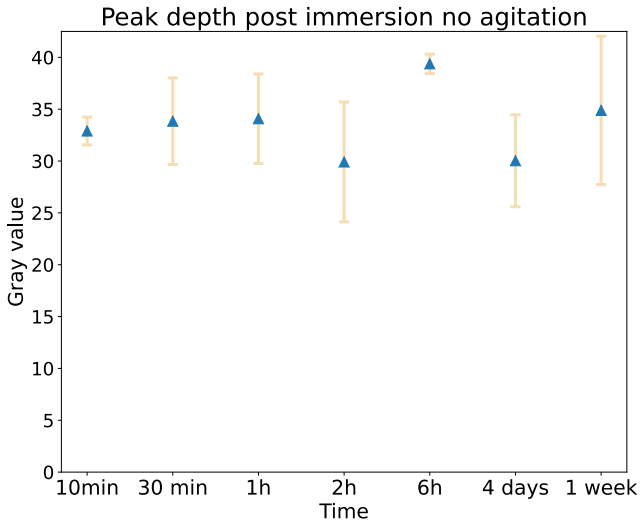

Figure 7.7: Mean of the gray value peak depths at the control line after retention test.

7.4 Discussion

We have seen that the results of the retention test indicates that the MNP@Neutravidine have a tendency to stay on the stick, the release of nanoparticles was not massive to say the least. Of course this result is achieved with specific nanoparticles in specific conditions. The MNP@Neutravidine are big nanoparticles (1μm) coated with neutravidin that experienced a poor flow. The choice have been made to use those nanoparticles because I had less MNP@biotin at my disposal and at the time I still needed to conduct other experiment with them. The conditions of the tests, immersed in PBS 0.01M pH7.4 at ambient temperature, can also influence the test. Experiments closer to real environment, different pH (river water usually experience a pH between 6 and 8), cycle of temperature could be conducted. In fine, the nanoparticles will end-up in the environment with time and degradation of the nitrocellulose but a slow release of the nanoparticles could be beneficial because it would let time to disperse them in bigger volume, reducing the de facto

concentration.

I am not able to assess precisely the risk linked to the use of iron oxide nanoparticles let alone precise nanoparticle type use in LFA framework. But we can with the information gathered imagine what it would take to achieve a RCR, risk characterization ratio, of 1 (it begins to be concerning) in the Louvain-La-Neuve pound. As a reminder the RCR is given by : $RCR = \frac{PEC}{PNEC}$

We are therefore searching for the PEC (predicted environment concentration) at which it begins to be dangerous. For that we have to compute the PNEC (predicted no effect concentration) which is the EC50 (effect concentration) for the most sensitive species divided by the assessment factor. The only data I have is for *daphnia magna* a invertebrate, primary consumer. If we consider the more toxic iron oxide nanoparticle (5.2nm diameter, dextran coated) tested in the article, visible in the figure 7.3, we have a effect concentration of 20 [mg/L]. In this case the assessment factor would be 1000. Thus we have:

$$PEC = \frac{20[mg/L]}{1000}$$

Knowing that the pound of Louvain-La-Neuve has a volume of about 85 * 10^6 L, it would require 85 $10^6[L] \cdot 0.02\frac{[mg]}{[L]} = 1.7$ kg of nanoparticles. It might not seem a lot but for the comparison, in each stick used for the retention test there was 6.67 μg of nanoparticle. 1.7 kg thus correspond to about 250 millions of sticks discharged in the Louvain-La-Neuve pound without even considering the low release rate of the nanoparticles found in the retention test!

Of course this is more an experiment of thoughts. The properties of the iron oxide nanoparticle used for the EC50 greatly differs from the one used for LFA and I miss information on those nanoparticle to obtain something more close to what would be a real risk assessment. However, with regards to the content of this chapter the use of nanoparticle seems to represent a very mild risk for the environment especially regarding to other sources of iron oxide nanoparticles. Indeed magnetite nanospheres can be formed by combustion and/or friction-derived heating as reported in "*Magnetite pollution nanoparticles in the human brain*" from Maher and al.[108]. In this work, I focused on the IONP related toxicity but other components of the LFA could have detrimental effects as well (e.g. the PVA (polyvinyl alcohol) sometimes used can pollute ground water). More generally the extensive use of LFA can generate a lot of waste aside from nanoparticles (housing cassette, packaging, etc). To diminish the environmental impact a solution could be to recycle some parts [27] [109]. In parallel, the incineration of the used sticks could not be a suitable solution as study has indicated that nanostructures can be transformed or destroyed during the combustion process or remain unchanged. The knowledge and understanding of the behaviour of nanocomposites during the incineration process is lacking to draw definitive conclusion [110]. In short, the end-of-life of lateral flow assay should not be forgotten to avoid spreading used LFAs and the different components associated in the environment.

Chapter 8

Conclusion

The detection of microorganisms is tremendously important to assess the presence of pathogens that could induce diseases leading to dire consequences. Numerous biodetection methods are available but their limitations can be problematic for drinking water quality monitoring and, in a larger frame, for other field of application such as beverage industry, dairy industry, food industry, recreational water, etc. Indeed, conventional biodetection methods often require expensive equipment, laboratory facilities, skilled personal and time to run the process. To remedy those limitations development of point-of-care (PoC) devices are investigated to match the World Health Organization's REASSRED criteria ((Real-time connectivity, Ease of specimen collection, Affordable, Sensitive, Specific, User-friendly, Rapid and robust, Equipment-free or simple, and Deliverable to end-users). Among those, the lateral flow assay LFA stands out because of its low cost, known technology (Rapid pregnancy test, COVID-19 detection, etc.), end-user friendliness and short time on-site analysis. To improve the sensitivity and achieve quantitative measurements with lateral flow assay, a strategy is to use magnetic nanoparticles as signal transducer. In this work, lateral flow assay prototypes based on iron oxide nanoparticles were designed.

More precisely, 2 types of iron oxide nanoparticles were used: Neutravidin coated 1μm (nano)particles (MNP@Neutravidine) and biotin coated 10 nm nanoparticles (MNP@biotin). The strong affinity between biotin and Neutravidin was put into profit, the capture bioreceptor on the membrane being biotin or streptavidin in function of the nanoparticle used. To achieve LFA prototypes and improve the flow and signal, different chemicals were tested in running, blocking and conjugate pad buffers. Sonication, different suspension media of the nanoparticles and several concentration of capture bioreceptor were experimented as well as the use of different nitrocellulose membrane type.

The multiple conditions experimented allowed to highlight the importance of some parameters such as the presence of a detergent (here Tween 20) for the flow or the presence of sucrose for the good resolubilisation of the conjugate. The same way, the choice of the membrane is of great importance because of its implications on the flow, the size of the nanoparticles usable, the capture bioreceptors' loading capacity of the membrane and in fine on the sensitivity of the device. A comparison between the size of the 2 types of iron oxide nanoparticles (IONPs) used was drawn on the way it affects the flow and the detection (optical and magnetic). In order to have a global view of the implications of the use of IONPs in a LFA framework, the toxicity concerns of such nanoparticles were investigated. The way a risk assessment for environmental toxicity could be

done was explained and an experiment to have better understanding of the behaviour of IONPs on used sticks immersed was conducted. This investigation led to the conclusion that the use of iron oxide nanoparticles in LFA framework presents a low risk for the environment especially regarding to the other sources of IONPs. The end-of-life of the product should however not be neglected as knowledge and understanding of the behaviour of nanocomposites during a potential incineration is lacking and lateral flow assay can produce a quite large amount of other wastes (housing cassette, packaging,...).

As a result of this work, two LFA prototypes with control line were obtained and could be used to assess the limit of detection obtained with a to-be-designed magnetic reader. However the results obtained with MNP@Neutravidine are less convincing. Probably due to the too big size of those particles the binding at the control line is not uniform and there is a lot of non specific binding visible on the membrane. The performances of two LFA prototypes could yet be improved, particularly by loading the capture bioreceptor in a buffer with a pH equivalent to their isoelectric point. To go a step further, a MNP@biotin based lateral flow assay detecting streptavidin in solution up to 50μg/mL was manufactured. This way, the future magnetic detector could be tested in conditions closer to real. If the limit of detection of the working LFA detecting streptavidin is reduced with the use of this magnetic reader compared to what can be achieve optically, it would be a nice proof of concept and another step towards rapid and sensitive paper-based biosensor.

Appendix A

Standard protocol for MNP@neutra

- Cut 1.5 cm of conjugate pad (glass fiber)
- Take 10 μL of NMNP diluted 10 times (1mg/mL) and put it in 90 μL of conjugate pad buffer (5% (w/v) sucrose,1% (wt/vol) BSA and 0.5% (vol/vol) Tween-20 **in 0.01M PBS ?**) The proportions stay the same for bigger ones conjugate pad(e.g. 20NMNP and 180 CPB for 6cm conjugate pad).
- *Optional (sonication):* fill the tank of the ultra sonicator, place the eppendorf on an attach and dip it into the tank, it must be partly immersed at least the part with the CPB.
- Pour the CPB containing the NP onto the conjugate pad drop wise in order to avoid over flooding in the petri dish
- Place the conjugate pad in vacuum for 2 hours. After 2 hours, verify that the conjugate pad is completely dried. If not let under vacuum.
- Cut 1.5 cm of nitrocellulose membrane
- Place the dots of the control line (biotin-BSA, 1mg/mL) at 1cm from the conjugate pad.
- Set the membrane in the oven for 20 min (2 hours better) at 37 °C
- *Optional (blocking):* Dip the membrane in blocking buffer (2%(wt/vol) BSA, 0.01M PBS pH7.4) for 20 min at 150 rpm. Then at least 2 times washing step with washing buffer (0.05% (wt/vol) SDS, 0.005 M PBS, pH 7.4):2 x 15 min at 150 rpm. Then dry the membrane 2 hours in the oven at 37 °C.
- Cut 2 times 3 cm of cellulose (sample and absorbent pad with margin for the cutting)
- Cut 1.5cm of backing card
- Once all is dried, assemble the different pads on the backing card beginning with the membrane. The membrane is to be handled carefully to avoid introducing damage. The pads that are added should overlap on about 3 mm. cellulose is place with the smaller pore size up for the absorbent pad and down for the sample pad for capillarity.
- Cut the cards with the strip cutter 5mm width

- Run the test by pouring drop-wise 140μL of PBS 0.01M

For the MNP@biotin, the protocol is similar. The concentration of capture bioreceptor (streptavidin) is higher for better results (5mg/mL) and should be kept in the oven at 37°C for 2 hours.

List of the reagents and material used

Name	Reference
MNP@biotin	Iron oxide(II,III), magnetic nanoparticles solution Sigma Aldrich 747424
MNP@Neutravidine	GE78152104010150 SpeedBeads Magnetic Neutravidin Coated particles
BSA	Bovine Serum Albumin Fraction V, Roche 10735108001
SDS	Dodecyl sulfate sodium salt, 1.13760.0100 EMD milipore corporation
PBS	P4417 Sigma Aldrich P4417 Phosphate buffered saline
Tween20	P1379 Sigma-Aldrich Tween 20
Sucrose	D(+)Saccharose 27480.294 AnalaR NORMAPUR VWRchemicals
Streptavidin 1	S4762 Sigma-Aldrich Streptavidin from Streptomyces avidinii
Streptavidin 2	189730 Streptavidin Merck Milipore
Biotin-BSA	Albumin, biotin labeled bovine. Sigma Aldrich A8549
Cellulose	CFSP001700 EMD Milipore cellulose (nonwoven cotton fiber)
Glass fiber	Merck Milipore GFDX001000 glass fiber with PVA binder
Nitrocellulose 1	UniSart Satorius CN95 polyester backing 100μm
Nitrocellulose 2	UniSart Satorius CN140 polyester backing 100μm
Nitrocellulose 3	Hi-Flow^{T}M Plus 75 (60x301mm) HF075MC5PK Merck Milipore
Backing card	Kenosha (60mm x 300mm) KN-PS1060.45

Table A.1: References of the reagents and pads used

Appendix B

Test with HF75 membrane

Due to the problem of flow of the big nanoparticles MNP@Neutravidine (about 1 μm diameter) another membrane was tested. The membrane is the HI-Flow Plus HF075 membrane nitrocellulose from Merck Milipore with a pore size which is estimated by the manufacturer from 12 to 17 µm. As we can see on the figure B.1, the use of this new membrane with bigger pores enable to achieve a more coloured control line. On the figure B.2 we can see the 3 types of membranes tested with the MNP@Neutravidine. Unfortunately the HF75 did not allowed to obtain a fully coloured dot. The dot is, in his 'quarter moon' shape, similar to the dot we might see with a CN95 membrane from Satorius. As the range of the pore size given by the manufacturer is quite large, it is difficult to know to which extend the pore size are bigger than the ones of CN95. However, they are not big enough for the MNP@Neutravidine as it did not allowed to obtain a dot similar to what is obtained with the MNP@biotin. Nitrocellulose membrane with even bigger pore size up to 20 μm exist and could be tested with the MNP@Neutravidine but here we approach the limit achievable with nitrocellulose. Nanoparticles of 1 μm may just be too big for lateral flow assay. On the figure B.2,the conjugate pad for the HF75 seems bigger, it is only due to the fact that the HF75 sample was delivered already mounted on a backing card whose dimensions differs a bit from the one I used for the other membrane. We can see on the photos presented on the figure B.2 the colouring of the membrane which differs with the membrane being lighter with bigger pore size.

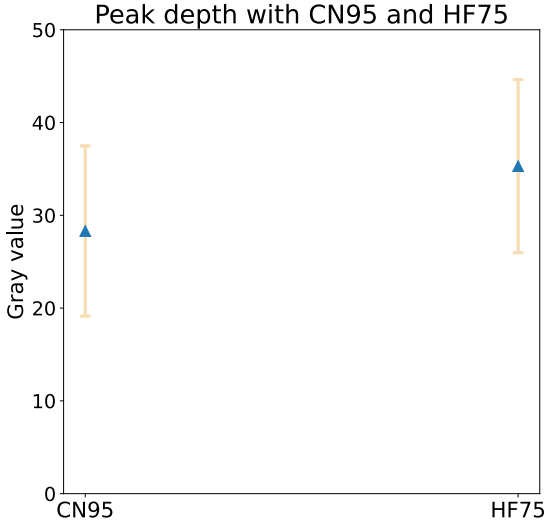

Figure B.1: Peak depth for MNP@Neutravidine with CN95 membrane (*left*) and HF75 (*right*)

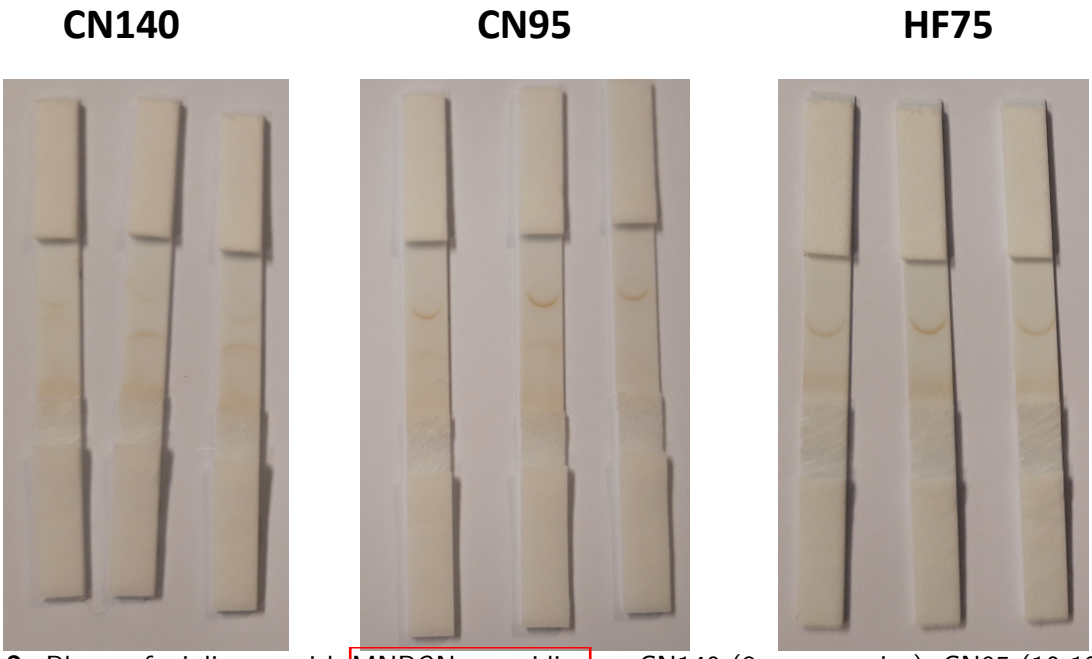

Figure B.2: Photo of triplicates with MNP@Neutravidine on CN140 (8 μm poresize), CN95 (10-12 μm pore size), HF75 (12-15 μm pore size)

Bibliography

[1] World Health Organisation. *Drinking-water*. Last access: 09/04/2023. 2022. URL: https://www.who.int/news-room/fact-sheets/detail/drinking-water.

[2] World Health Organization. *Guidelines for drinking-water quality: fourth edition incorporating first addendum*. 4th ed + 1st add. World Health Organization, 2017, 541 p.

[3] Kate Medlicott et al. *Guidelines on recreational water quality: Volume 1 coastal and fresh waters*. July 2021. ISBN: 978-92-4-003130-2.

[4] Naveen Minhas et al. "Cost-analysis of real time RT-PCR test performed for COVID-19 diagnosis at India's national reference laboratory during the early stages of pandemic mitigation". In: *PLOS ONE* 18.1 (Jan. 2023). Ed. by Aneesh Basheer, e0277867. DOI: 10.1371/journal.pone.0277867. URL: https://doi.org/10.1371/journal.pone.0277867.

[5] Raphael Chukwuka Nnachi et al. "Biosensors for rapid detection of bacterial pathogens in water, food and environment". In: *Environment International* 166 (2022), p. 107357. ISSN: 0160-4120. DOI: https://doi.org/10.1016/j.envint.2022.107357. URL: https://www.sciencedirect.com/science/article/pii/S0160412022002847.

[6] Saima Hameed, Lijuan Xie, and Yibin Ying. "Conventional and emerging detection techniques for pathogenic bacteria in food science: A review". In: *Trends in Food Science and Technology* 81 (2018), pp. 61–73. ISSN: 0924-2244. DOI: https://doi.org/10.1016/j.tifs.2018.05.020. URL: https://www.sciencedirect.com/science/article/pii/S0924224417307689.

[7] Seokheun Choi. "Powering point-of-care diagnostic devices". In: *Biotechnology Advances* 34.3 (2016). Trends in In Vitro Diagnostics and Mobile Healthcare, pp. 321–330. ISSN: 0734-9750. DOI: https://doi.org/10.1016/j.biotechadv.2015.11.004. URL: https://www.sciencedirect.com/science/article/pii/S0734975015300549.

[8] Jonas A. Otoo and Travis S. Schlappi. "REASSURED Multiplex Diagnostics: A Critical Review and Forecast". In: *Biosensors* 12.2 (2022). ISSN: 2079-6374. DOI: 10.3390/bios12020124. URL: https://www.mdpi.com/2079-6374/12/2/124.

[9] Hans R Boehringer and Brendan J O'Farrell. "Lateral Flow Assays in Infectious Disease Diagnosis". In: *Clinical Chemistry* 68.1 (Dec. 2021), pp. 52–58. DOI: 10.1093/clinchem/hvab194. URL: https://doi.org/10.1093/clinchem/hvab194.

[10] Grace Wu and Muhammad H Zaman. "Low-cost tools for diagnosing and monitoring HIV infection in low-resource settings". In: *Bulletin of the World Health Organization* 90.12 (Oct. 2012), pp. 914–920. DOI: 10.2471/blt.12.102780. URL: https://doi.org/10.2471/blt.12.102780.

[11] Josquin Vandeputte. "Nanoparticles for paper-based biosensors and environmental impact assessment". In: *Ecole polytechnique de Louvain, Université catholique de Louvain, Prom. : Raskin, Jean- Pierre.* (2021). DOI: http://hdl.handle.net/2078.1/thesis:30695.

[12] in BW. *Qualité de l'eau: PARAMÈTRES ET NORMES.* https://www.inbw.be/parametres-et-normes. Accessed: 2023-05-31.

[13] Dirk Wildeboer and Robert Price. "Methods of analysis for bacterial contamination in environmental waters". In: Nov. 2015. ISBN: 9781634835770.

[14] World Health Organization. *Quantitative Microbial Risk Assessment: Application for Water Safety Management.* 4th ed + 1st add. ISBN 978 92 4 156537 0, 2016, 183 p.

[15] Jacques Mahillon. *LBRAL2104 - Food Microbiology: Slides D Detection methods for microorganisms.* 2022.

[16] Regina Bailey. *Phases of the Bacterial Growth Curve.* https://www.thoughtco.com/bacterial-growth-curve-phases-4172692. Accessed: 2023-06-1.

[17] Kate M. Scow et al. "Microbial Biodiversity, Measurement of". In: *Encyclopedia of Biodiversity.* Elsevier, 2001, pp. 259–270. DOI: 10.1016/b978-0-12-384719-5.00434-2. URL: https://doi.org/10.1016/b978-0-12-384719-5.00434-2.

[18] Ozioma Forstinus Nwabor et al. "Water and Waterborne Diseases: A Review". In: *International Journal of TROPICAL DISEASE and Health* 12 (Jan. 2016), pp. 1–14. DOI: 10.9734/IJTDH/2016/21895.

[19] Nisha Rijal. "Most Probable Number (MPN) Test: Principle, Procedure, Results". In: (2022). URL: https://microbeonline.com/probable-number-mpn-test-principle-procedure-results/.

[20] LLC Molecular Devices. *Contrôle qualité et tests de sécurité dans l'agroalimentaire à l'aide des analyses sur plaque.* https://fr.moleculardevices.com/applications/food-and-beverage/quality-control-safety-testing. Accessed: 2023-05-31.

[21] Sarah Neidler. *What are the differences between PCR, RT-PCR, qPCR, and RT-qPCR?* https://www.enzolifesciences.com/science-center/technotes/2017/march/what-are-the-differences-between-pcr-rt-pcr-qpcr-and-rt-qpcr?/. Accessed: 2023-06-1.

[22] Ali Kemal Yetisen, Muhammad Safwan Akram, and Christopher R. Lowe. "Paper-based microfluidic point-of-care diagnostic devices". In: *Lab Chip* 13 (12 2013), pp. 2210–2251. DOI: 10.1039/C3LC50169H. URL: http://dx.doi.org/10.1039/C3LC50169H.

[23] Yilin Liu et al. "Ultrasensitive and Highly Specific Lateral Flow Assays for Point-of-Care Diagnosis". In: *ACS Nano* 15.3 (Feb. 2021), pp. 3593–3611. DOI: 10.1021/acsnano.0c10035. URL: https://doi.org/10.1021/acsnano.0c10035.

[24] Hélène Frouard. *Enceinte ou pas ? Le test de grossesse a 40 ans.* Ed. by Figaro. https://sante.lefigaro.fr/actualite/2013/04/05/20182-enceinte-pas-test-grossesse-40-ans. Accessed: 2023-04-07.

[25] Committee of Public Accounts. *House of Commons Committee of Public Accounts: Test and Trace update, Twenty-Third Report of Session 2021–22.* https://committees.parliament.uk/publications/7651/documents/79945/default/. Accessed: 2023-04-06.

[26] Mark Drakesmith et al. "Cost-effectiveness of a whole-area testing pilot of asymptomatic SARS-CoV-2 infections with lateral flow devices: a modelling and economic analysis study". In: *BMC Health Services Research* 22.1 (Sept. 2022). DOI: 10.1186/s12913-022-08511-3. URL: https://doi.org/10.1186/s12913-022-08511-3.

[27] Jobie Budd et al. "Lateral flow test engineering and lessons learned from COVID-19". In: *Nature Reviews Bioengineering* 1.1 (Jan. 2023), pp. 13–31. DOI: 10.1038/s44222-022-00007-3. URL: https://doi.org/10.1038/s44222-022-00007-3.

[28] Indiamart. *Pregnancy tests kit*. https://www.indiamart.com/proddetail/pregnancy-kit-13358530448.html?pos=8&pla=n. Accessed: 2023-06-1.

[29] Claudio Parolo et al. "Tutorial: design and fabrication of nanoparticle- based lateral-flow immunoassays". In: *Nature Protocol* 15 (Oct. 2020). DOI: 10.1038/s41596-020-0357-x.

[30] Radetec Pty Ltd. *Lateral flow assays*. https://www.lateralflows.com/lateral-flow-assays/. Accessed: 2023-05-01.

[31] Raphael Wong and Harley Tse, eds. *Lateral Flow Immunoassay*. Humana Press, 2009. DOI: 10.1007/978-1-59745-240-3. URL: https://doi.org/10.1007/978-1-59745-240-3.

[32] Elif Bahadir and Mustafa Sezgintürk. "Lateral flow assays: Principles, designs and labels". In: *TrAC Trends in Analytical Chemistry* 82 (Sept. 2016), pp. 286–306. DOI: 10.1016/j.trac.2016.06.006.

[33] David Gasperino et al. "Improving Lateral Flow Assay Performance Using Computational Modeling". In: *Annual Review of Analytical Chemistry* 11.1 (June 2018), pp. 219–244. DOI: 10.1146/annurev-anchem-061417-125737. URL: https://doi.org/10.1146/annurev-anchem-061417-125737.

[34] Merck Millipore. *Rapid lateral flow test strips: considerations for product development*. https://www.merckmillipore.com/INTERSHOP/web/WFS/Merck-RU-Site/ru_RU/-/USD/ShowDocument-Pronet?id=201306.15671. Accessed: 2023-05-01. 2013.

[35] Ruihua Tang et al. "Nitrocellulose Membrane for Paper-based Biosensor". In: *Applied Materials Today* 26 (Mar. 2022), p. 101305. DOI: 10.1016/j.apmt.2021.101305. URL: https://doi.org/10.1016/j.apmt.2021.101305.

[36] Richard Jenny. "Drugs of Abuse, Body Fluid Testing. Raphael C. Wong and Harley Y. Tse, editors. Totowa, NJ: Humana Press, 2005, 305 pp., 145.00, hardcover. ISBN 1-58829-435-8". In: *Clinical Chemistry - CLIN CHEM* 52 (May 2006), pp. 911–912. DOI: 10.1373/clinchem.2005.063446.

[37] Satorius. *UniSart Nitrocellulose Membranes, The Substrate of Choice for Protein Assays*. https://www.sartorius.com/download/613622/broch-unisart-nitro-sl-1536-e-pdf-data.pdf. Accessed: 2023-05-09.

[38] Wikipedia. *Nitrocellulose*. https://fr.wikipedia.org/wiki/Nitrocellulose. Accessed: 2023-06-2.

[39] Walport M Janeway CA Jr Travers P. "The Immune System in Health and Disease: The structure of a typical antibody molecule." In: *Garland Science* (2001). URL: %5Curl%7Bhttps://www.ncbi.nlm.nih.gov/books/NBK27144/#%7D.

[40] Wikipedia. *Antibody*. Accessed: 2023-05-11. URL: %5Curl%7Bhttps://en.wikipedia.org/wiki/Antibody#cite_note-pmid8450761-3%7D.

[41] Marjan Majdinasab, Mihaela Badea, and Jean Louis Marty. "Aptamer-Based Lateral Flow Assays: Current Trends in Clinical Diagnostic Rapid Tests". In: *Pharmaceuticals* 15.1 (Jan. 2022), p. 90. DOI: 10.3390/ph15010090. URL: https://doi.org/10.3390/ph15010090.

[42] Ailiang Chen and Shuming Yang. "Replacing antibodies with aptamers in lateral flow immunoassay". In: *Biosensors and Bioelectronics* 71 (Sept. 2015). DOI: 10.1016/j.bios.2015.04.041.

[43] Lorenz Leitner, Thomas M. Kessler, and Jochen Klumpp. "Bacteriophages: a Panacea in Neuro-Urology?" In: *European Urology Focus* 6.3 (May 2020), pp. 518–521. DOI: 10.1016/j.euf.2019.10.018. URL: https://doi.org/10.1016/j.euf.2019.10.018.

[44] Honglin Yang et al. "Lateral flow assay of methicillin-resistant Staphylococcus aureus using bacteriophage cellular wall-binding domain as recognition agent". In: *Biosensors and Bioelectronics* 182 (June 2021), p. 113189. DOI: 10.1016/j.bios.2021.113189. URL: https://doi.org/10.1016/j.bios.2021.113189.

[45] Minsuk Kong et al. "Lateral flow assay-based bacterial detection using engineered cell wall binding domains of a phage endolysin". In: *Biosensors and Bioelectronics* 96 (May 2017). DOI: 10.1016/j.bios.2017.05.010.

[46] Mir Hadi Jazayeri et al. "Various methods of gold nanoparticles (GNPs) conjugation to antibodies". In: *Sensing and Bio-Sensing Research* 9 (July 2016), pp. 17–22. DOI: 10.1016/j.sbsr.2016.04.002. URL: https://doi.org/10.1016/j.sbsr.2016.04.002.

[47] Yi-Ting Chen et al. "Biosensing Using Magnetic Particle Detection Techniques". In: *Sensors* 17 (Oct. 2017), p. 2300. DOI: 10.3390/s17102300.

[48] Nguyen T.K. Thanh and Luke A.W. Green. "Functionalisation of nanoparticles for biomedical applications". In: *Nano Today* 5.3 (June 2010), pp. 213–230. DOI: 10.1016/j.nantod.2010.05.003. URL: https://doi.org/10.1016/j.nantod.2010.05.003.

[49] Jinchuan Yang et al. "Detection platforms for point-of-care testing based on colorimetric, luminescent and magnetic assays: A review". In: *Talanta* 202 (2019), pp. 96–110. ISSN: 0039-9140. DOI: https://doi.org/10.1016/j.talanta.2019.04.054. URL: https://www.sciencedirect.com/science/article/pii/S0039914019304436.

[50] Daniel Quesada-González and Arben Merkoçi. "Nanoparticle-based lateral flow biosensors". In: *Biosensors and Bioelectronics* 73 (2015), pp. 47–63. ISSN: 0956-5663. DOI: https://doi.org/10.1016/j.bios.2015.05.050. URL: https://www.sciencedirect.com/science/article/pii/S0956566315301482.

[51] Wenqiang Yan et al. "Machine Learning Approach to Enhance the Performance of MNP-Labeled Lateral Flow Immunoassay". In: *Nano-Micro Letters* 11.1 (Jan. 2019). DOI: 10.1007/s40820-019-0239-3. URL: https://doi.org/10.1007/s40820-019-0239-3.

[52] Yilin Liu et al. "fM–aM Detection of the SARS-CoV-2 Antigen by Advanced Lateral Flow Immunoassay Based on Gold Nanospheres". In: *ACS Applied Nano Materials* 4.12 (Dec. 2021), pp. 13826–13837. DOI: 10.1021/acsanm.1c03217. URL: https://doi.org/10.1021/acsanm.1c03217.

[53] Wenjuan Sun et al. “A novel multi-walled carbon nanotube-based antibody conjugate for quantitative and semi-quantitative lateral flow assays”. In: *Bioscience, Biotechnology, and Biochemistry* 81.10 (2017). PMID: 28840780, pp. 1874–1882. DOI: 10.1080/09168451.2017.1365590. eprint: https://doi.org/10.1080/09168451.2017.1365590. URL: https://doi.org/10.1080/09168451.2017.1365590.

[54] Shi Ying Lim, Wei Shen, and Zhiqiang Gao. “Carbon quantum dots and their applications”. In: *Chemical Society Reviews* 44.1 (2015), pp. 362–381. DOI: 10.1039/c4cs00269e. URL: https://doi.org/10.1039/c4cs00269e.

[55] Birui Jin et al. “Lateral flow aptamer assay integrated smartphone-based portable device for simultaneous detection of multiple targets using upconversion nanoparticles”. In: *Sensors and Actuators B: Chemical* 276 (2018), pp. 48–56. ISSN: 0925-4005. DOI: https://doi.org/10.1016/j.snb.2018.08.074. URL: https://www.sciencedirect.com/science/article/pii/S0925400518315156.

[56] Lokesh Srinath Ganapathe et al. “Magnetite (Fe3O4) Nanoparticles in Biomedical Application: From Synthesis to Surface Functionalisation”. In: *Magnetochemistry* 6.4 (2020). ISSN: 2312-7481. DOI: 10.3390/magnetochemistry6040068. URL: https://www.mdpi.com/2312-7481/6/4/68.

[57] Wei Wu et al. “Recent progress on magnetic iron oxide nanoparticles: synthesis, surface functional strategies and biomedical applications”. In: *Science and Technology of Advanced Materials* 16.2 (Apr. 2015), p. 023501. DOI: 10.1088/1468-6996/16/2/023501. URL: https://doi.org/10.1088/1468-6996/16/2/023501.

[58] Yiseul Ryu et al. “Increase in the detection sensitivity of a lateral flow assay for a cardiac marker by oriented immobilization of antibody”. In: *BioChip Journal* 5.3 (Sept. 2011), pp. 193–198. DOI: 10.1007/s13206-011-5301-2. URL: https://doi.org/10.1007/s13206-011-5301-2.

[59] Wikipedia. *Tunnel magnetoresistance*. https://en.wikipedia.org/wiki/Tunnel_magnetoresistance. Accessed: 2023-06-2.

[60] Etelka Tombácz et al. “Magnetic iron oxide nanoparticles: Recent trends in design and synthesis of magnetoresponsive nanosystems”. In: *Biochemical and Biophysical Research Communications* 468.3 (2015). Nanomedicine, pp. 442–453. ISSN: 0006-291X. DOI: https://doi.org/10.1016/j.bbrc.2015.08.030. URL: https://www.sciencedirect.com/science/article/pii/S0006291X15304204.

[61] Nur Alam et al. “Improving the sensitivity of cellulose fiber-based lateral flow assay by incorporating a water-dissolvable polyvinyl alcohol dam”. In: *Cellulose* 28.13 (July 2021), pp. 8641–8651. DOI: 10.1007/s10570-021-04083-3. URL: https://doi.org/10.1007/s10570-021-04083-3.

[62] Lourdes Rivas et al. “Improving sensitivity of gold nanoparticle-based lateral flow assays by using wax-printed pillars as delay barriers of microfluidics”. In: *Lab Chip* 14.22 (Sept. 2014), pp. 4406–4414. DOI: 10.1039/c4lc00972j. URL: https://doi.org/10.1039/c4lc00972j.

[63] Tsung-Ting Tsai et al. “Development a stacking pad design for enhancing the sensitivity of lateral flow immunoassay”. In: *Scientific Reports* 8.1 (Nov. 2018). DOI: 10.1038/s41598-018-35694-9. URL: https://doi.org/10.1038/s41598-018-35694-9.

[64] Hyun Jung Min et al. "Development of a smartphone-based lateral-flow imaging system using machine-learning classifiers for detection of Salmonella spp." In: *Journal of Microbiological Methods* 188 (Sept. 2021), p. 106288. DOI: 10.1016/j.mimet.2021.106288. URL: https://doi.org/10.1016/j.mimet.2021.106288.

[65] Kathryn H. Ching. "Lateral Flow Immunoassay". In: *Methods in Molecular Biology*. Springer New York, 2015, pp. 127–137. DOI: 10.1007/978-1-4939-2742-5_13. URL: https://doi.org/10.1007/978-1-4939-2742-5_13.

[66] Cytiva. *Sera-Mag and Sera-Mag SpeedBeads Magnetic Particles*. Accessed: 2023-05-15. URL: https://www.cytivalifesciences.com/en/be/shop/molecular-and-immunodiagnostics/magnetic-beads-and-kits/sera-mag-speedbeads-neutravidin-coated-magnetic-particles-p-06375#related-documents.

[67] ThermoFisher. *Avidin-Biotin Interaction*. Accessed: 2023-05-15. URL: https://www.thermofisher.com/be/en/home/life-science/protein-biology/protein-biology-learning-center/protein-biology-resource-library/pierce-protein-methods/avidin-biotin-interaction.html.

[68] Wasim Abuillan. "Fine-Structures, Lateral Correlation and Diffusion of Membrane-Associated Proteins on Biological Membrane Surfaces". In: (Jan. 2013).

[69] Scott C. Meyer, Thomas Gaj, and Indraneel Ghosh. "Highly Selective Cyclic Peptide Ligands for NeutrAvidin and Avidin Identified by Phage Display". In: *Chemical Biology* 68.1 (July 2006), pp. 3–10. DOI: 10.1111/j.1747-0285.2006.00401.x. URL: https://doi.org/10.1111/j.1747-0285.2006.00401.x.

[70] Grégoire Le Brun. "Design of paper-based sensors for PoC pathogen diagnostics". In: (Apr. 2023). PhD thesis, Ecole Polytechnique de Louvain, Université catholique de Louvain.

[71] Julian Taurozzi, Vincent Hackley, and Mark Wiesner. "Ultrasonic dispersion of nanoparticles for environmental, health and safety assessment issues and recommendations". In: *Nanotoxicology* 5 (Nov. 2010), pp. 711–29. DOI: 10.3109/17435390.2010.528846.

[72] Avin Abdullah and Azad Mohammed. "Scanning Electron Microscopy (SEM): A Review". In: Jan. 2019, pp. 77–85.

[73] Anwar Ul-Hamid. "Introduction". In: *A Beginners' Guide to Scanning Electron Microscopy*. Springer International Publishing, 2018, pp. 1–14. DOI: 10.1007/978-3-319-98482-7_1. URL: https://doi.org/10.1007/978-3-319-98482-7_1.

[74] Frank Babick. "Dynamic light scattering (DLS)". In: *Characterization of Nanoparticles*. Elsevier, 2020, pp. 137–172. DOI: 10.1016/b978-0-12-814182-3.00010-9. URL: https://doi.org/10.1016/b978-0-12-814182-3.00010-9.

[75] IMPLEN. *UV-Vis Spectrophotometers*. Accessed: 2023-05-16. URL: https://www.implen.de/uv-vis-spectrophotometer/.

[76] *Ultraviolet–visible spectroscopy*. Accessed: 2023-05-16. URL: https://en.wikipedia.org/wiki/Ultraviolet%E2%80%93visible_spectroscopy.

[77] SMACgig WORLD. *How Does a Modern UV-Vis Spectrophotometer Work?* Accessed: 2023-05-16. URL: https://www.smacgigworld.com/blog/working-of-modern-uv-vis-spectrophotometer.php.

[78] Baihui Wang et al. “Nanozyme-Based Lateral Flow Immunoassay (LFIA) for Extracellular Vesicle Detection”. In: *Biosensors* 12 (July 2022), p. 490. DOI: 10.3390/bios12070490.

[79] Shayesteh Bazsefidpar et al. “Lipid–Polymer Hybrids Encapsulating Iron-Oxide Nanoparticles as a Label for Lateral Flow Immunoassays”. In: *Biosensors* 11.7 (July 2021), p. 218. DOI: 10.3390/bios11070218. URL: https://doi.org/10.3390/bios11070218.

[80] Mohammed Alnajrani and Omar Alsager. “Lateral flow aptasensor for progesterone: Competitive target recognition and displacement of short complementary sequences”. In: *Analytical Biochemistry* 587 (Sept. 2019), p. 113461. DOI: 10.1016/j.ab.2019.113461.

[81] Zhiying Wang et al. “A strip of lateral flow gene assay using gold nanoparticles for point-of-care diagnosis of African swine fever virus in limited environment”. In: *Analytical and Bioanalytical Chemistry* 413 (May 2021). DOI: 10.1007/s00216-021-03408-2.

[82] Janeway CA Jr Travers P Walport M and al. *Immunobiology: The Immune System in Health and Disease*. Garland Science, 2001. URL: https://www.ncbi.nlm.nih.gov/books/NBK27144/#:~:text=IgG%5C%20antibodies%5C%20are%5C%20large%5C%20molecules,different%5C%20kinds%5C%20of%5C%20polypeptide%5C%20chain.

[83] Wanwisa Poonlapdecha et al. “Antibody-conjugated ferromagnetic nanoparticles with lateral flow test strip assay for rapid detection of Campylobacter jejuni in poultry samples”. In: *International Journal of Food Microbiology* 286 (2018), pp. 6–14. ISSN: 0168-1605. DOI: https://doi.org/10.1016/j.ijfoodmicro.2018.07.009. URL: https://www.sciencedirect.com/science/article/pii/S016816051830360X.

[84] Baihui Wang et al. “Nanozyme-Based Lateral Flow Immunoassay (LFIA) for Extracellular Vesicle Detection”. In: *Biosensors* 12.7 (July 2022), p. 490. DOI: 10.3390/bios12070490. URL: https://doi.org/10.3390/bios12070490.

[85] Dian-Bing Wang et al. “Rapid detection of Bacillus anthracis spores using a super-paramagnetic lateral-flow immunological detectionsystem”. In: *Biosensors and Bioelectronics* 42 (Apr. 2013), pp. 661–667. DOI: 10.1016/j.bios.2012.10.088. URL: https://doi.org/10.1016/j.bios.2012.10.088.

[86] Myriam Oliveira-Rodriguez et al. “Point-of-care detection of extracellular vesicles: Sensitivity optimization and multiple-target detection”. In: *Biosensors and Bioelectronics* 87 (Jan. 2017), pp. 38–45. DOI: 10.1016/j.bios.2016.08.001. URL: https://doi.org/10.1016/j.bios.2016.08.001.

[87] Mary Johnson. “Detergents: Triton X-100, Tween-20, and More”. In: *Materials and Methods* 3 (Jan. 2013). DOI: 10.13070/mm.en.3.163. URL: https://doi.org/10.13070/mm.en.3.163.

[88] Wikipedia. *Sucrose*. https://en.wikipedia.org/wiki/Sucrose. Accessed: 2023-05-29.

[89] Sulena Pradhan et al. “Effect of sonication on particle dispersion, administered dose and metal release of non-functionalized, non-inert metal nanoparticles”. In: *Journal of Nanoparticle Research* 18 (Sept. 2016). DOI: 10.1007/s11051-016-3597-5.

[90] S.C. Low et al. "Electrophoretic interactions between nitrocellulose membranes and proteins: Biointerface analysis and protein adhesion properties". In: *Colloids and Surfaces B: Biointerfaces* 110 (2013), pp. 248–253. ISSN: 0927-7765. DOI: https://doi.org/10.1016/j.colsurfb.2013.05.001. URL: https://www.sciencedirect.com/science/article/pii/S0927776513003093.

[91] Gina E. Fridley et al. "The evolution of nitrocellulose as a material for bioassays". In: *MRS Bulletin* 38.4 (Apr. 2013), pp. 326–330. DOI: 10.1557/mrs.2013.60. URL: https://doi.org/10.1557/mrs.2013.60.

[92] Nikolai Khlebtsov et al. "Quantifying the Numbers of Gold Nanoparticles in the Test Zone of Lateral Flow Immunoassay Strips". In: 2 (June 2019), 5020−5028. DOI: 10.1021/acsanm.9b00956.

[93] Chunyan Liu et al. "Lateral Flow Immunochromatographic Assay for Sensitive Pesticide Detection by Using Fe304 Nanoparticle Aggregates as Color Reagents". In: *Analytical Chemistry* 83.17 (Aug. 2011), pp. 6778–6784. DOI: 10.1021/ac201462d. URL: https://doi.org/10.1021/ac201462d.

[94] Shouhu Xuan et al. "Tuning the Grain Size and Particle Size of Superparamagnetic Fe3O4 Microparticles". In: *Chemistry of Materials* 21 (Nov. 2009). DOI: 10.1021/cm901618m.

[95] Zhila Shaterabadi et al. "The effect of the magnetically dead layer on the magnetization and the magnetic anisotropy of the dextran-coated magnetite nanoparticles". In: *Applied Physics A* 128.8 (July 2022). DOI: 10.1007/s00339-022-05675-x. URL: https://doi.org/10.1007/s00339-022-05675-x.

[96] Ke Luo et al. "Paper-based lateral flow strip assay for the detection of foodborne pathogens: principles, applications, technological challenges and opportunities". In: *Critical Reviews in Food Science and Nutrition* 60 (Oct. 2018), pp. 1–14. DOI: 10.1080/10408398.2018.1516623.

[97] Nemi Malhotra et al. "Potential Toxicity of Iron Oxide Magnetic Nanoparticles: A Review". In: *Molecules* 25 (July 2020), p. 3159. DOI: 10.3390/molecules25143159.

[98] Ayse Sengul and Eylem Asmatulu. "Toxicity of metal and metal oxide nanoparticles: a review". In: *Environmental Chemistry Letters* 18 (June 2020). DOI: 10.1007/s10311-020-01033-6.

[99] Roghayyeh Vakili-Ghartavol et al. "Toxicity assessment of superparamagnetic iron oxide nanoparticles in different tissues". In: *Artificial Cells, Nanomedicine, and Biotechnology* 48 (Dec. 2020), pp. 443–451. DOI: 10.1080/21691401.2019.1709855.

[100] Tony Baker, Charles Tyler, and Tamara Galloway. "Impacts of metal and metal oxide nanoparticles on marine organisms". In: *Environmental pollution (Barking, Essex : 1987)* 186 (Dec. 2013). DOI: 10.1016/j.envpol.2013.11.014.

[101] Gang Liu et al. "Applications and Potential Toxicity of Magnetic Iron Oxide Nanoparticles". In: *Small (Weinheim an der Bergstrasse, Germany)* 9 (May 2013). DOI: 10.1002/smll.201201531.

[102] Quaiser Saquib et al., eds. *Cellular and Molecular Toxicology of Nanoparticles*. Springer International Publishing, 2018. DOI: 10.1007/978-3-319-72041-8. URL: https://doi.org/10.1007/978-3-319-72041-8.

[103] Qiyi Feng et al. "Uptake, distribution, clearance, and toxicity of iron oxide nanoparticles with different sizes and coatings". In: *Scientific Reports* 8 (Feb. 2018). DOI: 10.1038/s41598-018-19628-z.

[104] Graeme Batley, Jason Kirby, and Mike McLaughlin. "Fate and Risks of Nanomaterials in Aquatic and Terrestrial Environments". In: *Accounts of chemical research* 46 (July 2012). DOI: 10.1021/ar2003368.

[105] Sarah Vellemans. *LBRTE2201 – Human and environmental toxicology course given by Debier Cathy and Hantson Philippe: Environmental risk assessment Theory*. 2022.

[106] Thomas Backhaus and Michael Faust. "Predictive Environmental Risk Assessment of Chemical Mixtures: A Conceptual Framework". In: *Environmental science and technology* 46 (Mar. 2012), pp. 2564–73. DOI: 10.1021/es2034125.

[107] Jonas Baumann et al. "The coating makes the difference: Acute effects of iron oxide nanoparticles on Daphnia magna". In: *The Science of the total environment* 484C (Apr. 2014), pp. 176–184. DOI: 10.1016/j.scitotenv.2014.03.023.

[108] Barbara A. Maher et al. "Magnetite pollution nanoparticles in the human brain". In: *Proceedings of the National Academy of Sciences* 113.39 (Sept. 2016), pp. 10797–10801. DOI: 10.1073/pnas.1605941113. URL: https://doi.org/10.1073/pnas.1605941113.

[109] BBC. *Should we be recycling Covid tests?* https://www.youtube.com/watch?v=pIuJw5yFXrA. Accessed: 2023-05-30. 2022.

[110] European Chemicals Agency. et al. *Study on the product lifecycles, waste recycling and the circular economy for nanomaterials: November 2021*. Publications Office, 2021. DOI: 10.2823/708711. URL: https://data.europa.eu/doi/10.2823/708711.

[111] Claudio Parolo et al. "Simple paper architecture modifications lead to enhanced sensitivity in nanoparticle based lateral flow immunoassays". In: *Lab Chip* 13.3 (2013), pp. 386–390. DOI: 10.1039/c2lc41144j. URL: https://doi.org/10.1039/c2lc41144j.

[112] Yanyan Wang et al. "Study of superparamagnetic nanoparticles as labels in the quantitative lateral flow immunoassay". In: *Materials Science and Engineering: C* 29.3 (2009). Development of Nanostructures for Medicine Special Issue, pp. 714–718. ISSN: 0928-4931. DOI: https://doi.org/10.1016/j.msec.2009.01.011. URL: https://www.sciencedirect.com/science/article/pii/S0928493109000113.

UNIVERSITÉ CATHOLIQUE DE LOUVAIN
École polytechnique de Louvain
Rue Archimède, 1 bte L6.11.01, 1348 Louvain-la-Neuve, Belgique | **www.uclouvain.be/epl**